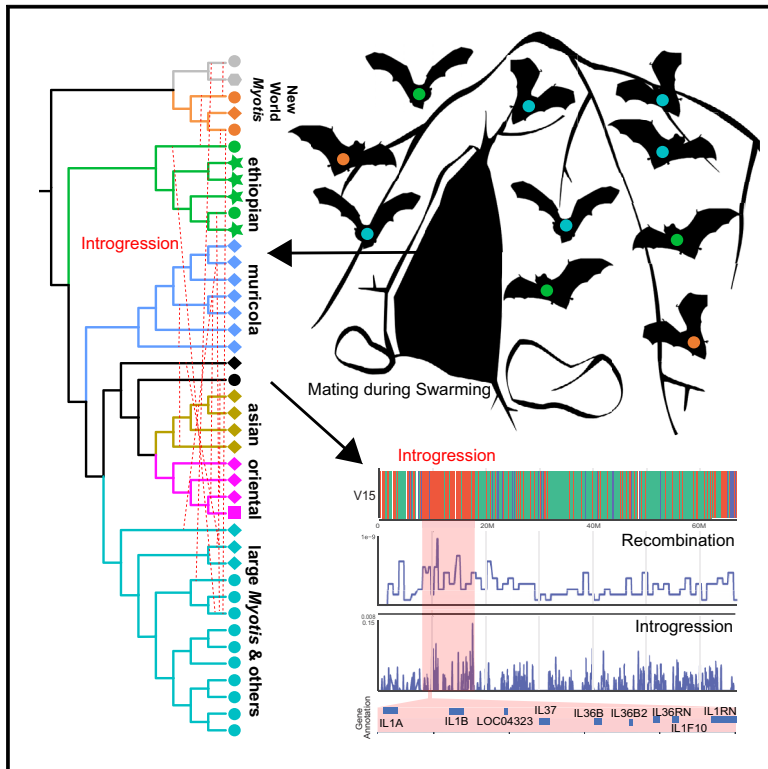Article

Karyotypic stasis and swarming influenced the evolution of viral tolerance in a species-rich bat radiation

Graphical abstract

Authors

Nicole M. Foley, Andrew J. Harris,
Kevin R. Bredemeyer, ...,
Emma C. Teeling, Michael F. Criscitiello,
William J. Murphy

Correspondence

nfoley@cvm.tamu.edu (N.M.F.),
wmurphy@cvm.tamu.edu (W.J.M.)

In brief

In their recombination-aware phylogenomic analyses, Foley et al. demonstrate pervasive introgression among *Myotis* bats, likely promoted by their use of cryptic swarming behavior during mating. Introgression has acted to restrict the species tree to low recombining regions of the genome. In contrast, immune loci are enriched in introgressed regions.

Highlights

- Phylogenomics reveals pervasive introgression among Old World *Myotis* bats

- A cryptic bat mating behavior called swarming promotes interspecific introgression

- Genomic regions of low recombination repel introgression and retain the species tree

- Immune loci are among those most frequently introgressed

CellPress

Cell Genomics

Article

Karyotypic stasis and swarming influenced the evolution of viral tolerance in a species-rich bat radiation

Nicole M. Foley,[1,*] Andrew J. Harris,[1,2] Kevin R. Bredemeyer,[1,2] Manuel Ruedi,[3] Sebastien J. Puechmaille,[4,5] Emma C. Teeling,[6] Michael F. Criscitiello,[2,7] and William J. Murphy[1,2,8,*]

[1]Veterinary Integrative Biosciences, Texas A&M University, College Station, TX, USA
[2]Interdisciplinary Program in Genetics & Genomics, Texas A&M University, College Station, TX, USA
[3]Department of Mammalogy and Ornithology, Natural History Museum of Geneva, Route de Malagnou 1, BP 6434, 1211 Geneva 6, Switzerland
[4]Institut des Sciences de l'Évolution, Montpellier (ISEM), Université de Montpellier, CNRS, EPHE, IRD, Montpellier, France
[5]Institut Universitaire de France, Paris, France
[6]School of Biology and Environmental, Science, Science Centre West, University College Dublin, Belfield, Ireland
[7]Department of Veterinary Pathobiology, Texas A&M University, College Station, TX 77843, USA
[8]Lead contact
*Correspondence: nfoley@cvm.tamu.edu (N.M.F.), wmurphy@cvm.tamu.edu (W.J.M.)
https://doi.org/10.1016/j.xgen.2023.100482

SUMMARY

The emergence of COVID-19 and severe acute respiratory syndrome (SARS) has prioritized understanding bats' viral tolerance. *Myotis* bats are exceptionally species rich and have evolved viral tolerance. They also exhibit swarming, a cryptic behavior where large, multi-species assemblages gather for mating, which has been hypothesized to promote interspecific hybridization. To resolve the coevolution of genome architecture and their unusual antiviral tolerance, we undertook a phylogenomic analysis of 60 Old World *Myotis* genomes. We demonstrate an extensive history of introgressive hybridization that has replaced the species phylogeny across 17%−93% of the genome except for pericentromeric regions of macrochromosomes. Introgression tracts were enriched on microchromosome regions containing key antiviral pathway genes overexpressed during viral challenge experiments. Together, these results suggest that the unusual *Myotis* karyotype may have evolved to selectively position immune-related genes in high recombining genomic regions prone to introgression of divergent alleles, including a diversity of interleukin loci responsible for the release of pro-inflammatory cytokines.

INTRODUCTION

The observation that several bat species are tolerant to some viruses of significant concern to human and animal health[1,2] has led global public health initiatives to prioritize understanding the basis of this phenotype.[3] Hypotheses for this enhanced tolerant, antiviral immunity include the coordinated evolution of bat flight,[4] unique immune system adaptations, and bat/virus coevolution.[2,5–9] The hypothesized coevolution of bats and viruses[1,10] suggests that interrogating phylogenomic discordance may be instrumental in understanding the genetic basis of viral tolerance. Resolved species-level phylogenies may also aid in monitoring future disease emergence through the identification of related species that host similar viruses.[11] *Myotis* bats comprise the most species-rich bat genus and have an almost global distribution.[12] However, their phylogenomic relationships lack consensus, most likely due to some combination of gene flow and incomplete lineage sorting during their evolution, the resolution of which has been hampered by limited surveys of genomic variation.[12–15]

Adaptive introgression of immune loci is frequently observed between species pairs across the mammalian phylogeny.[16–20] Additionally, mating strategy has been shown to result in systematic differences in immune responses, conferring enhanced protection again sexually transmitted diseases in promiscuous primates and adenovirus infection in promiscuous bats.[21,22] Temperately distributed bats, including numerous *Myotis* species, exhibit autumnal swarming, a cryptic behavior where large, multi-species assemblages gather for mating.[23] During the swarming period between August and October, thousands of bats from multiple bat genera form nightly gatherings at cave entrances.[24] At these transient meetings, bats exhibit intense flight activity, chasing, and increased communication, including echolocation and human-audible social calls, which facilitate interspecific communication.[24–26] Additionally, these assemblages are typically 80% male biased,[27,28] suggesting intense competition for mates.[29] Although the phenology of swarming varies by species, elevation, and seasonal timing,[26,30,31] many bat species and genera still overlap at swarming sites.

Initially, the purpose of swarming was thought to be locating suitable hibernation sites and orienting juveniles to their whereabouts.[25] Later, swarming was shown to facilitate gene flow between isolated populations of the same species.[32] Most recently, genetic analyses of microsatellites have suggested that swarming may promote interspecific hybridization among *Myotis* species, but the strength and consistency of this process during the evolution of the genus is unknown.[23] We hypothesized that an excess of historical gene flow, facilitated by swarming, has contributed to the acquisition and maintenance of novel and divergent genomic diversity. Some of this novel variation may include immune gene loci that enhance viral tolerance.

RESULTS

Whole-genome phylogenies

To test this hypothesis, we sequenced and aligned 60 new *Myotis* genomes representing 42 species to a chromosome-level long-read reference genome assembly for *Myotis myotis* (Tables S1 and S2).[33] We improved this assembly by initially using the associated gene annotation and previously generated ZooFISH maps[34] to predict the location of unassigned scaffolds.

The original Hi-C data[33] were remapped to the assembly, and assignments were made if contacts in the Juicebox Analysis Toolkit[35,36] matched predictions made by the ZooFISH and gene annotation analysis. In this way, we placed 37 scaffolds that were previously chromosomally unassigned (Table S3). Notably, these contained large clusters of immune-related genes (e.g., major histocompatibility complex [MHC], immunoglobulin heavy-chain genes, and interleukin receptors) (Figure S1), which have previously been implicated in adaptive introgression.[37,38] Our analysis localized these scaffolds predominantly to chromosome ends, which typically possess elevated recombination rates (Figure S2).

To establish a baseline phylogeny for the Old World *Myotis*, we sampled phylogenomic signal across the chromosome alignments, analyzing 1,463,340 single-nucleotide variants (SNVs) with site pattern frequency-based coalescent methods in SVDquartets.[39] The same dataset was also concatenated to generate a maximum likelihood tree using IQ-TREE 2.[40] The concatenation- and coalescent-based SNV phylogenies were highly congruent. Both trees identified six primary Old World *Myotis* clades (Figure 1A) and differed only in the positions of the whiskered and muricola clades and a few rogue taxa, including *M. annatessae* and *M. welwitschii* (Figures 1A and S3). By contrast, there was a considerable degree of phylogenomic conflict between the nuclear and mitogenome topologies. Widespread clade switching occurred for several focal species (Figures 1A and 1B), similar to results from small-scale analyses of nuclear and mitochondrial gene fragments (Figures 1B, 1C, and S4).[12] Resolving the basis for this discordance was critical to distinguishing species relationships and associations that may arise due to gene flow and other types of phylogenetic noise.[41–45]

Mitonuclear discordance is generally predictive of gene flow in other mammals, although there are some exceptions.[46,47] Among species with a history of post-speciation gene flow, it has been demonstrated that the species tree is not the dominant phylogenomic signal across the genome.[42,43] However, majority-rule phylogenomic approaches assume that the most frequent topology represents the species tree and therefore often mask underlying signatures of discordance.[41,43,44] In several hybridizing radiations, episodes of post-speciation gene flow have erased the historical branching events of the species tree from large swaths of the genome.[42,43,45] Therefore, we implemented a recombination-aware locus tree approach, which has proved crucial to distinguishing the phylogenetic signal of speciation from introgression.

All surveyed *Myotis* species shared an identical G-banded karyotype (2n = 44) except *M. annectans*, with (2n = 46),[34,48] an interesting trait given that animal radiations with histories of post-speciation gene flow typically possess conserved karyotypes.[41–43,49] The *Myotis* karyotype is also unusual among mammals, comprising three large autosomes (∼228–217 Mb) and 18 much smaller chromosomes (∼108–14 Mb) (Figure 2A),[34] which superficially resemble macro- and microchromosomes commonly observed in avian and reptilian karyotypes.[50,51] We used ReLERNN,[52] a deep learning approach, to infer a sex-averaged recombination map for *M. myotis* (Figure S5). A comparative analysis indicated the recombination landscape is conserved between *M. brandtii* and *M. myotis* (Figure S6). Therefore, we proceeded to use the *M. myotis* map as a representative for all *Myotis*. Low recombining regions were narrowly restricted to the pericentromeric regions of the largest macrochromosomes (V1, V3, and V5) and the X chromosome (chrX) (Figure 2B). The highest recombination rates were predictably found on the smallest autosomes, which also exhibit elevated gene densities and GC content (Figure 2C), similar to the microchromosomes of birds and some reptiles.[50,51]

Recombination-aware phylogenomics

To investigate phylogenomic variation across the recombination landscape, we computed 36,264 maximum likelihood (ML) locus trees for 60 species from the whole-genome dataset using the GTR + GHOST model of rate heterogeneity[53] in IQ-TREE 2 from 50 kilobase (kb) alignment windows covering 91% of the *M. myotis* genome. The GHOST model was chosen given that recent studies have demonstrated that some tests of introgression are highly sensitive to rate variation across clades.[54] Ten subtrees (Table S4) were pruned from these datasets to determine the genomic stability of relationships among the principal clades and between individual species whose positions were difficult to resolve in the whole-genome and mitogenome analyses (Figures 1A and 1B). These analyses revealed widespread locus tree discordance otherwise masked in the whole-genome concatenation and coalescence phylogenies (Figures 3 and S7–S15). Locus tree frequencies varied markedly between chrX and the autosomes and between high and low recombining regions (Figure S16).

Phylogenomic relationships within the whiskered bats and most *Myotis* clades exhibited asymmetric tree topology frequencies, considered one of the clearest indicators of the presence of gene flow (Figures 3 and S16).[55] Previous studies have shown that in the presence of gene flow, the species tree is enriched in low recombining regions of the genome (particularly pericentromeric regions and the chrX) (Figure S17), while trees
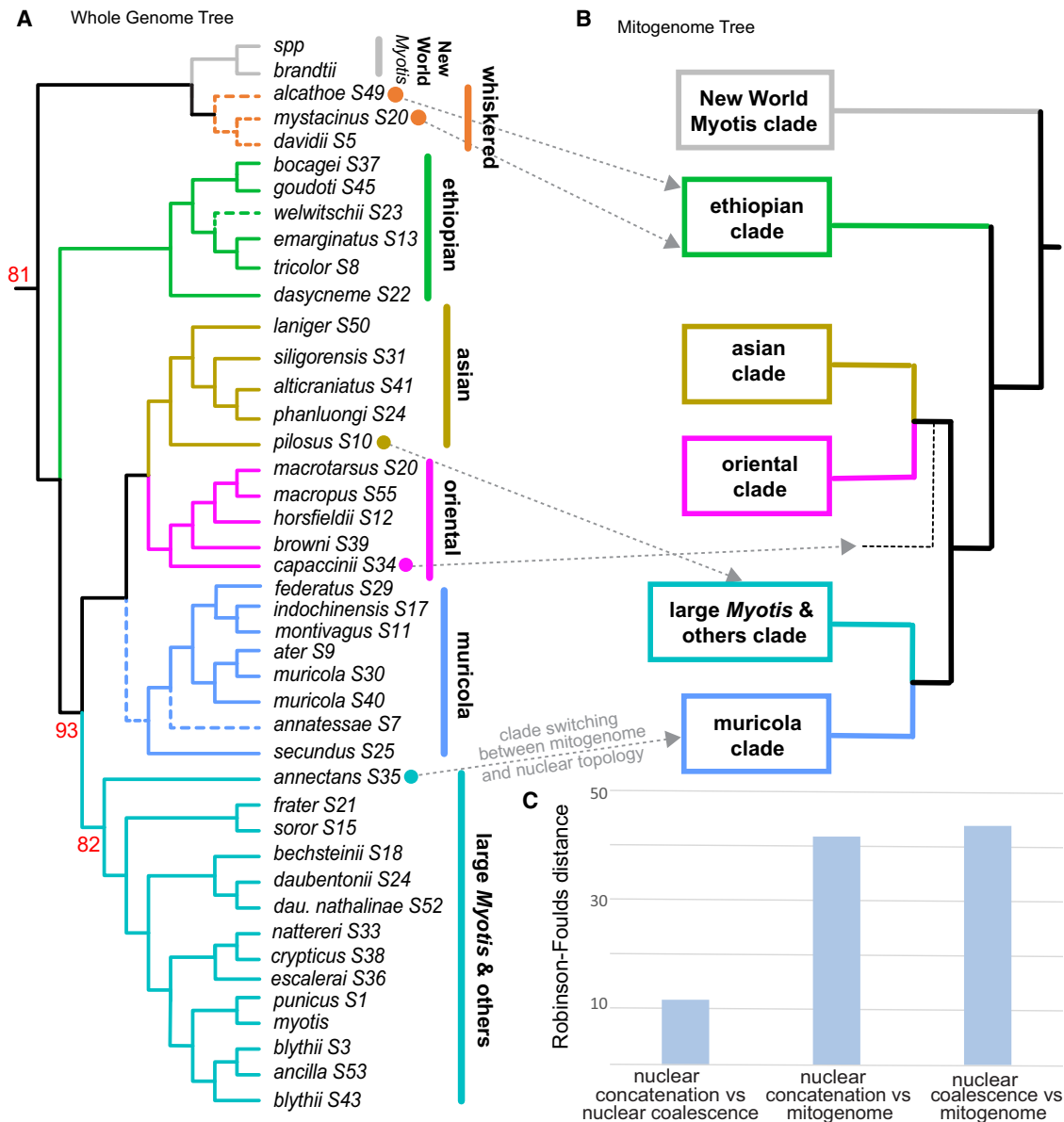
Figure 1. Clade switching between the whole-genome nuclear and mitogenome topologies

(A) Maximum likelihood cladogram from ~1.5 million genome-wide SNVs, showing only one sample per species where multiple exist. Bootstrap support is 100% for all nodes unless indicated otherwise. Dashed branches show which relationships differ between concatenation and coalescent analyses of the same dataset. Concatenation bootstrap values are shown in red.

(B) The mitogenome phylogeny is illustrated to highlight, via gray dashed arrows, clade switching relative to the nuclear phylogeny for the species indicated with colored dots.

(C) Robinson-Foulds (RF) distances between the nuclear and mitogenome topologies.

reflective of gene flow will be enriched in high recombining regions.[41,43–45] Using a combined approach to infer the species tree, our distributions of phylogenomic signal were validated by three statistical measures that distinguish introgression from incomplete lineage sorting (ILS): (1) whole-genome D-statistics[56] (Table S5), (2) windowed f(D) statistics (Figures 3C, S16, and S17), and (3) QuIBL (Table S6). While D-statistics can yield insights into the genome-wide presence of introgression, f(D) can provide information on more precise genomic locations

of introgression. QuIBL takes a distribution of internal branch lengths from a set of locus trees and uses a coalescence-based model to infer the proportion of locus trees derived from introgression or ILS. For the whiskered clade, topology 1 (t1) is most frequent in low recombining regions and in regions with reduced introgression, while t2 becomes more frequent in introgressed, high recombining regions (Figure 3B). Similar observations across numerous eukaryotic clades have increasingly demonstrated the predictive power of using regions of low
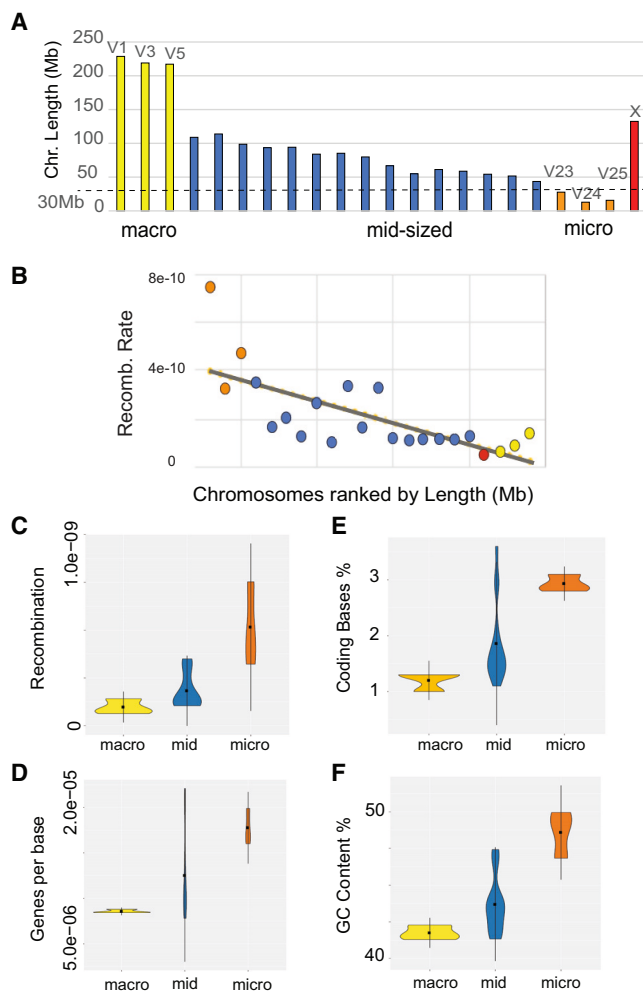
Figure 2. An unusual mammalian karyotype
(A) The dashed line indicates 30 Mb, which previous studies have used as a cutoff to define microchromosomes.[50]
(B) Chromosome length is inversely related to recombination rate.
(C–F) Comparison of recombination rate (C), genes per base (D), coding bases (E), and GC content (F) between macro-, mid-sized, and microchromosomes.

recombination to infer the species tree, as they are depleted of ILS and gene flow.[41,43–45,57–60]

Remarkably, the inferred species tree uniting the whiskered clade with New World species was restricted to less than ~60% of the genome, clustering in the pericentromeric regions of the three macrochromosomes, and chrX, which possessed the lowest rates of recombination (Figures 3 and S16). This pattern, as well as patterns of alpha and internal branch length (ibl) parameter distributions along chromosomes (Figure 3C) , was mirrored in a highly predictable manner across other *Myotis* clades (Figure S18) where the species tree was commonly observed in less than 50% of the genome. Crucially, there are numerous differences between the recombination-aware inferred species tree (Figure 4A) and the whole-genome concatenation and coalescence analyses inferred from SNVs. *D*-statistics show that analyses of the genome-wide SNV dataset return

the most frequent introgressed topology for the relationships between the muricola, large myotis, Asian, and Oriental clades, the respective positions of *M. annatessae*, *M. capaccinii*, and *M. pilosus*, and the relationship among *M. pilosus*, *M. capaccinii*, and *M. laniger* (Figure 4B; Table S5). *D*-statistics and QuIBL (Table S6) also show that clade switching between nuclear and mitogenome topologies (Figure 1B) is due to historical interclade introgression likely due to range overlap between Asian-distributed *M. annectans* and *M. indochinensis* (Figure 4).

Previous studies have demonstrated that whole-genome *D*-statistics maintain sensitivity when there is up to 20% genetic distance among the ingroup species in the test[62] and are also relatively robust to the genetic distance between the outgroup and ingroup species. In our analysis, the genetic distance between component species of Old and New World clades is ~16%, which spans the deepest divergence in our dataset. In conclusion, our findings support a scenario for Old World *Myotis* evolution where a long history of interspecific hybridization involving species from multiple clades has resulted in massive depletion of the species tree across the arms of the macrochromosomes increasing toward telomere ends, with a near-complete replacement by introgression signatures on the smallest microchromosomes.

A link between introgression and swarming behavior?

Introgression is exceptionally pervasive among *Myotis* bats, even when compared to other mammalian clades with histories of ancient introgressive hybridization.[43,49,63] This may be due to the use of swarming behavior in many *Myotis* species. Swarming behavior is characterized by multi-species, male-biased mating assemblages often numbering from hundreds to thousands of individuals.[23] Many records of species present at swarming sites come from predominantly European studies and overlap our sampling (Figure 5A; Table S7). Therefore, we pruned subtrees derived from the 50 kb windows from the whole-genome 60 species sliding-windows dataset (Table S4) to test the hypothesis that hybridization is common among species within and between clades recorded at swarming sites (Figure 4B). Asymmetry in genome-wide frequency and *D*-statistics estimated among swarming species indicated that introgression was the dominant driver of phylogenetic discordance in these analyses (Figures 5B, S19, and S20). Additionally, we show that introgressed topologies with the highest f(*D*) values are the most enriched on microchromosomes (Figure S21). Introgression was observed not only among species within clades but also between species from divergent clades (Figure 5B), like the large *Myotis*, whiskered, and New World clades. Note, due to our sampling scheme, we could only infer the presence of historical introgression among *Myotis* species. Population-level data or data sampled from species found contemporaneously at swarming sites would be required to accurately determine the prevalence of ongoing hybridization at swarming sites, which has been documented for some of the species we sampled.[15,63,64]

The Ethiopian clade (Figure 1A) contains important contrasts to other predominantly swarming *Myotis* clades. At least one species lacks swarming behavior: *M. bocagei* employs a harem system where a single male and 6–8 females gather in a banana leaf for mating.[65] This behavior should minimize the probability of introgression. Although not all mating strategies employed by
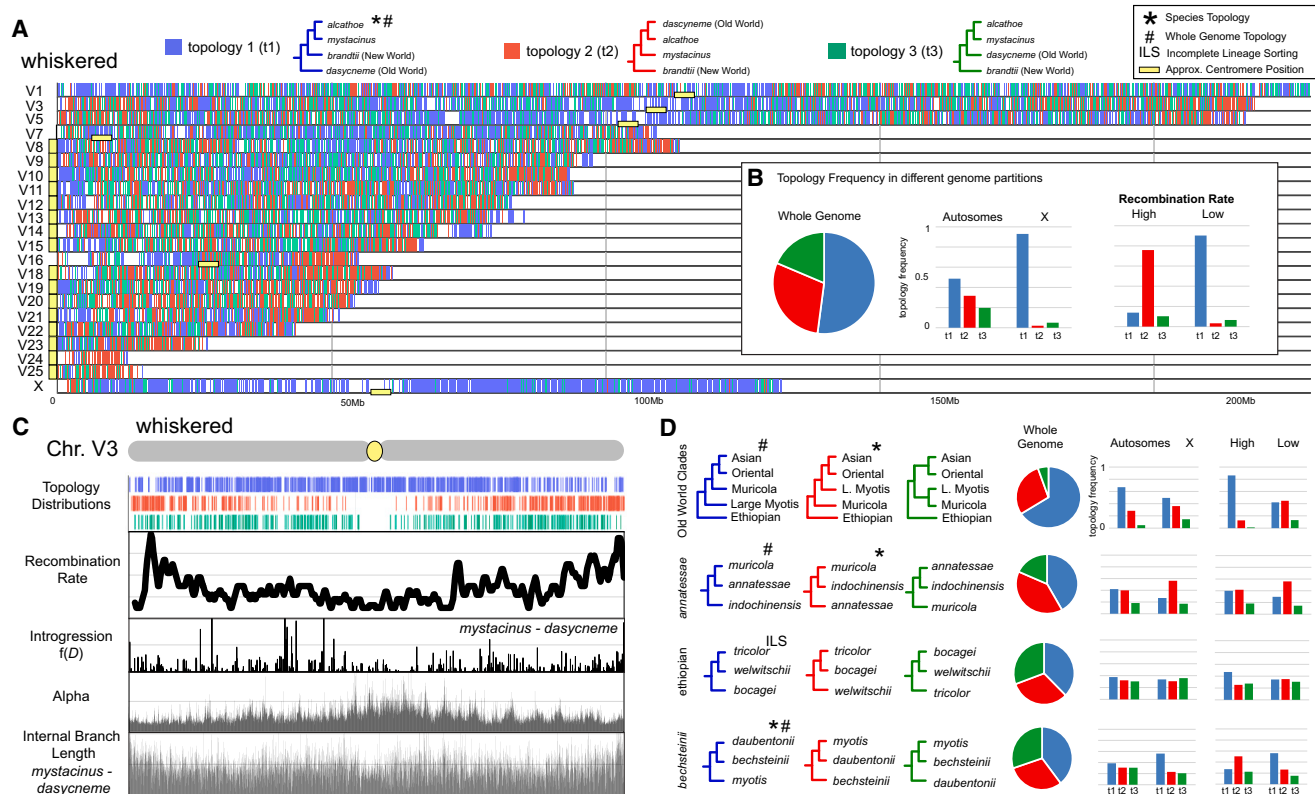
Figure 3. Genome-wide distribution of phylogenomic discordance across the Old World *Myotis* radiation

(A) Distribution of phylogenomic signal for the whiskered clade visualized using Tree House Explorer[61] in 50 kb locus alignment windows across the genome. Vertical bars along each chromosome are color coded to depict the distribution of the most frequent topologies.

(B) Comparison of the frequency of t1, t2, and t3 across the whole genome (left) and between the autosomes and the X (middle) and between high and low recombining regions of the genome (right).

(C) Whole-chromosome view for ChrV3 illustrates local relationship between recombination rate, f(*D*), the alpha parameter of the gamma model, and the internal branch length (ibl) for relationships between *M. mystacinus* and *M. dasycneme*. Note the depletion of topologies associated with introgression (t2 [red], t3 [green]) in the low recombining region at the center of the chromosome.

(D) Distributions of phylogenomic signal for additional *Myotis* clades in relation to chromosome type and recombination rate (reference the key in B).

the Ethiopian clade species are well characterized, the roughly equal frequency of locus trees for the clade are consistent with ILS, and not introgression, being the dominant source of phylogenomic discordance (Figure 3C). This is notable given that *M. bocagei*, *M. tricolor*, and *M. welwitschii* are sympatric over much of their current distributions. Conversely, two members of the Ethiopian clade, *M. emarginatus* and *M. dasycneme*, have a European distribution and are frequently reported at swarming sites (Figures 4A and 5A). Whole-genome *D*-statistics consistently show significant ancient introgression signatures between *M. emarginatus* and numerous European distributed species, yet there is minimal evidence of ancient introgression with *M. bocagei* (Figure 5C). In summary, these contrasting phylogenomic patterns between swarming and non-swarming species support the hypothesis that swarming sites have acted as crucibles of genetic exchange.

Introgression at immune loci

We hypothesized that viral tolerance in *Myotis* bats may be enhanced by a long history of immune gene introgression involving species from multiple phylogenetic lineages interacting at swarming sites.[66] Introgression from Neanderthals into modern humans has had measurable impacts on the expression of genes associated with immunity.[16,67,68] Most notable among these is differential expression of an *OAS1* isoform, which has previously been shown to contribute to differential susceptibility and severity of COVID-19 outcomes in humans.[69] To further examine if the apparent genome-wide intersection between introgression and immune-related processes has had any potential effect on gene expression in *Myotis* bats, we used a database of differentially expressed genes from a study that performed viral challenge experiments on *M. daubentonii* cell lines.[70] These cells were treated with a modified Rift Valley fever virus or supplemented with interferon, and gene expression was compared 6 h before and after treatment.[70] Our results demonstrate that genes that were differentially expressed in response to viral challenges in *M. daubentonii* were among the most frequently introgressed across microchromosomes (Figure S22) and were also significantly introgressed genome-wide across numerous *Myotis* clades (Figure S23). Notably, these include
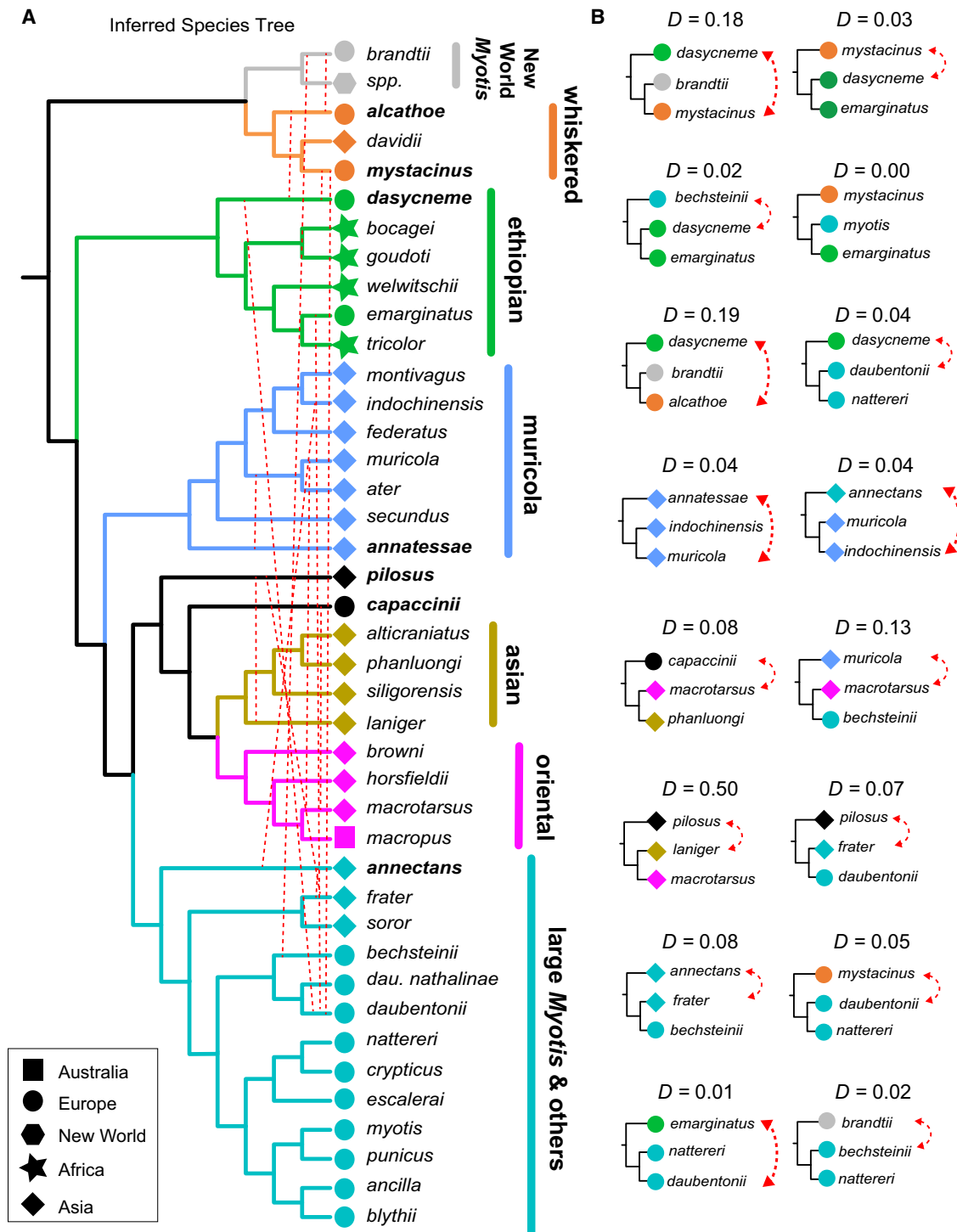
Figure 4. Discordance due to gene flow

(A) Species tree inferred from recombination-aware phylogenomic approaches. Crucially, our analyses show that standard whole-genome analyses in Figure 1 do not recover the species tree and instead depict relationships consistent with introgression for some species (e.g., *M. capaccinii*). Dashed lines indicate where within and between introgression is detected. Note that we illustrate introgression only for the analyses presented in (B) for the purpose of clarity. Additional instances of genome-wide introgression are depicted in Figure 5.

(B) Whole-genome-based *D*-statistics generated using ABBA-BABA tests in ANGSD illustrate significant evidence for introgression (*Z* score > 3) in (A). Trees are represented top to bottom in the format (H1, (H2, H3), O), where the outgroup O (*S. latirostris*) is not shown. See Table S5 for detailed results.
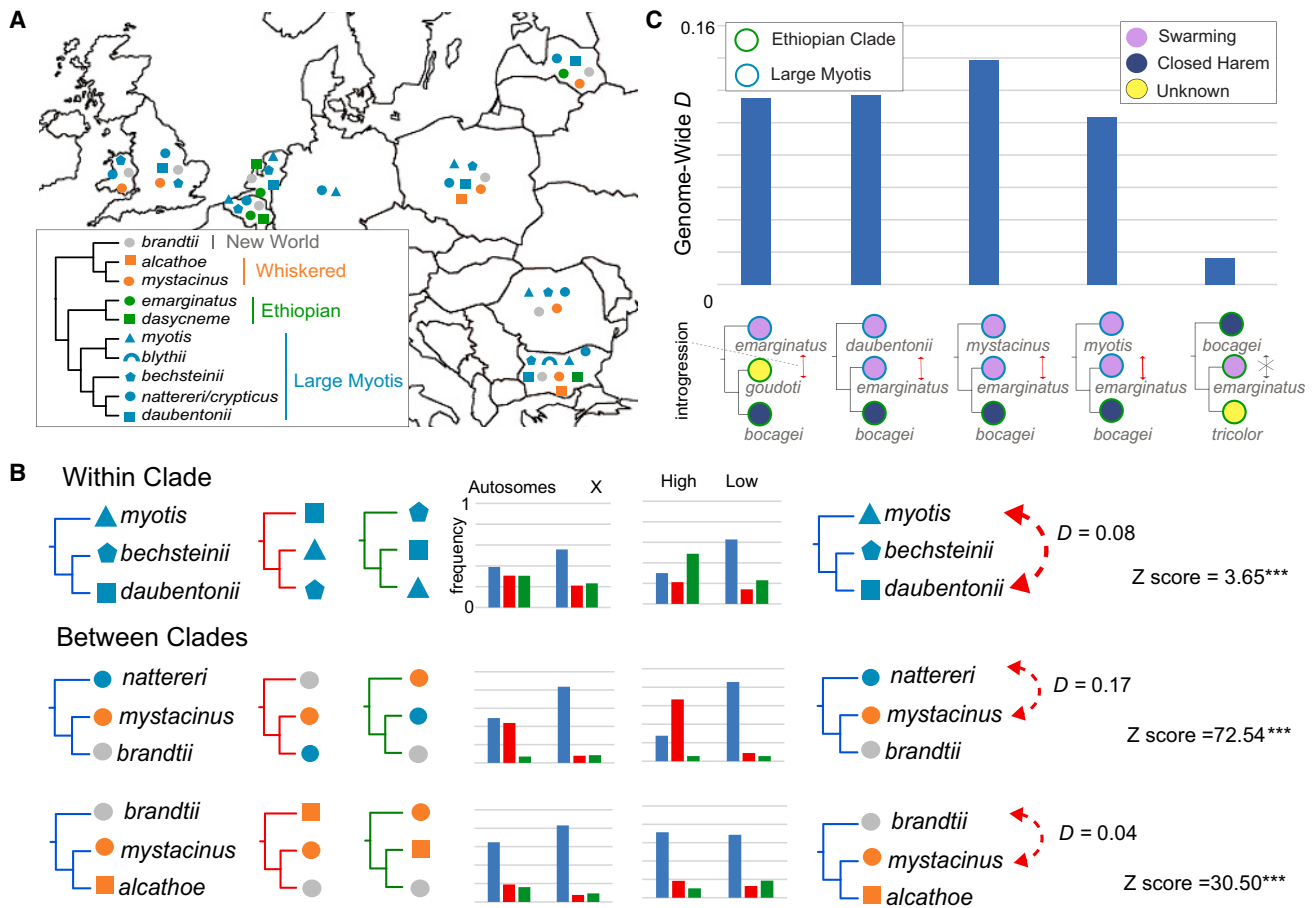
Figure 5. Introgression occurs among species that co-occur at swarming sites

(A) Species assemblages reported at swarming sites throughout Europe (Table S6). The tree inset shows the species tree and clade membership of each species.

(B) Examples of within and between clade introgression. Variation in topological frequency is observed between autosomal, X, and high and low recombining genomic partitions. Whole–genome D-statistics demonstrate phylogenomic conflict is due to introgression.

(C) Comparisons of the genome-wide D-statistic for species representing the large myotis clade, with a promiscuous mating system, and M. bocagei from the Ethiopian clade, which employs a conservative (closed harem) mating system. The same analysis was repeated using M. yumanensis as the reference genome to demonstrate that our results are not confounded by reference bias (Figure S25; Table S5). Trees for introgression tests are represented top to bottom in the format (H1, (H2, H3)), O), where the outgroup O (S. latirostris) is not shown. See Table S5 for detailed results.

microchromosome-linked genes *OAS1*, *OAS3*, and *OASL*, which exhibit up to a 6-fold change in expression in response to viral challenge.[70] Because one of the common outcomes of interspecific hybridization is altered gene expression,[68,71–73] these results suggest that frequent hybridization-induced modulation of immune gene expression in bats might be adaptive and is worthy of further investigation in natural and experimental populations.

Recombination acts to break down introgressed haplotype blocks over time. While long blocks representing more recent introgression events are expected to be rare in our dataset due to low population genomic sampling, one of the largest haplotypes spans ~10 Mb on the subtelomeric region of V15 and possesses an introgressed topology uniting *M. myotis* and *M. daubentonii* (Figures 6 and S24). Measures of recombination rate, ibl, and f(D) were all elevated inside the block relative to the remainder of the chromosome. A STRING analysis of this haplo- type block identified a significant enrichment (false discovery rate [FDR] < 0.05) of genes associated with cytokine receptor activity, the interleukin-36 pathway, and the interleukin-1 family signaling pathway (Table S8). *IL36* is notable as a member of the *IL1* superfamily of pro-inflammatory cytokines, which help regulate the adaptive and innate immune systems.[74] *IL36* promotes antiviral immunity by increasing cellular sensitivity to interferon[75] in human and mouse models to herpes simplex virus[75] and a host of other viruses.[74]

DISCUSSION

Collectively, our results support a scenario where swarming-mediated interspecific hybridization can impact antiviral immune responses in bats. High rates of introgression have also been reported in animal clades where multiple, closely related species are present during mating, including species of *Stenella* and
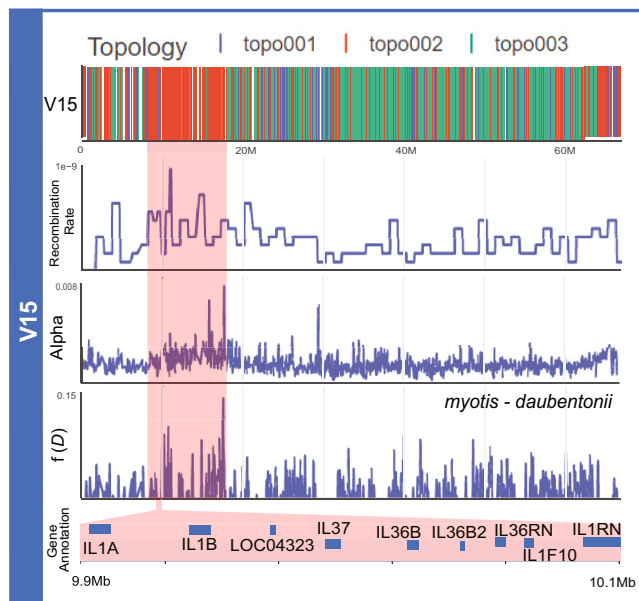
Figure 6. Evidence for a potential link between immunity and the recombination landscape in *Myotis* bats

Distribution of phylogenomic signal, recombination rate, ibl, and f(D) values for chromosome V15 for the *bechsteinii* clade. A large introgressed block for *myotis* and *daubentonii* (Figure S24) is highlighted in red and is significantly enriched for *IL-36* and *IL-1* signaling pathways (FDR < 0.05) (Table S8).

Tursiops dolphins[76–78] and *Anopheles* mosquitoes.[42,79] Swarming has specifically contributed to the introgression-mediated evolution of insecticide resistance at several loci in anopheline mosquitoes.[80,81] Promiscuous mating behaviors may frequently evolve to promote adaptive interspecific hybridization, providing access to divergent genomic variants and/or quantitative variation in gene expression as a rapid means to counter frequent and novel pathogen exposure.[71] The extraordinarily large number of mammalian congeners present in large colonies of bats (sometimes thousands of individuals) and mating during swarming would impose a unique burden on mucosal viral immunity. Under this model, frequent introgression at swarming sites would conceivably afford myriad opportunities for adjusting viral symbiont management and/or defense mechanisms using pooled immunogenomic resources from species across the genus. As such, swarming behavior may have provided a singular opportunity for the evolution of a novel mechanism for viral management/symbiosis through introgression biased toward chromosome termini enriched for immune loci. Such innovations are not unprecedented in nature. Radical and profound innovations in immunogenetic diversification have previously evolved from horizontal genetic transfer in other taxa (Table S9)—for example, the CRISPR-Cas9 prokaryotic adaptive immune system from IscB and IS200/IS605 transposons[82] and the somatic cell recombination capability of immunoglobulin and T cell receptor genes via domestication of ProtoRAG transposase[83] in an early chordate. Further investigations into understanding how karyotype evolution, the recombination rate landscape, and the introduction of divergent genomic variants via introgres-

sion and/or ILS intersect to hone bats' genomes for viral and cancer tolerance may yield novel innovations for viral immunotherapeutics and even oncology.[84] Finally, our results suggest that swarming sites may merit recognition as special sites of conservation given the unique evolutionary processes to which they play host.[23,28,31,85]

Limitations of the study

All data were mapped to *M. myotis*, which is part of the ingroup in our analysis, and so may lead to spurious inference of introgression due to reference bias. To account for this potentially confounding factor, we also mapped the data to the long-read *M. yumanensis* genome assembly[86] from the New World clade. Although this analysis confirmed our initial results for the Old World ingroup, ideally a closely related outgroup, which is roughly equidistant to all ingroup species, should be used to mitigate any potential reference bias and data loss due to mapping to a divergent reference genome. Our analysis was also constrained to the detection of historical introgression. Although some studies indicate that contemporary introgression occurs at swarming sites,[23] our dataset was not selected to formally test this hypothesis. Further comparative phylogenomic analyses of species with conservative and promiscuous mating behaviors would be useful to fully characterize the contribution of swarming behavior to introgression in bats.

STAR★METHODS

Detailed methods are provided in the online version of this paper and include the following:

- **KEY RESOURCES TABLE**
- **RESOURCE AVAILABILITY**
  - ○ Lead contact
  - ○ Materials availability
  - ○ Data and code availability
- **METHOD DETAILS**
  - ○ Taxonomic sampling and sequencing
  - ○ Sequence QC and read mapping
  - ○ Mitogenome assembly and analysis
  - ○ Improving the *Myotis myotis* reference genome
  - ○ A recombination map for *Myotis myotis*
  - ○ Phylogenomics
  - ○ Sliding windows
  - ○ Detection of gene flow
  - ○ Hybridization at swarming sites?
  - ○ Anti-viral immunity and introgression
  - ○ Large introgressed haplotype blocks

AUTHOR CONTRIBUTIONS

Conceptualization, W.J.M. and N.M.F.; data curation, N.M.F. and K.R.B.; investigation, N.M.F., A.J.H., K.R.B., M.F.C., and W.J.M.; software, A.J.H.; project administration, W.J.M.; samples, M.R., S.J.P., and E.C.T.; writing – original draft, W.J.M. and N.M.F.; writing – review & editing, all authors.

DECLARATION OF INTERESTS

The authors declare no competing interests.

REFERENCES

1. Ruiz-Aravena, M., McKee, C., Gamble, A., Lunn, T., Morris, A., Snedden, C.E., Yinda, C.K., Port, J.R., Buchholz, D.W., Yeo, Y.Y., et al. (2022). Ecology, evolution and spillover of coronaviruses from bats. Nat. Rev. Microbiol. 20, 299–314.

2. Carlson, C.J., Albery, G.F., Merow, C., Trisos, C.H., Zipfel, C.M., Eskew, E.A., Olival, K.J., Ross, N., and Bansal, S. (2022). Climate change increases cross-species viral transmission risk. Nature 607, 555–562.

3. Streicker, D.G., and Gilbert, A.T. (2020). Contextualizing bats as viral reservoirs. Science 370, 172–173.

4. Zhang, G., Cowled, C., Shi, Z., Huang, Z., Bishop-Lilly, K.A., Fang, X., Wynne, J.W., Xiong, Z., Baker, M.L., Zhao, W., et al. (2013). Comparative analysis of bat genomes provides insight into the evolution of flight and immunity. Science 339, 456–460.

5. O'Shea, T.J., Cryan, P.M., Cunningham, A.A., Fooks, A.R., Hayman, D.T.S., Luis, A.D., Peel, A.J., Plowright, R.K., and Wood, J.L.N. (2014). Bat flight and zoonotic viruses. Emerg. Infect. Dis. 20, 741–745.

6. Brook, C.E., and Dobson, A.P. (2015). Bats as 'special' reservoirs for emerging zoonotic pathogens. Trends Microbiol. 23, 172–180.

7. Calisher, C.H., Childs, J.E., Field, H.E., Holmes, K.V., and Schountz, T. (2006). Bats: important reservoir hosts of emerging viruses. Clin. Microbiol. Rev. 19, 531–545.

8. Cui, J., Han, N., Streicker, D., Li, G., Tang, X., Shi, Z., Hu, Z., Zhao, G., Fontanet, A., Guan, Y., et al. (2007). Evolutionary relationships between bat coronaviruses and their hosts. Emerg. Infect. Dis. 13, 1526–1532.

9. Scheben, A., Ramos, O.M., Kramer, M., Goodwin, S., Oppenheim, S., Becker, D.J., Schatz, M.C., Simmons, N.B., Siepel, A., and Richard McCombie, W. (2021). Long-read sequencing reveals rapid evolution of immunity- and cancer-related genes in bats. Preprint at bioRxiv.

10. Wynne, J.W., and Wang, L.-F. (2013). Bats and viruses: friend or foe? PLoS Pathog. 9, e1003651.

11. Gouilh, M.A., Puechmaille, S.J., Gonzalez, J.-P., Teeling, E., Kittayapong, P., and Manuguerra, J.-C. (2011). SARS-Coronavirus ancestor's footprints in South-East Asian bat colonies and the refuge theory. Infect. Genet. Evol. 11, 1690–1702.

12. Ruedi, M., Stadelmann, B., Gager, Y., Douzery, E.J.P., Francis, C.M., Lin, L.-K., Guillén-Servent, A., and Cibois, A. (2013). Molecular phylogenetic reconstructions identify East Asia as the cradle for the evolution of the cosmopolitan genus Myotis (Mammalia, Chiroptera). Mol. Phylogenet. Evol. 69, 437–449.

13. Platt, R.N., 2nd, Faircloth, B.C., Sullivan, K.A.M., Kieran, T.J., Glenn, T.C., Vandewege, M.W., Lee, T.E., Jr., Baker, R.J., Stevens, R.D., and Ray, D.A. (2018). Conflicting Evolutionary Histories of the Mitochondrial and Nuclear Genomes in New World Myotis Bats. Syst. Biol. 67, 236–249.

14. Morales, A.E., Ruedi, M., Field, K., and Carstens, B.C. (2019). Diversification rates have no effect on the convergent evolution of foraging strategies in the most speciose genus of bats, Myotis. Evolution 73, 2263–2280.

15. Morales, A.E., Jackson, N.D., Dewey, T.A., O'Meara, B.C., and Carstens, B.C. (2017). Speciation with Gene Flow in North American Myotis Bats. Syst. Biol. 66, 440–452.

16. Jagoda, E., Xue, J.R., Reilly, S.K., Dannemann, M., Racimo, F., Huerta-Sanchez, E., Sankararaman, S., Kelso, J., Pagani, L., Sabeti, P.C., and Capellini, T.D. (2022). Detection of Neanderthal Adaptively Introgressed Genetic Variants That Modulate Reporter Gene Expression in Human Immune Cells. Mol. Biol. Evol. 39, msab304.

17. Enard, D., and Petrov, D.A. (2018). Evidence that RNA Viruses Drove Adaptive Introgression between Neanderthals and Modern Humans. Cell 175, 360–371.e13.

18. Chiou, K.L., Bergey, C.M., Burrell, A.S., Disotell, T.R., Rogers, J., Jolly, C.J., and Phillips-Conroy, J.E. (2021). Genome-wide ancestry and introgression in a Zambian baboon hybrid zone. Mol. Ecol. 30, 1907–1920.

19. Upadhyay, M., Kunz, E., Sandoval-Castellanos, E., Hauser, A., Krebs, S., Graf, A., Blum, H., Dotsev, A., Okhlopkov, I., Shakhin, A., et al. (2021). Whole genome sequencing reveals a complex introgression history and the basis of adaptation to subarctic climate in wild sheep. Mol. Ecol. 30, 6701–6717.

20. Song, Y., Endepols, S., Klemann, N., Richter, D., Matuschka, F.-R., Shih, C.-H., Nachman, M.W., and Kohn, M.H. (2011). Adaptive introgression of anticoagulant rodent poison resistance by hybridization between old world mice. Curr. Biol. 21, 1296–1301.

21. Nunn, C.L., Gittleman, J.L., and Antonovics, J. (2000). Promiscuity and the primate immune system. Science 290, 1168–1170.

22. Rossetto, F., Iglesias-Caballero, M., Liedtke, H.C., Gomez-Mestre, I., Berciano, J.M., Pérez-Suárez, G., de Paz, O., Ibáñez, C., Echevarría, J.E., Casas, I., and Juste, J. (2020). Mating strategy is determinant of adenovirus prevalence in European bats. PLoS One 15, e0226203.

23. Bogdanowicz, W., Piksa, K., and Tereba, A. (2012). Hybridization hotspots at bat swarming sites. PLoS One 7, e53334.

24. Bergmann, A., Gloza-Rausch, F., Wimmer, B., Kugelschafter, K., and Knörnschild, M. (2022). Similarities in social calls during autumn swarming may facilitate interspecific communication between Myotis bat species. Front. Ecol. Evol. 10.

25. Fenton, M.B. (1969). Summer activity of Myotis lucifugus (Chiroptera:Vespertilionidae) at hibernacula in Ontario and Quebec. Can. J. Zool. 47, 597–602.

26. Parsons, K.N., Jones, G., and Greenaway, F. (2003). Swarming activity of temperate zone microchiropteran bats: effects of season, time of night and weather conditions. J. Zool. 261, 257–264.

27. Thomas, R.J., and Davison, S.P. (2022). Seasonal swarming behavior of Myotis bats revealed by integrated monitoring, involving passive acoustic monitoring with automated analysis, trapping, and video monitoring. Ecol. Evol. 12, e9344.

28. Glover, A.M., and Altringham, J.D. (2008). Cave selection and use by swarming bat species. Biol. Conserv. 141, 1493–1504.

29. Senior, P., Butlin, R.K., and Altringham, J.D. (2005). Sex and segregation in temperate bats. Proc. Biol. Sci. 272, 2467–2473.

30. Piksa, K., Bogdanowicz, W., and Tereba, A. (2011). Swarming of Bats at Different Elevations in the Carpathian Mountains. Acta Chiropterol. 13, 113–122.

31. van Schaik, J., Janssen, R., Bosch, T., Haarsma, A.-J., Dekker, J.J.A., and Kranstauber, B. (2015). Bats Swarm Where They Hibernate: Compositional Similarity between Autumn Swarming and Winter Hibernation Assemblages at Five Underground Sites. PLoS One 10, e0130850.

32. Kerth, G., Kiefer, A., Trappmann, C., and Weishaar, M. (2003). High gene diversity at swarming sites suggest hot spots for gene flow in the endangered Bechstein's bat. Conserv. Genet. *4*, 491–499.

33. Jebb, D., Huang, Z., Pippel, M., Hughes, G.M., Lavrichenko, K., Devanna, P., Winkler, S., Jermiin, L.S., Skirmuntt, E.C., Katzourakis, A., et al. (2020). Six reference-quality genomes reveal evolution of bat adaptations. Nature *583*, 578–584.

34. Volleth, M., Heller, K.G., Pfeiffer, R.A., and Hameister, H. (2002). A comparative ZOO-FISH analysis in bats elucidates the phylogenetic relationships between Megachiroptera and five microchiropteran families. Chromosome Res. *10*, 477–497.

35. Dudchenko, O., Shamim, M.S., Batra, S.S., Durand, N.C., Musial, N.T., Mostofa, R., Pham, M., Glenn St Hilaire, B., Yao, W., Stamenova, E., et al. (2018). The Juicebox Assembly Tools module facilitates de novo assembly of mammalian genomes with chromosome-length scaffolds for under $1000. Preprint at bioRxiv.

36. Durand, N.C., Robinson, J.T., Shamim, M.S., Machol, I., Mesirov, J.P., Lander, E.S., and Aiden, E.L. (2016). Juicebox Provides a Visualization System for Hi-C Contact Maps with Unlimited Zoom. Cell Syst. *3*, 99–101.

37. Abi-Rached, L., Jobin, M.J., Kulkarni, S., McWhinnie, A., Dalva, K., Gragert, L., Babrzadeh, F., Gharizadeh, B., Luo, M., Plummer, F.A., et al. (2011). The shaping of modern human immune systems by multiregional admixture with archaic humans. Science *334*, 89–94.

38. Chen, N., Cai, Y., Chen, Q., Li, R., Wang, K., Huang, Y., Hu, S., Huang, S., Zhang, H., Zheng, Z., et al. (2018). Whole-genome resequencing reveals world-wide ancestry and adaptive introgression events of domesticated cattle in East Asia. Nat. Commun. *9*, 2337.

39. Chifman, J., and Kubatko, L. (2014). Quartet inference from SNP data under the coalescent model. Bioinformatics *30*, 3317–3324.

40. Minh, B.Q., Schmidt, H.A., Chernomor, O., Schrempf, D., Woodhams, M.D., von Haeseler, A., and Lanfear, R. (2020). IQ-TREE 2: New models and efficient methods for phylogenetic inference in the genomic era. Mol. Biol. Evol. *37*, 1530–1534.

41. Edelman, N.B., Frandsen, P.B., Miyagi, M., Clavijo, B., Davey, J., Dikow, R.B., García-Accinelli, G., Van Belleghem, S.M., Patterson, N., Neafsey, D.E., et al. (2019). Genomic architecture and introgression shape a butterfly radiation. Science *366*, 594–599.

42. Fontaine, M.C., Pease, J.B., Steele, A., Waterhouse, R.M., Neafsey, D.E., Sharakhov, I.V., Jiang, X., Hall, A.B., Catteruccia, F., Kakani, E., et al. (2015). Extensive introgression in a malaria vector species complex revealed by phylogenomics. Science *347*, 1258524.

43. Li, G., Figueiró, H.V., Eizirik, E., and Murphy, W.J. (2019). Recombination-aware phylogenomics reveals the structured genomic landscape of hybridizing cat species. Mol. Biol. Evol. *36*, 2111–2126.

44. Nelson, T.C., Stathos, A.M., Vanderpool, D.D., Finseth, F.R., Yuan, Y.-W., and Fishman, L. (2021). Ancient and recent introgression shape the evolutionary history of pollinator adaptation and speciation in a model monkeyflower radiation (*Mimulus* section *Erythranthe*). PLoS Genet. *17*, e1009095.

45. Hennelly, L.M., Habib, B., Modi, S., Rueness, E.K., Gaubert, P., and Sacks, B.N. (2021). Ancient divergence of Indian and Tibetan wolves revealed by recombination-aware phylogenomics. Mol. Ecol. *30*, 6687–6700.

46. Li, G., Davis, B.W., Eizirik, E., and Murphy, W.J. (2016). Phylogenomic evidence for ancient hybridization in the genomes of living cats (Felidae). Genome Res. *26*, 1–11.

47. Mao, X., Tsagkogeorga, G., Thong, V.D., and Rossiter, S.J. (2019). Resolving evolutionary relationships among six closely related taxa of the horseshoe bats (*Rhinolophus*) with targeted resequencing data. Mol. Phylogenet. Evol. *139*, 106551.

48. O'Brien, S.J., Graphodatsky, A.S., and Perelman, P.L. (2020). In Atlas of Mammalian Chromosomes S (Wiley Blackwell).

49. Chafin, T.K., Douglas, M.R., and Douglas, M.E. (2020). Genome-wide local ancestries discriminate homoploid hybrid speciation from secondary introgression in the red wolf (Canidae: *Canis rufus*). Preprint at bioRxiv.

50. Perry, B.W., Schield, D.R., Adams, R.H., and Castoe, T.A. (2021). Microchromosomes Exhibit Distinct Features of Vertebrate Chromosome Structure and Function with Underappreciated Ramifications for Genome Evolution. Mol. Biol. Evol. *38*, 904–910.

51. Waters, P.D., Patel, H.R., Ruiz-Herrera, A., Álvarez-González, L., Lister, N.C., Simakov, O., Ezaz, T., Kaur, P., Frere, C., Grützner, F., et al. (2021). Microchromosomes are building blocks of bird, reptile, and mammal chromosomes. Proc. Natl. Acad. Sci. USA *118*, e2112494118.

52. Adrion, J.R., Galloway, J.G., and Kern, A.D. (2020). Predicting the Landscape of Recombination Using Deep Learning. Mol. Biol. Evol. *37*, 1790–1808.

53. Crotty, S.M., Minh, B.Q., Bean, N.G., Holland, B.R., Tuke, J., Jermiin, L.S., and Haeseler, A.V. (2020). GHOST: Recovering historical signal from heterotachously evolved sequence alignments. Syst. Biol. *69*, 249–264.

54. Frankel, L.E., and Ané, C. (2023). Summary tests of introgression are highly sensitive to rate variation across lineages. Preprint at bioRxiv.

55. Hibbins, M.S., and Hahn, M.W. (2022). Phylogenomic approaches to detecting and characterizing introgression. Genetics *220*, iyab173.

56. Korneliussen, T.S., Albrechtsen, A., and Nielsen, R. (2014). ANGSD: Analysis of Next Generation Sequencing Data. BMC Bioinf. *15*, 356.

57. Feng, C., Wang, J., Liston, A., and Kang, M. (2023). Recombination Variation Shapes Phylogeny and Introgression in Wild Diploid Strawberries. Mol. Biol. Evol. *40*, msad049.

58. Ottenburghs, J., Honka, J., Heikkinen, M.E., Madsen, J., Müskens, G.J.D.M., and Ellegren, H. (2023). Highly differentiated loci resolve phylogenetic relationships in the Bean Goose complex. BMC Ecol. Evol. *23*, 2.

59. Stubbs, R.L., Theodoridis, S., Mora-Carrera, E., Keller, B., Yousefi, N., Potente, G., Léveillé-Bourret, É., Celep, F., Kochjarová, J., Tedoradze, G., et al. (2023). Whole-genome analyses disentangle reticulate evolution of primroses in a biodiversity hotspot. New Phytol. *237*, 656–671.

60. Owens, G.L., Huang, K., Todesco, M., and Rieseberg, L.H. (2023). Re-evaluating Homoploid Reticulate Evolution in Helianthus Sunflowers. Mol. Biol. Evol. *40*, msad013.

61. Harris, A.J., Foley, N.M., Williams, T.L., and Murphy, W.J. (2022). Tree House Explorer: A novel genome browser for phylogenomics. Mol. Biol. Evol. *39*, msac130.

62. Zheng, Y., and Janke, A. (2018). Gene flow analysis method, the D-statistic, is robust in a wide parameter space. BMC Bioinf. *19*, 10.

63. Morales, A.E., and Carstens, B.C. (2018). Evidence that *Myotis lucifugus* "Subspecies" are Five Nonsister Species, Despite Gene Flow. Syst. Biol. *67*, 756–769.

64. Korstian, J.M., Paulat, N.S., Platt, R.N., 2nd, Stevens, R.D., and Ray, D.A. (2022). SINE-Based Phylogenomics Reveal Extensive Introgression and Incomplete Lineage Sorting in *Myotis*. Genes *13*, 399.

65. Zachos, F.E. (2020). Handbook of the Mammals of the World. Bats. Mamm. Biol. *9*, 335. 100.

66. Letko, M., Seifert, S.N., Olival, K.J., Plowright, R.K., and Munster, V.J. (2020). Bat-borne virus diversity, spillover and emergence. Nat. Rev. Microbiol. *18*, 461–471.

67. Silvert, M., Quintana-Murci, L., and Rotival, M. (2019). Impact and Evolutionary Determinants of Neanderthal Introgression on Transcriptional and Post-Transcriptional Regulation. Am. J. Hum. Genet. *104*, 1241–1250.

68. Dannemann, M., Prüfer, K., and Kelso, J. (2017). Functional implications of Neandertal introgression in modern humans. Genome Biol. *18*, 61.

69. Zhou, S., Butler-Laporte, G., Nakanishi, T., Morrison, D.R., Afilalo, J., Afilalo, M., Laurent, L., Pietzner, M., Kerrison, N., Zhao, K., et al. (2021). A

Neanderthal *OAS1* isoform protects individuals of European ancestry against COVID-19 susceptibility and severity. Nat. Med. *27*, 659–667.

70. Hölzer, M., Schoen, A., Wulle, J., Müller, M.A., Drosten, C., Marz, M., and Weber, F. (2019). Virus- and Interferon Alpha-Induced Transcriptomes of Cells from the Microbat *Myotis daubentonii*. iScience *19*, 647–661.

71. Hibbins, M.S., and Hahn, M.W. (2021). The effects of introgression across thousands of quantitative traits revealed by gene expression in wild tomatoes. PLoS Genet. *17*, e1009892.

72. Michalak, P., and Noor, M.A.F. (2003). Genome-wide patterns of expression in *Drosophila* pure species and hybrid males. Mol. Biol. Evol. *20*, 1070–1076.

73. Mack, K.L., and Nachman, M.W. (2017). Gene Regulation and Speciation. Trends Genet. *33*, 68–80.

74. Wang, X., Yi, P., and Liang, Y. (2021). The Role of *IL-36* in Infectious Diseases: Potential Target for COVID-19? Front. Immunol. *12*, 662266.

75. Wang, P., Gamero, A.M., and Jensen, L.E. (2019). *IL-36* promotes antiviral immunity by boosting sensitivity to $IFN-\alpha/\beta$ in *IRF1* dependent and independent manners. Nat. Commun. *10*, 1–17.

76. Moura, A.E., Shreves, K., Pilot, M., Andrews, K.R., Moore, D.M., Kishida, T., Möller, L., Natoli, A., Gaspari, S., McGowen, M., et al. (2020). Phylogenomics of the genus *Tursiops* and closely related Delphininae reveals extensive reticulation among lineages and provides inference about eco-evolutionary drivers. Mol. Phylogenet. Evol. *146*, 106756.

77. Herzing, D.L., and Elliser, C.R. (2013). Directionality of Sexual Activities During Mixed-Species Encounters between Atlantic Spotted Dolphins (*Stenella frontalis*) and Bottlenose Dolphins (*Tursiops truncatus*). Int. J. Comp. Psychol. *26*.

78. Guo, W., Sun, D., Cao, Y., Xiao, L., Huang, X., Ren, W., Xu, S., and Yang, G. (2021). Extensive Interspecific Gene Flow Shaped Complex Evolutionary History and Underestimated Species Diversity in Rapidly Radiated Dolphins. J. Mamm. Evol. *29*, 353–367.

79. Mozūraitis, R., Hajkazemian, M., Zawada, J.W., Szymczak, J., Pålsson, K., Sekar, V., Biryukova, I., Friedländer, M.R., Koekemoer, L.L., Baird, J.K., et al. (2020). Male swarming aggregation pheromones increase female attraction and mating success among multiple African malaria vector mosquito species. Nat. Ecol. Evol. *4*, 1395–1401.

80. Grau-Bové, X., Lucas, E., Pipini, D., Rippon, E., van 't Hof, A.E., Constant, E., Dadzie, S., Egyir-Yawson, A., Essandoh, J., Chabi, J., et al. (2021). Resistance to pirimiphos-methyl in West African *Anopheles* is spreading via duplication and introgression of the Ace1 locus. PLoS Genet. *17*, e1009253.

81. Grau-Bové, X., Tomlinson, S., O'Reilly, A.O., Harding, N.J., Miles, A., Kwiatkowski, D., Donnelly, M.J., and Weetman, D.; Anopheles gambiae 1000 Genomes Consortium (2020). Evolution of the Insecticide Target Rdl in African *Anopheles* Is Driven by Interspecific and Interkaryotypic Introgression. Mol. Biol. Evol. *37*, 2900–2917.

82. Altae-Tran, H., Kannan, S., Demircioglu, F.E., Oshiro, R., Nety, S.P., McKay, L.J., Dlakić, M., Inskeep, W.P., Makarova, K.S., Macrae, R.K., et al. (2021). The widespread IS200/IS605 transposon family encodes diverse programmable RNA-guided endonucleases. Science *374*, 57–65.

83. Escudero, J.A., Nivina, A., Kemble, H.E., Loot, C., Tenaillon, O., and Mazel, D. (2020). Primary and promiscuous functions coexist during evolutionary innovation through whole protein domain acquisitions. Elife *9*, e58061.

84. O'Brien, S.J. (1995). Genomic prospecting. Nat. Med. *1*, 742–744.

85. Rivers, N.M., Butlin, R.K., and Altringham, J.D. (2005). Genetic population structure of Natterer's bats explained by mating at swarming sites and philopatry. Mol. Ecol. *14*, 4299–4312.

86. Curti, J.N., Fraser, D., Escalona, M., Fairbairn, C.W., Sacco, S., Sahasrabudhe, R., Nguyen, O., Seligmann, W., Sudmant, P.H., Toffelmier, E., et al. (2023). A genome assembly of the Yuma myotis bat, Myotis yumanensis. J. Hered. esad053.

87. Martin, S.H., Davey, J.W., and Jiggins, C.D. (2015). Evaluating the Use of ABBA–BABA Statistics to Locate Introgressed Loci. Mol. Biol. Evol. *32*, 244–257.

88. Pease, J.B., and Hahn, M.W. (2015). Detection and Polarization of Introgression in a Five-Taxon Phylogeny. Syst. Biol. *64*, 651–662.

89. Laine, V.N., Sävilammi, T., Wahlberg, N., Meramo, K., Ossa, G., Johnson, J.S., Blomberg, A.S., Yeszhanov, A.B., Yung, V., Paterson, S., and Lilley, T.M. (2023). Whole-genome Analysis Reveals Contrasting Relationships Among Nuclear and Mitochondrial Genomes Between Three Sympatric Bat Species. Genome Biol. Evol. *15*, evac175.

90. Krueger, F. (2015). Trim Galore!: A Wrapper Around Cutadapt and FastQC to Consistently Apply Adapter and Quality Trimming to FastQ Files, with Extra Functionality for RRBS Data (Babraham Institute).

91. Li, H., and Durbin, R. (2009). Fast and accurate short read alignment with Burrows–Wheeler transform. Bioinformatics *25*, 1754–1760.

92. Li, H. (2013). Aligning sequence reads, clone sequences and assembly contigs with BWA-MEM. Preprint at arXiv.

93. García-Alcalde, F., Okonechnikov, K., Carbonell, J., Cruz, L.M., Götz, S., Tarazona, S., Dopazo, J., Meyer, T.F., and Conesa, A. (2012). Qualimap: evaluating next-generation sequencing alignment data. Bioinformatics *28*, 2678–2679.

94. Li, H., Handsaker, B., Wysoker, A., Fennell, T., Ruan, J., Homer, N., Marth, G., Abecasis, G., and Durbin, R.; 1000 Genome Project Data Processing Subgroup (2009). The sequence alignment/map format and SAMtools. Bioinformatics *25*, 2078–2079.

95. McKenna, A., Hanna, M., Banks, E., Sivachenko, A., Cibulskis, K., Kernytsky, A., Garimella, K., Altshuler, D., Gabriel, S., Daly, M., and DePristo, M.A. (2010). The Genome Analysis Toolkit: a MapReduce framework for analyzing next-generation DNA sequencing data. Genome Res. *20*, 1297–1303.

96. DePristo, M.A., Banks, E., Poplin, R., Garimella, K.V., Maguire, J.R., Hartl, C., Philippakis, A.A., del Angel, G., Rivas, M.A., Hanna, M., et al. (2011). A framework for variation discovery and genotyping using next-generation DNA sequencing data. Nat. Genet. *43*, 491–498.

97. Poplin, R., Ruano-Rubio, V., DePristo, M.A., Fennell, T.J., Carneiro, M.O., Van der Auwera, G.A., Kling, D.E., Gauthier, L.D., Levy-Moonshine, A., Roazen, D., et al. (2017). Scaling accurate genetic variant discovery to tens of thousands of samples. Preprint at bioRxiv.

98. Van der Auwera, G.A., Carneiro, M.O., Hartl, C., Poplin, R., Del Angel, G., Levy-Moonshine, A., Jordan, T., Shakir, K., Roazen, D., Thibault, J., et al. (2013). From FastQ data to high confidence variant calls: the Genome Analysis Toolkit best practices pipeline. Current Protocols in Bioinformatics *11*, 11.10.1–11.10.33.

99. Braun, E.L., and Kimball, R.T. (2021). Data types and the phylogeny of Neoaves. Birds *2*, 1–22.

100. Gurevich, A., Saveliev, V., Vyahhi, N., and Tesler, G. (2013). QUAST: quality assessment tool for genome assemblies. Bioinformatics *29*, 1072–1075.

101. Danecek, P., and McCarthy, S.A. (2017). BCFtools/csq: haplotype-aware variant consequences. Bioinformatics *33*, 2037–2039.

102. Danecek, P., Auton, A., Abecasis, G., Albers, C.A., Banks, E., DePristo, M.A., Handsaker, R.E., Lunter, G., Marth, G.T., Sherry, S.T., et al. (2011). The variant call format and VCFtools. Bioinformatics *27*, 2156–2158.

103. Page, A.J., Taylor, B., Delaney, A.J., Soares, J., Seemann, T., Keane, J.A., and Harris, S.R. (2016). SNP-sites: rapid efficient extraction of SNPs from multi-FASTA alignments. Microb. Genom. *2*, e000056.

104. Posada, D. (2003). Using MODELTEST and PAUP* to select a model of nucleotide substitution. In Current Protocols in Bioinformatics (Wiley Online Library). Unit 6.5.

105. Capella-Gutiérrez, S., Silla-Martínez, J.M., and Gabaldón, T. (2009). trimAl: a tool for automated alignment trimming in large-scale phylogenetic analyses. Bioinformatics *25*, 1972–1973.

106. R Core Team (2022). R: A Language and Environment for Statistical Computing.

107. Altschul, S.F., Gish, W., Miller, W., Myers, E.W., and Lipman, D.J. (1990). Basic local alignment search tool. J. Mol. Biol. *215*, 403–410.

108. Larsen, R.J., Larsen, P.A., Genoways, H.H., Catzeflis, F.M., Geluso, K., Kwiecinski, G.G., Pedersen, S.C., Simal, F., and Baker, R.J. (2012). Evolutionary history of Caribbean species of Myotis, with evidence of a third Lesser Antillean endemic. Mamm. Biol. *77*, 124–134.

109. Seim, I., Fang, X., Xiong, Z., Lobanov, A.V., Huang, Z., Ma, S., Feng, Y., Turanov, A.A., Zhu, Y., Lenz, T.L., et al. (2013). Genome analysis reveals insights into physiology and longevity of the Brandt's bat *Myotis brandtii*. Nat. Commun. *4*, 2212.

110. Luo, R., Liu, B., Xie, Y., Li, Z., Huang, W., Yuan, J., He, G., Chen, Y., Pan, Q., Liu, Y., et al. (2012). SOAPdenovo2: an empirically improved memory-efficient short-read de novo assembler. GigaScience *1*, 18.

111. Jebb, D., Foley, N.M., Puechmaille, S.J., and Teeling, E.C. (2017). The complete mitochondrial genome of the Greater Mouse-Eared bat, *Myotis myotis* (Chiroptera: Vespertilionidae). Mitochondrial DNA A DNA Mapp. Seq. Anal. *28*, 347–349.

112. Miller, W., Drautz, D.I., Janecka, J.E., Lesk, A.M., Ratan, A., Tomsho, L.P., Packard, M., Zhang, Y., McClellan, L.R., Qi, J., et al. (2009). The mitochondrial genome sequence of the Tasmanian tiger (*Thylacinus cynocephalus*). Genome Res. *19*, 213–220.

113. Minh, B.Q., Nguyen, M.A.T., and von Haeseler, A. (2013). Ultrafast approximation for phylogenetic bootstrap. Mol. Biol. Evol. *30*, 1188–1195.

114. Hoang, D.T., Chernomor, O., von Haeseler, A., Minh, B.Q., and Vinh, L.S. (2018). UFBoot2: Improving the ultrafast bootstrap approximation. Mol. Biol. Evol. *35*, 518–522.

115. Wang, L.-F., Gamage, A.M., Chan, W.O.Y., Hiller, M., and Teeling, E.C. (2021). Decoding bat immunity: the need for a coordinated research approach. Nat. Rev. Immunol. *21*, 269–271.

116. Irving, A.T., Ahn, M., Goh, G., Anderson, D.E., and Wang, L.-F. (2021). Lessons from the host defences of bats, a unique viral reservoir. Nature *589*, 363–370.

117. Afonso, E., Goydadin, A.-C., Giraudoux, P., and Farny, G. (2017). Investigating Hybridization between the Two Sibling Bat Species *Myotis myotis* and *M. blythii* from Guano in a Natural Mixed Maternity Colony. PLoS One *12*, e0170534.

118. Berthier, P., Excoffier, L., and Ruedi, M. (2006). Recurrent replacement of mtDNA and cryptic hybridization between two sibling bat species *Myotis myotis* and *Myotis blythii*. Proc. Biol. Sci. *273*, 3101–3109.

119. Peterson, A.L., and Payseur, B.A. (2021). Sex-specific variation in the genome-wide recombination rate. Genetics *217*, 1–11.

120. Kumar, S., and Subramanian, S. (2002). Mutation rates in mammalian genomes. Proc. Natl. Acad. Sci. USA *99*, 803–808.

121. Posada, D., and Crandall, K.A. (2002). The effect of recombination on the accuracy of phylogeny estimation. J. Mol. Evol. *54*, 396–402.

122. Lemey, P., Salemi, M., and Vandamme, A.-M. (2009). The Phylogenetic Handbook: A Practical Approach to Phylogenetic Analysis and Hypothesis Testing (Cambridge University Press).

123. Schierup, M.H., and Hein, J. (2000). Recombination and the molecular clock. Mol. Biol. Evol. *17*, 1578–1579.

124. Paradis, E., and Schliep, K. (2019). ape 5.0: an environment for modern phylogenetics and evolutionary analyses in R. Bioinformatics *35*, 526–528.

125. Green, R.E., Krause, J., Briggs, A.W., Maricic, T., Stenzel, U., Kircher, M., Patterson, N., Li, H., Zhai, W., Fritz, M.H.-Y., et al. (2010). A draft sequence of the Neandertal genome. Science *328*, 710–722.

126. Zoonomia Consortium (2020). A comparative genomics multitool for scientific discovery and conservation. Nature *587*, 240–245.

127. Szklarczyk, D., Kirsch, R., Koutrouli, M., Nastou, K., Mehryary, F., Hachilif, R., Gable, A.L., Fang, T., Doncheva, N.T., Pyysalo, S., et al. (2023). The STRING database in 2023: protein–protein association networks and functional enrichment analyses for any sequenced genome of interest. Nucleic Acids Res. *51*, D638–D646.

STAR★METHODS

KEY RESOURCES TABLE

REAGENT or RESOURCE	SOURCE	IDENTIFIER
Deposited data		
HLmyoMyo6	Jebb et al.[33]	GCA_014108235.1
Myotis myotis Hi-C data	Jebb et al.[33]	SRR11732436
Myotis myotis ZooFISH map	Volleth et al.[34]	N/A
Myotis yumanensis reference genome	Curti et al.[87]	mMyoYum1.0.hap1
Myotis myotis SRA data	Zoonomia Consortium[88]	SRS3678524
List of differentially expressed genes from a study that treated *Myotis daubentonii* cell lines with a modified Rift Valley Fever virus or supplemented with IFN to measure response to a viral challenge	Holzer et al.[69]	Supplementary Material
WGS phylogenomic data generated in this study	This study	PRJNA1035163
WGS data used to generate *Myotis myotis* recombination map	This study	PRJNA1035163
WGS data used to generate *Myotis brandtii* recombination map	Laine et al.[89]	SRR18788643, SRR18788644, SRR18788646, SRR18788647
Myotis myotis recombination map	This study	https://doi.org/10.5281/zenodo.7044479
Myotis brandtii recombination map	This study	https://doi.org/10.5281/zenodo.7044479
Alignments	This study	https://doi.org/10.5281/zenodo.7044479
Newick Tree files	This study	https://doi.org/10.5281/zenodo.7044479
Software and algorithms		
Trim Galore! v0.6.5	Krueger et al.[90]	https://github.com/FelixKrueger/TrimGalore
bwa-mem v0.7.17	Li et al.[91]; Li[92]	https://github.com/lh3/bwa
Qualimap	Garcia-Alcalde et al.[93]	http://qualimap.conesalab.org/
Samtools v1.9	Li et al.[94]	https://github.com/samtools/samtools
GATK v4.1.2	McKenna et al.[95]; DePriesto et al.[96]; Poplin et al.[97]; Van der Auwera et al.[98]	https://github.com/broadinstitute/gatk
ANGSD v0.916	Korneliussen et al.[56]	http://www.popgen.dk/angsd/index.php/Installation
SOAPdenovo2 vr242	Luo et al.[98]	https://github.com/aquaskyline/SOAPdenovo2
Geneious Prime 2019.04	Dotmatics	https://www.geneious.com/
RYcode	Braun et al.[99]	https://github.com/ebraun68/RYcode)
IQtree2 v2.2.1	Minh et al.[40]	https://github.com/iqtree/iqtree2
Quast v5.2.0	Gurevich et al.[100]	https://github.com/ablab/quast
Bcftools v1.14	Danecek et al.[101]	https://github.com/samtools/bcftools
VCFtools v1.16	Danecek et al.[102]	https://vcftools.sourceforge.net/
ReLERNN	Adrion et al.[52]	https://github.com/kr-colab/ReLERNN
SVDquartets	Chifman and Kubatko[39]	https://paup.phylosolutions.com/
SNP-sites v2.5.1	Page et al.[103]	v2.5.1
PAUP* v4a168	Posada et al.[104]	https://paup.phylosolutions.com/
trimAl v1.4.1	Capella-Gutierrez et al.[105]	https://vicfero.github.io/trimal/
Tree House Explorer (THEx)	Harris et al.[61]	https://github.com/harris-2374/THEx
R v4.2.2	R Core Team[106]	https://www.r-project.org/
f(D)	Martin et al.[87]	https://github.com/simonhmartin/genomics_general

(Continued on next page)

Continued		
REAGENT or RESOURCE	SOURCE	IDENTIFIER
QuIBL	Edelman et al.[41]	https://github.com/miriammiyagi/QuIBL
STRING v12.0	Szklarczyk et al.[87]	https://string-db.org/
Dfoil	Pease and Hahn[88]	https://github.com/jbpease/dfoil
Critical commercial assays		
Qiagen Puregene kit	Qiagen	Cat. No./ID: 158063
NEBNext Ultra II DNA Library Prep Kit for Illumina	New England Biolabs	E7805L
NEBNext Multiplex Oligos for Illumina	New England Biolabs	E7600S

RESOURCE AVAILABILITY

Lead contact
Further information and requests for resources and reagents should be directed to and will be fulfilled by the lead contact, William Murphy (wmurphy@cvm.tamu.edu).

Materials availability
This study did not generate new unique reagents.

Data and code availability
All code used to generate the analysis is publicly available and are cited in the text. All short-read data generated as part of this study have been submitted to the NCBI Short Read Archive under the following BioProject PRJNA1035163. Recombination maps for *M. myotis* and *M. brandtii*, whole-genome SNP datasets used for concatenation and coalescence analyses, a FASTA-formatted version of the updated *M. myotis* genome assembly, and whole-genome alignments are deposited in the following Zenodo repository: https://doi.org/10.5281/zenodo.7044479. The updated *M. myotis* genome assembly can be found under BioProject PRJNA628559.

METHOD DETAILS

Taxonomic sampling and sequencing
We isolated genomic DNA from museum specimens, sampling 58 individual bats, putatively representing 58 individuals and 42 putative Old World *Myotis* species for the ingroup, selected to index the major clades and nodes in the tree.[12] An unknown New World species, *Myotis* spp. (see below), and *Submyotodon latirostris* were also sequenced as outgroup species (Table S1). BLASTn[107] was used to try determine a more specific nomenclature for *Myotis* spp. using the mitogenome and Cyt-b sequences derived from this sample. The top hit for the mitogenome was *Myotis martiniquensis* with 94.6% pairwise identity and 91.81% query coverage. The top hit for the Cyt-b sequence was the GenBank: JN020572, a *Myotis* sp. individual from Suriname which grouped in a clade including *Myotis nyctor* and *Myotis nesopolus* in the following analysis.[108] Pairwise identity was 94.7% and query coverage was 99.91%.

DNA was extracted using the Qiagen Puregene kit following the manufacturer's protocol, except 10μL of linear acrylamide was added to the lysis buffer to aid the recovery of DNA from small starting amounts of tissue. Standard Illumina fragment libraries (300-bp) were prepared for each DNA sample using the NEBNext Ultra II DNA Library Prep Kit for Illumina. Samples were sequenced to ~20× genome-wide depth of coverage with 2 × 150-bp reads on the Illumina HISeq X platform. We combined these data with published genomes from two other bat species: *Myotis brandtii*[109] and *Myotis myotis*.

Sequence QC and read mapping
Raw reads were trimmed using Trim Galore (http://www.bioinformatics.babraham.ac.uk/projects/trim_galore). All but one species of *Myotis* possess a karyotype of 2n = 44, the exception being *Myotis annectans* (2n = 46). G-banding similarities indicate a high degree of collinearity across the genus.[48] All trimmed and filtered reads, using default trimgalore parameters,[90] were mapped to the *Myotis myotis* reference genome, HLmyoMyo6. Sequence alignment was carried out using bwa-mem[91,92] using the -M and -R parameters. Mapping results were evaluated and summarized using the Qualimap function bamqc.[93] Samtools[94] was used to remove duplicate reads. Local realignment and variant calling was performed using GATK.[95–98] Consensus pseudohaploid variants were called for each species using ANGSD[56] where the minimum required mapping quality was 30 and minimum base quality of 20. Short-read Illumina assemblies struggle to accurately resolve highly repetitive and duplicated regions within a genome. This can introduce erroneous variant calls which can confound branch length inference in downstream phylogenomic analyses. To control for this, we also used ANGSD to identify and exclude all alignment regions with read depth greater than 200% of the average coverage per genome and positions with a minimum depth of 5 reads. Average mapped read depth and the proportion of the reference covered by mapped reads was calculated to assess the degree of missing data per species across the genome (Table S2)

Mitogenome assembly and analysis

To avoid incorporating nuclear copies of mitochondrial genes in our mitogenome assemblies, we aimed to sample small subsets of reads to capture only reads belonging to the mitochondria, as nuclear copies of mitochondrial genes would be rare in such small subsets. Random subsets (2, 4, and 8 million) of raw reads were extracted for each sample and trimmed as described above. SOAPdenovo2[110] was used to assemble the mitogenome by evaluating a range of k-mer sizes (71, 81, and 91), with a read length of 150bp and 300bp as the insert size; all other parameters were set to default. Typically, the longest scaffold represented the majority of the assembled mitogenome. The assembly of the highly repetitive D Loop region was incomplete and highly variable across species and so was excluded from further analysis. To orient, annotate and align scaffolds for downstream analyses, each scaffold was mapped to the *M. myotis* mitogenome,[111] with a final alignment of ~17kb. Coding regions were extracted from the mitogenome using Geneious Prime 2019.04. Coding regions were RY coded using RYcode (https://github.com/ebraun68/RYcode)[99] to reduce the potential impact of compositional bias.[112] Alignments were then concatenated to form a single matrix. We prepared a second mitochondrial dataset which included the whole mitogenome, D Loop excluded. For both datasets, a Maximum likelihood (ML) tree was generated using IQtree2[40] under a GTR+I+G4 model of sequence evolution. The tree was evaluated with 1000 bootstrap replicates using the ultrafast bootstrap approximation (Figure S4).[113,114]

Improving the *Myotis myotis* reference genome

The reference genomes for bats described in[33] reported 96–99% of data assembled to 'chromosome-level scaffolds'. However, upon examination of the assembly for key regions like the pseudoautosomal region and the major histocompatibility complex (MHC) locus, we determined that many genic regions were not assembled on chromosomes and would limit downstream inferences. We used two complementary approaches to further improve the completeness of the chromosome-level scaffolds. First, we used the gene annotation and a previously published ZOO-FISH map of human autosomal probes painted on *Myotis myotis* autosomes[34] to predict, based on gene content, which scaffolds in the HLmyoMyo6 assembly corresponded to chromosome paints in the ZOO-FISH map. We re-mapped the original *Myotis myotis* Hi-C (SRR11732436) data to test these predictions and re-scaffolded HLmyoMyo6 (GCA_014108235.1).[33] The Hi-C contact map was visualized using Juicebox.[36] We searched for contacts uniting scaffold associations identified using the gene annotations and ZOO-FISH maps and adjusted the assembly accordingly. This way, more data were assigned to chromosomes, most often to chromosome ends (Figure S2). Differences between the original assembly and the improved version are summarized via Quast[100] in Table S3. Assembling regions with high rates of recombination regions is key to polarizing and accurately interpreting the distribution of phylogenomic signal. Further, we noted that many previously unassigned scaffolds contained immune genes, including the Major Histocompatibility Complex (MHC) and immunoglobin clusters (Figure S1), genomic regions of particular interest given bats' exceptional immunity[115] and role in emerging pathogens.[116] Placing these important genomic regions in the correct genomic context furthers our understanding of the evolution of immune genes in bats.

A recombination map for *Myotis myotis*

We generated a recombination map for *M. myotis* to help interpret the chromosomal distribution of phylogenomic signal in our data. Studies have shown that hybridization occurs between the closely related sister species *M. myotis* and *Myotis blythii*, where they occur in sympatry throughout much of South and Central Europe.[117,118] To avoid bias due to potential genomic introgression between the species, we selected bats from Brittany, north-west France, which occur outside the range of *M. blythii*. Procedures were approved and permits were issued by 'Arrete' by the Prefet du Morbihan. *M. myotis* were sampled in western France, 2013 from three roost locations Ferel (FER), La Roche Bernard (LRB) and Beganne (BEG). Bats were captured in custom harp traps as they left the roost and were placed in individual cloth bags until sampled. A 3mm biopsy punch was obtained from the wing membrane. Samples were flash frozen in liquid nitrogen. Before release all bats were offered food and water. As the recombination landscape of genomes has been shown to vary between different sexes of the same species,[119] we selected samples from two males MMY78 (LRB) and MMY243 (BEG) and one female (MMY4) to construct a sex averaged map.

DNA was extracted, and Illumina libraries were prepared and sequenced as described above. Raw reads were filtered, and mapped to the *M. myotis* reference genome, and the resulting bam files were processed with GATK as before. Variants were called, and all samples were jointly genotyped, then filtered to remove variants in repeatmasked regions using GATK. Variants were further filtered, removing variants within 5bps of an indel and those which did not meet the following quality criteria -e'%QUAL<30 | INFO/DP < 16 | INFO/DP > 62 | QD < 2 | FS > 60 | SOR>10 | ReadPosRankSum <-8 | MQRankSum <-12.5 | MQ < 40' in bcftools (https://github.com/samtools/bcftools).[101] VCFtools (https://vcftools.github.io/man_latest.html) was used to remove indels, leaving 12,273,471 biallelic SNPs (referred to as Mm recombination dataset) for further analysis. ReLERNN, a deep learning approach that uses recurrent neural networks, was used to model the genome-wide recombination rate for *M. myotis*. The average mammalian mutation rate 2.2×10^{-9}[120] was used for this analysis. ReLERNN was run using the simulate, train, predict and bscorrect modules with default settings. Finally, inferred recombination rates were averaged in 2Mb blocks in 50kb sliding windows for use in downstream analyses.

To determine if the *Myotis myotis* recombination landscape was representative of the overall *Myotis* recombination landscape we used the same methods to generate a recombination map for the New World species, *Myotis brandtii*.[89] Publicly available SRA data were mapped to the *Myotis brandtii* pseudohaploid assembly generated as part of this study.

Phylogenomics

Coalescent and concatenation whole-genome phylogenies

SVDquartets[39] was chosen as the coalescence-based species tree approach to satisfy the assumption of no intra-locus recombination under the Multispecies Coalescent model (MSC). Variant sites were used to impute quartet trees which were then aggregated to infer a species tree. Many published coalescence-based analyses have included or been comprised only of protein coding regions or ultraconserved elements, thereby violating the MSC's neutrality assumption. Variable sites were extracted from the per chromosome fasta alignments in vcf format using SNP-sites v2.5.1.[103] Variable sites were thinned to a minimum of 1000bp between sites using VCFtools v1.16[102] and were converted to nexus format using the script vcf2phylip.py (https://github.com/edgardomortiz/vcf2phylip). By using widely spaced variable sites, we aimed to account for the requirement of free recombination between loci, an assumption of coalescent methods like SVDquartets. The dataset was further filtered on missingness, stripping columns from the alignment with more than 10% missingness. While data were initially thinned to a minimum distance of 1000bp apart to avoid intralocus recombination, the final distance between most variable sites is likely much larger. Data from all chromosomes were concatenated using Geneious Prime 2019.04 for a final dataset comprising 1,463,340 SNVs (referred to as the genome-wide SNV dataset). A 50% majority rule tree was estimated using SVDquartets implemented in PAUP* v4a168[104] using the QFM quartet amalgamation technique, sampling 99% of quartets.

The same genome-wide SNV dataset was concatenated into a supermatrix and analyzed with IQtree2 to generate a corresponding ML tree. Given that our nuclear datasets contained variable sites only, we used the +ASC option to correct for ascertainment bias due to the exclusion of constant sites in our analyses. Trees were analyzed as a single partition using a GTR + I + G model of sequence evolution to facilitate the use of the +ASC option. The +ASC option is currently incompatible with more complex mixture models. Trees were evaluated with 1000 bootstrap replicates using the ultrafast bootstrap approximation.[113,114]

Sliding windows

Many phylogenomic studies show that phylogenetic signal is non-randomly distributed throughout the genome. To sample phylogenomic signal, we performed a sliding window-based analysis signal across the 60-species whole genome alignment (referred to as the whole-genome dataset). Alignments were divided into 50-kb nonoverlapping, contiguous windows across the entire genome. Alignment columns were filtered in trimAl[105] using the setting -gt 0.50 to allow only 50% missing data per alignment column and an alignment filtering script (https://github.com/VCMason/Foley2021) with the following parameters: cutoff = 0.02, Z score = 0.5, windsize = 50, step = 1, *Myotis myotis* as the reference and PCcutoff = 50, where an alignment is excluded if one species is missing more than 50% than the total alignment length. After filtering, only windows retaining 10kb or more data were retained for further analysis. Maximum Likelihood locus trees were generated using IQtree2 under a GTR model of sequence evolution and the GHOST model of rate variation (GTR*H4). Trees were evaluated with 1000 bootstrap replicates using the ultrafast bootstrap approximation.[113,114] Relationships for the difficult-to-resolve relationships were summarized in subtrees extracted from the whole-genome dataset (Figure 1; Table S4). Data were visualized using Tree House Explorer (THEx).[61]

Detection of gene flow

Introgression causes phylogenomic distortion.[121,122] In a recent review, Hibbins and Hahn stated, "asymmetry in [the frequencies of] discordant tree topologies is one of the clearest signals of introgression".[55] Following this and other studies,[41,43] we estimated the relative frequency of each topology for the autosomes and X separately. We also investigated the relationship between recombination rate and phylogenomic signal by calculating the frequencies of topologies in high and low recombining regions, defined as 500 windows at either end of the distribution of recombination rates.

Models of rate heterogeneity are fitted to data as part of some tree-building procedures to account for rate variation among sites. Simulations and empirical studies have shown that genome regions subject to introgression have elevated rate heterogeneity due to the accumulation of discordant donor sites in these regions. Potential introgression regions can be identified via the alpha (or shape) parameter, which is estimated as part of fitting gamma models of rate heterogeneity. Alpha parameters are lower in regions of potential introgression as multiple changes are required to account for apparent homoplasy.[122,123] To estimate the alpha parameter per locus, alignments used to generate the 60 species locus trees pruned to represent subtrees (Table S4). As the GHOST model of rate heterogeneity was used to estimate locus trees, we re-ran IQtree2 for alignment loci to fit a gamma model of rate heterogeneity to the data. The alpha parameter, number of parsimony informative sites, and the sum of internal and external branch lengths per locus were extracted from the output using the bash command grep.

The combined effect of introgression and recombination can create local patchworks of phylogenomic histories, resulting in discordant tree topologies and branch lengths. The degree of discordance varies depending on the timing and direction of introgression and the relationship between hybridizing taxa.[55] Introgression between sister taxa will not produce discordant topologies but will result in compressed branch lengths or divergence times. Introgression among non-sister species will create discordant topologies with much older or much younger branch lengths or divergence times depending on the direction and age of the introgression events.[55] As such, we examined the genome-wide distribution of internal branch lengths extracted from quartet topologies using the ape package[124] in R.[106] Given the extreme morphological conservation observed among *Myotis* bats[12] we did not formally estimate divergence times given the difficulty in accurately assigning fossils branches in this phylogeny, particularly in the presence of

gene flow. In lieu of this, we examined the distribution of internal branch lengths to determine the distorting effect of introgression. In a divergence time analysis, the rate of substitution per site is simply scaled to time, thereby reflecting similar information.

Rather than relying solely upon genome-wide tests of introgression,[125] which do not identify specific regions of admixture, we used f (D),[87] which provides a point estimate of the admixture proportion at a given locus. More specifically, given a tree (((p1, p2), p3), O), f (D) describes the quantification of excess shared variation between p2 and p3 that is also not shared with p1. This approach also allows for the possibility of bidirectional introgression on a site-by-site basis. To test for evidence of admixture, we calculated f(D) for trios of species and an outgroup corresponding to the two most frequent introgressed topologies from each clade (Table S5). The whole-genome dataset chromosome alignments were pruned to the trio, and the outgroup and biallelic SNPs were called using SNPsites.[103] f(D) was calculated using scripts from (https://github.com/simonhmartin/genomics_general) following (https://github.com/simonhmartin/tutorials/blob/master/ABBA_BABA_windows/README.md). Introgression was estimated in 10kb windows requiring a minimum of 250 SNPs per window as a cut-off for analysis.

Given that f(D) can underestimate introgression if all three species in the ingroup taxa hybridize, we also used QuIBL[41] to determine to what extent discordance could be explained by ILS and introgression. This approach uses the distribution of internal branch lengths to distinguish between these two processes. Under ILS, internal branch lengths are expected to be exponentially distributed, while internal branches derived from introgressed regions will have a distribution with a non-zero mode.[41] The fit of models where all discordance is due to ILS or a mixture of ILS and introgression are compared via likelihood, and the proportion of trees that best fit either model are returned. Trees were pruned to a trio of focal species and an outgroup and run through QuIBL using default parameters.

To determine if there was a difference in the probability of the admixture between related species based on mating behavior, we estimated D the whole genome statistic used to detect introgression among species, in the form (((H1, H2), H3), O), where O is the outgroup S. latirostris in all cases. Within the Ethiopian Clade, M. bocagei uses a harem-based mating strategy where one male and several females gather in a banana leaf for mating. Conversely, M. emarginatus is frequently reported at swarming sites in Europe. Using subsets of the whole-genome dataset, a suite of whole genome D statistics[125] were calculated in Dfoil[88] using mode = dstat and all other default parameters for all trees shown in Figure 5C which are shown in the format (outgroup, (P1,(P2, P3))). We varied the individual used to represent M. bocagei, the position of species in the tree and varied the third species selected in addition to M. bocagei and M. emarginatus to represent a variety of species which have been found to co-occur with M. emarginatus at swarming sites or are within the Ethiopian clade, but the status of their mating behavior is unknown.

To investigate if our results were impacted by reference bias, we repeated the analysis described above, but instead mapped the data to both the Myotis myotis reference genome and the Myotis yumanensis reference genome (mMyoYum1.0.hap1).[86] As a member of the New World clade, M. yumanensis is roughly equally distant from all Old World species and so could be used to detect any possible bias from using a nested ingroup species as the reference. ABBA-BABA or whole genome D-statistics were estimated using ANGSD[56] for combinations of BAM files resulting in highly similar estimates of D and Z-scores, indicating the negligible impact of reference bias. As such, the remainder of introgression tests were conducted with data mapped to the M. myotis reference genome. To investigate if sampling a different individual from the same species changed our introgression results, we mapped an additional M. myotis individual (NCBI: SRS3678524)[126] and used this individual in our re-analysis. These results also showed negligible differences to our original results (Figures 5C and S25; Table S5).

Hybridization at swarming sites?

Typically swarming is thought to be limited to temperate bat species. However, data on the mating behavior of bats are limited and not widely known in families with large numbers of species. To better investigate this, we performed a literature search and aggregated data from multiple studies reporting species compositions at swarming sites across Europe (Table S7). As before, subtrees corresponding to the species which swarm within and between clades (Figure 5B) were pruned from the 60 species sliding windowed phylogenies derived from analyses of subsets of the whole-genome dataset. The number and frequency of genome-wide topologies were estimated using THEx.[61] Given the observed asymmetry in topology frequencies, introgression was determined to be the most likely source of phylogenomic discordance. To test this, we calculated whole genome D-statistics (Figure 5B) and windowed f(D) statistics (Figure S17) for trios of species and an outgroup corresponding to the two most frequent introgressed topologies using data derived from the whole-genome dataset.

Anti-viral immunity and introgression

Given that immune loci are frequently introgressed among mammals,[66] we sought to determine if genes associated with anti-viral immunity were introgressed in our dataset. Although the interferon pathway is a conserved anti-viral innate immune pathway, most species possess a repertoire of genes adapted for anti-viral defense. Given that standard gene enrichment analyses rely on data and function information for the best-studied model organisms, a traditional enrichment analysis would likely omit Myotis-specific components or features of anti-viral immunity. Therefore we used a custom database of differentially expressed genes from a study that treated Myotis daubentonii cell lines with a modified Rift Valley Fever virus or supplemented with IFN to look at differential gene expression in response to a viral challenge.[70] For our database, we selected all differentially expressed genes with an adjusted p value of 0.005 or less from both treatments after the 6h time point to capture an immediate acute response to viral infection. Of these genes, 731/984 were present in the windows represented by our 50kb sliding windows dataset. The 253 missing genes were likely

removed during the filtering of regions of poor alignment quality or were missing from the gene annotation. To determine if this gene set showed significant overlap with introgressed regions of the genome, defined as windows with a non-species tree topology, we performed a chi-squared test with a Yates correction in R using the native stats package.

Large introgressed haplotype blocks

A large introgressed haplotype block was identified through visual examination of genome-wide phylogenomic signal in THEx for the *bechsteinii* clade on chromosome V15. This corresponded to the topology where *M. myotis* and *M. daubentonii* were sister taxa relative to *M. bechsteinii* (red topology Figure 3C). Genes corresponding to this region were extracted as described previously, and an STRING enrichment analysis[127] was performed choosing human for the database, where FDR > 0.05 was considered significant, and all other parameters as default to determine if any function or pathway was enriched in this region.

Supplemental information

Karyotypic stasis and swarming

influenced the evolution of viral tolerance

in a species-rich bat radiation

Nicole M. Foley, Andrew J. Harris, Kevin R. Bredemeyer, Manuel Ruedi, Sebastien J. Puechmaille, Emma C. Teeling, Michael F. Criscitiello, and William J. Murphy
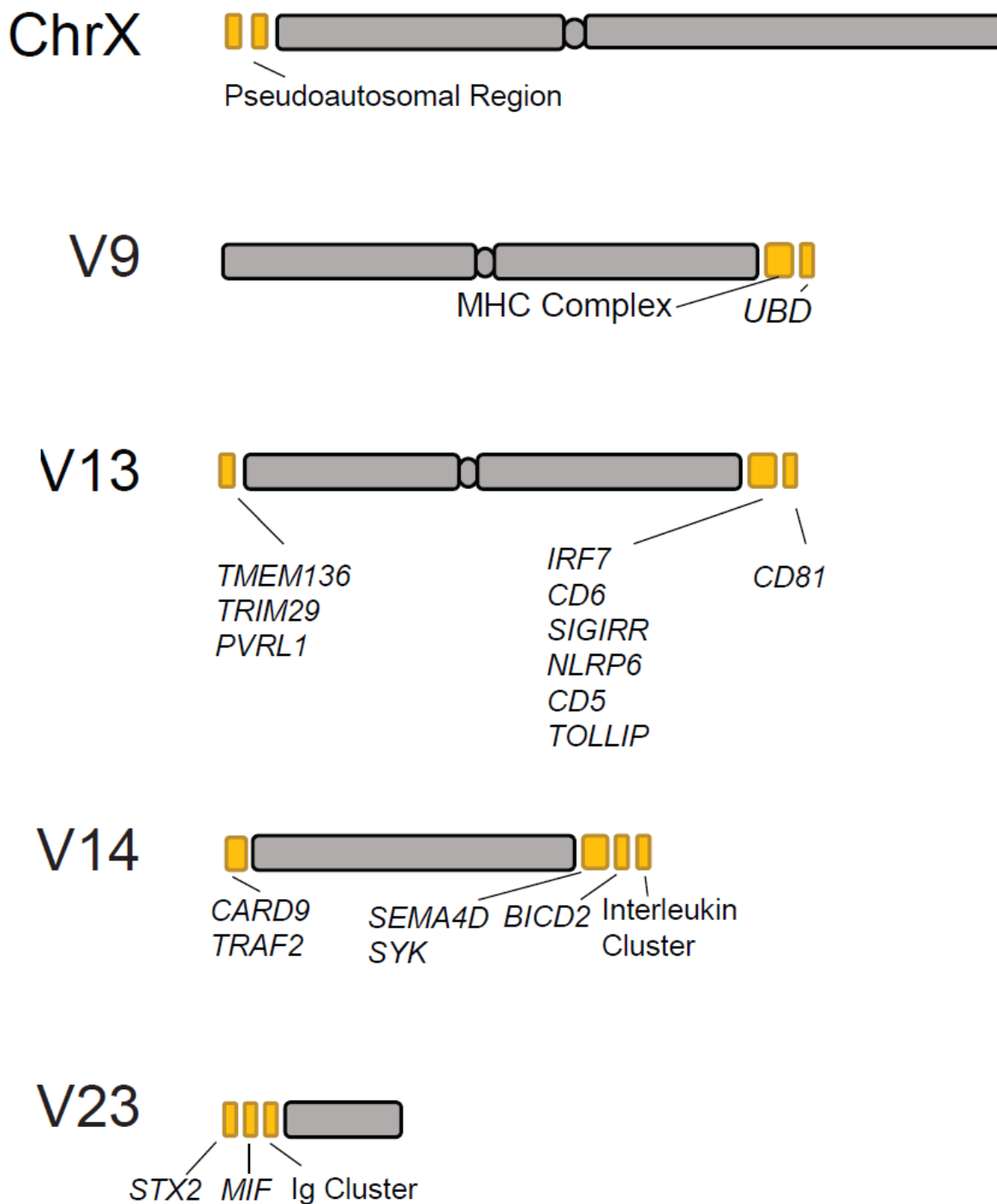
Figure S1: Previously unplaced assembly scaffolds contained many immune-related genes, related to the improved *Myotis myotis* genome assembly analyzed in Figure 2. Gray blocks depict the original chromosome-scale scaffolds from the original assembly (GCA_014108235.1). Yellow blocks represent unplaced scaffolds currently assigned to chromosomes. The yellow blocks are not drawn to scale.
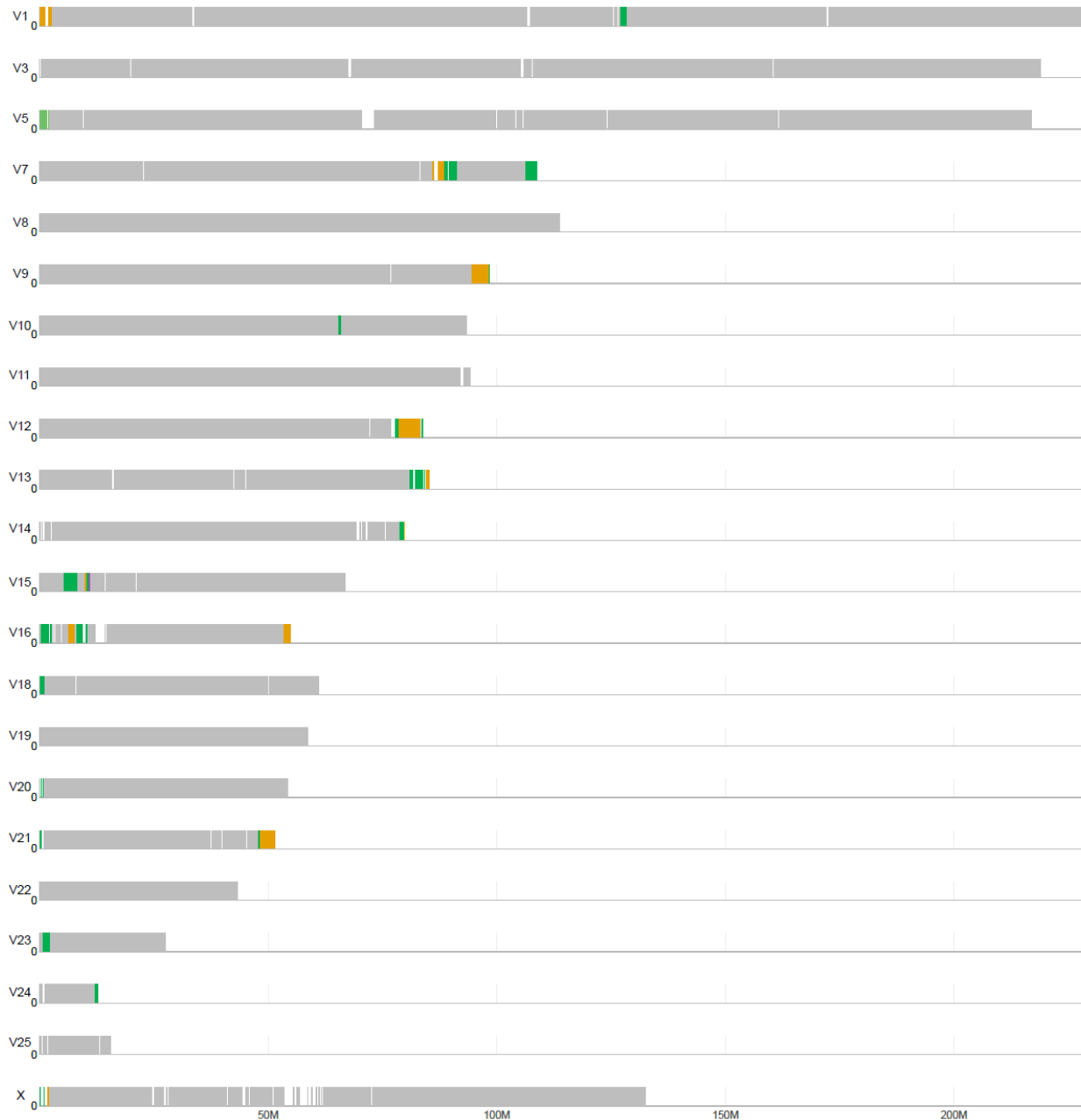
Figure S2: Most unplaced scaffolds were added to the terminal ends of chromosomes, related to the improved *Myotis myotis* genome analyzed in Figure 2. Portions of chromosomes colored gray represents the chromosome level scaffolds from the original assembly [S1]. Green and orange blocks, alternated to highlight where multiple scaffolds were added to the same region, illustrate where previously unplaced scaffolds were positioned in the new assembly based on Hi-C analysis and visualization in JBAT. All blocks and chromosomes are shown to scale. White spaces in blocks correspond to regions that were unassembled or removed due to missing data or poor alignment quality in the sliding window analysis.

2
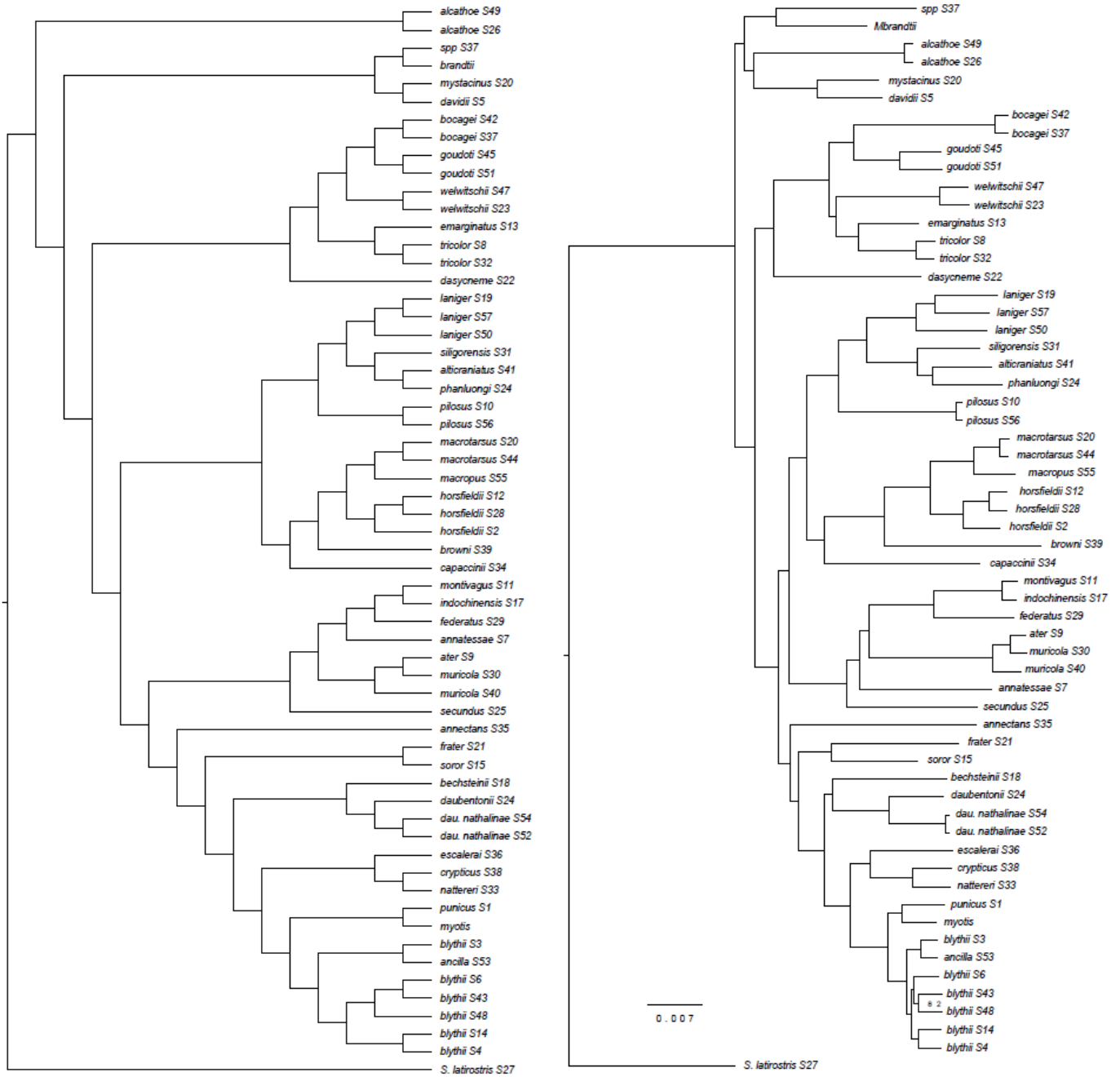
Figure S3: Whole genome nuclear topologies with all 60 individuals, related to Figure 1.
The tree on the left is the 50% Majority Rule tree derived from the SVDquartets analysis. The rightmost tree is the IQtree2 Maximum Likelihood with branch lengths. All bootstrap supports are 100 unless otherwise indicated.

3
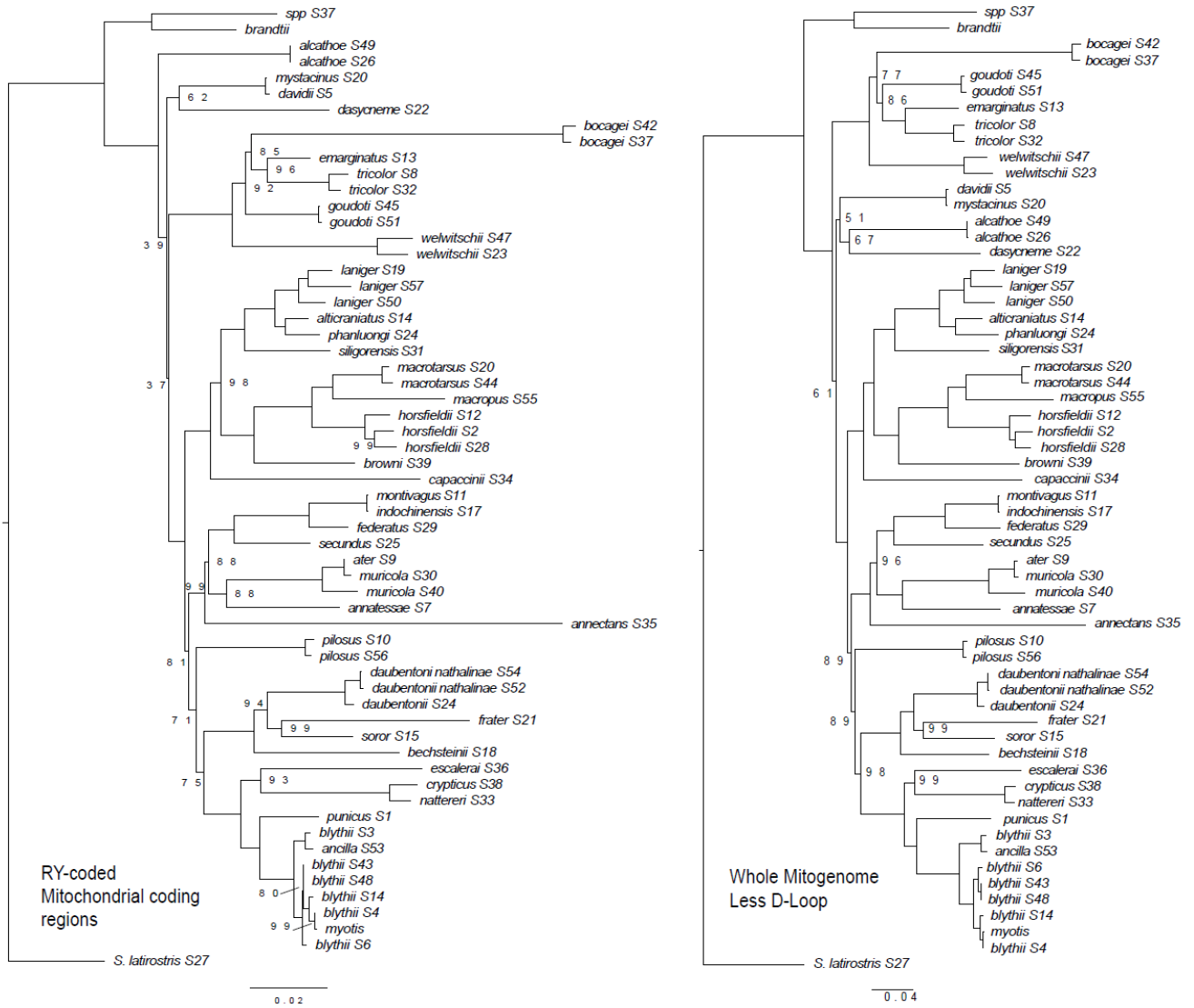
Figure S4: Mitogenome topologies with all 60 individuals, related to Figure 1. The tree on the left is RY-coded dataset. The tree on the right is the whole mitogenome with the D-Loop removed. All bootstrap supports are 100 unless otherwise indicated.

4
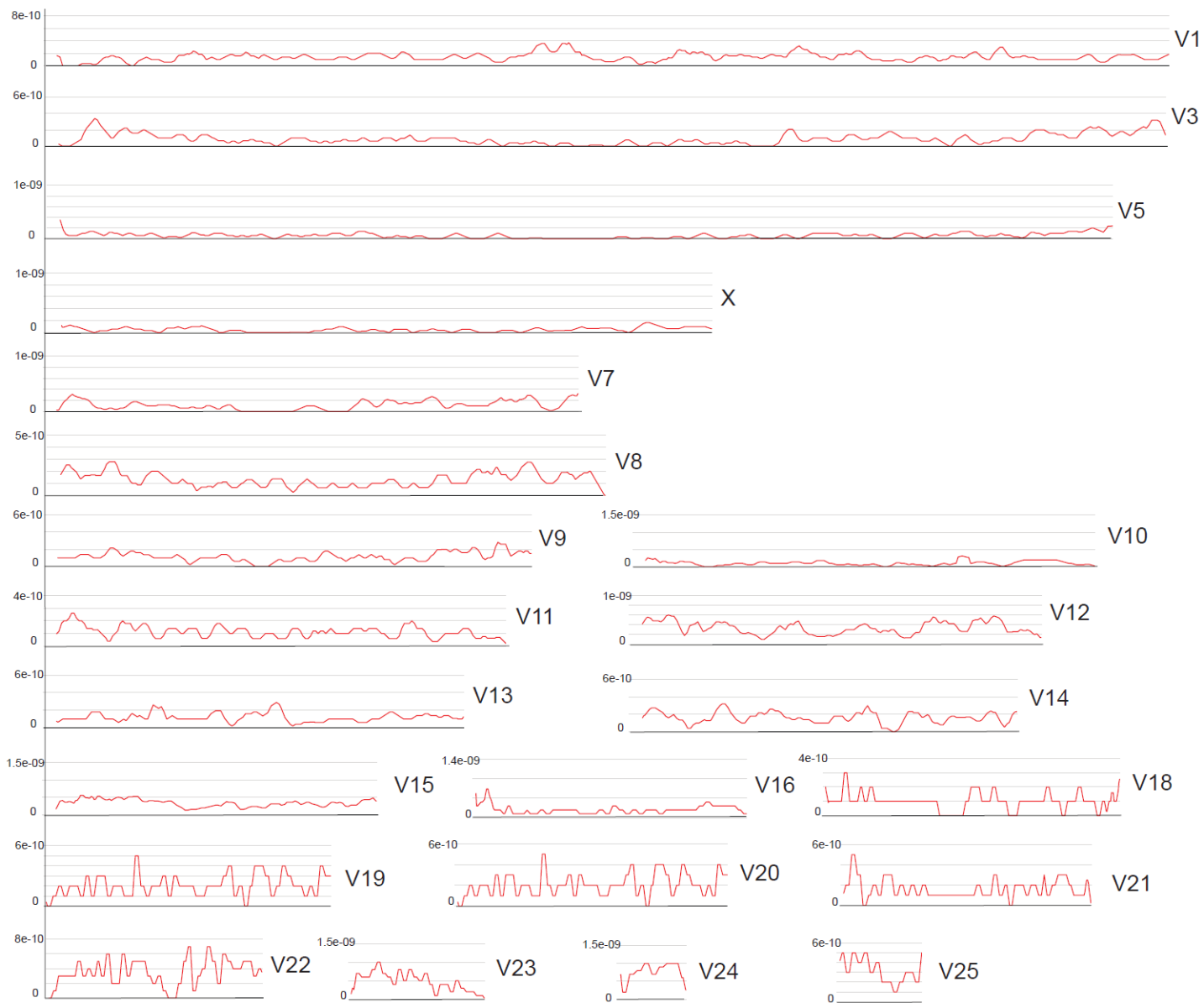
Figure S5.
***Myotis myotis* recombination map, related to Figure 2.** Genome-wide distribution of recombination rates inferred using ReLERNN. Rates are averaged every 2Mb in 50kb sliding windows. For illustrative purposes V1-V15 and chrX are displayed using a sliding average with a step of 50. Chromosomes V16-V25 are displayed using a sliding average with a step of 10.
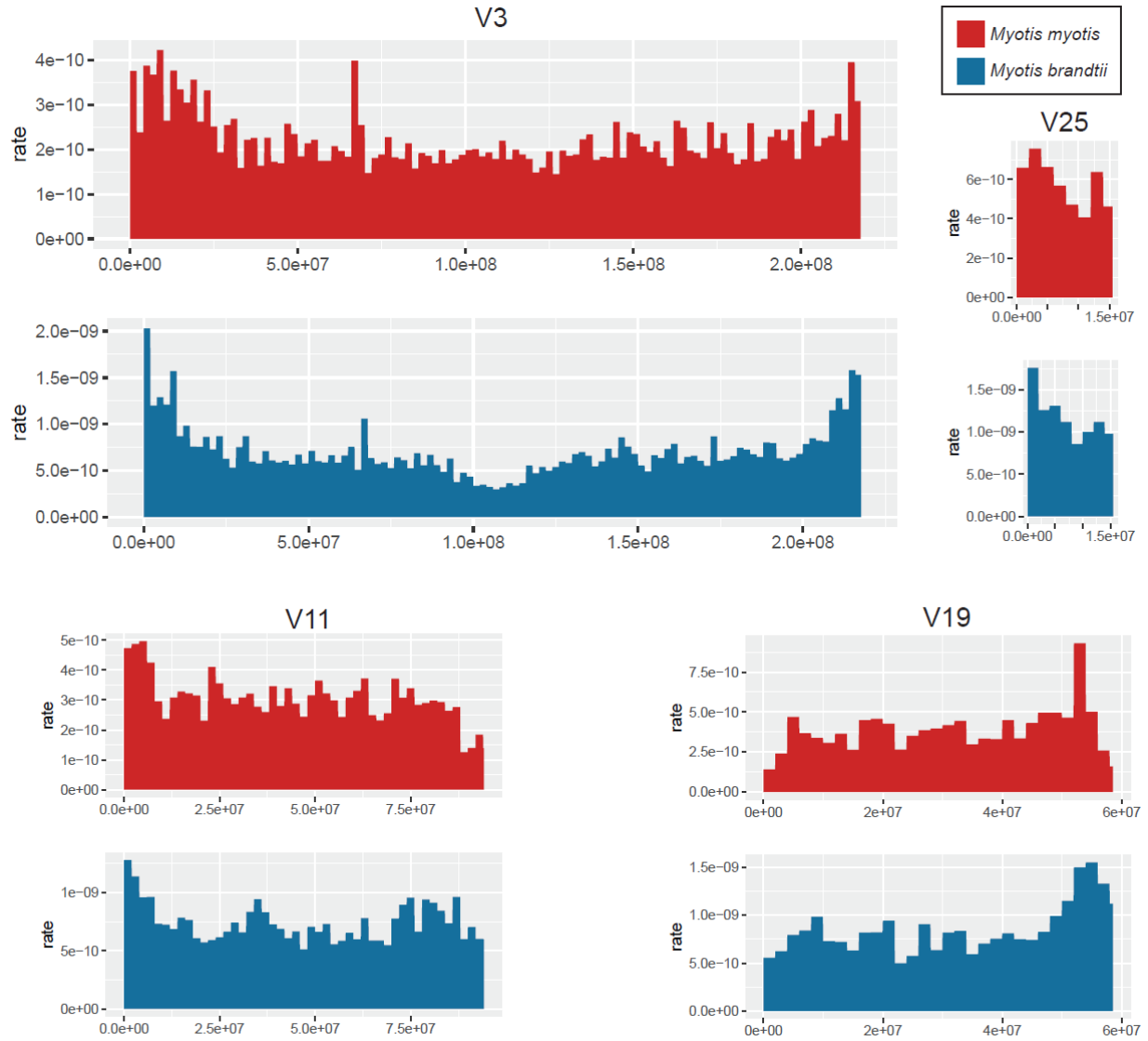
Figure S6: Comparison of select chromosomes from *M. myotis* and *M. brandtii* recombination maps, related to Figure 2.
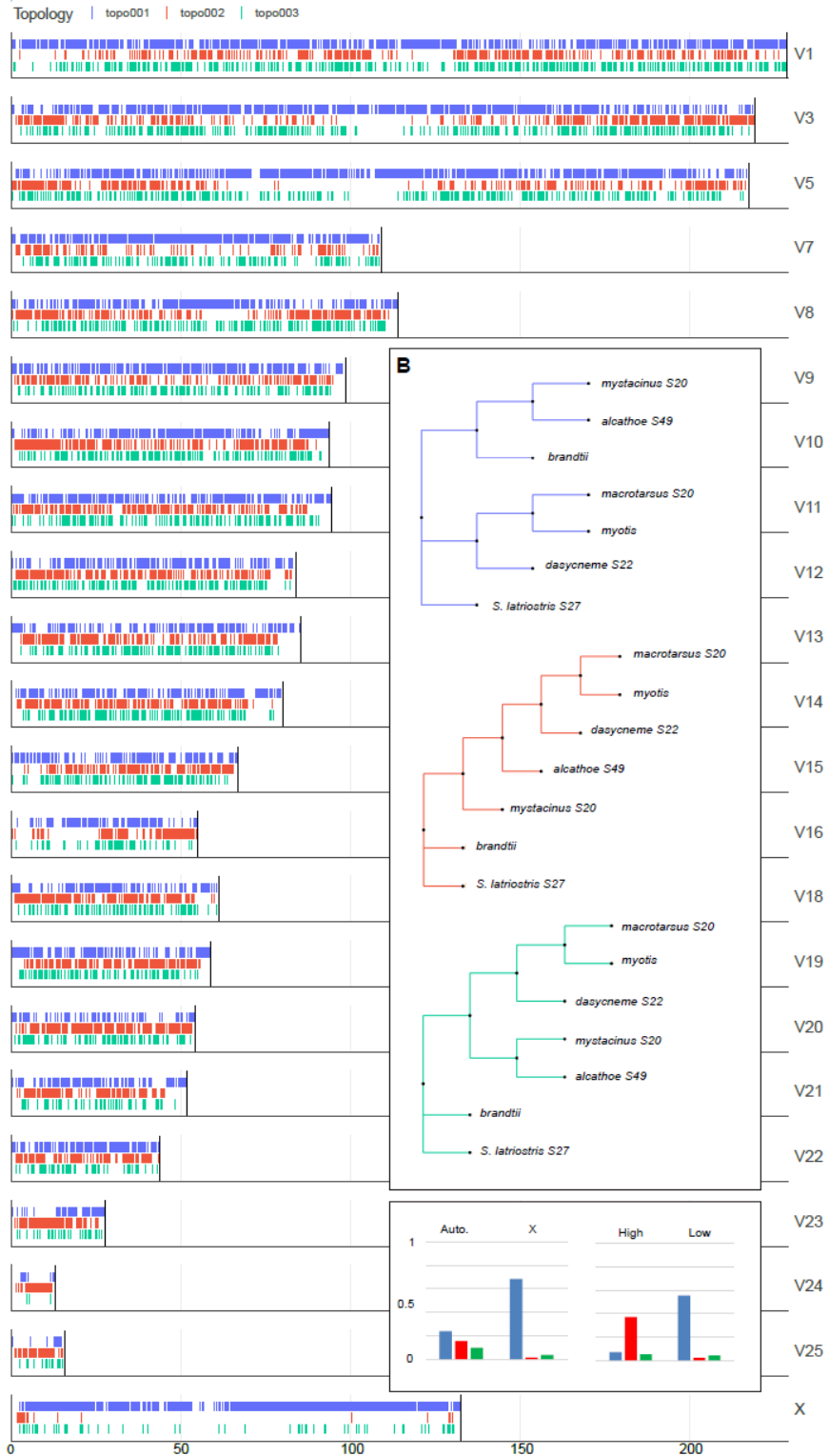
Figure S7: Genome-wide phylogenomic signal to determine the position of the whiskered bat clade, related to Figure 3. A) Genome-wide distribution of topologies shown in B). C) shows the frequency of each topology on the autosomes and X and in high and low recombining regions.
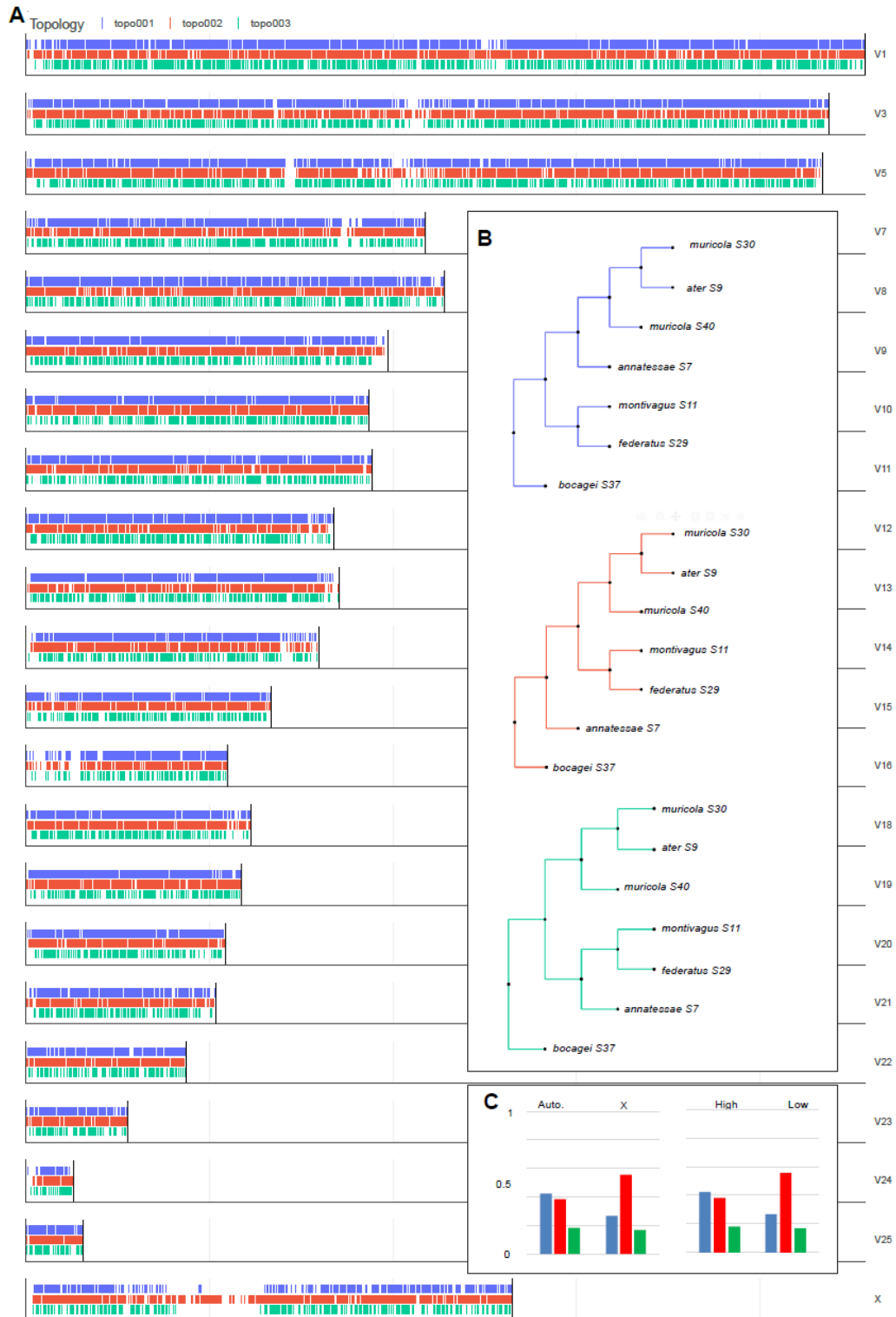
Figure S8: Genome-wide phylogenomic signal to determine the position of *M. annatessae*, related to Figure 3. A) Genome-wide distribution of topologies shown in B). C) shows the frequency of each topology on the autosomes and X and in high and low recombining regions.
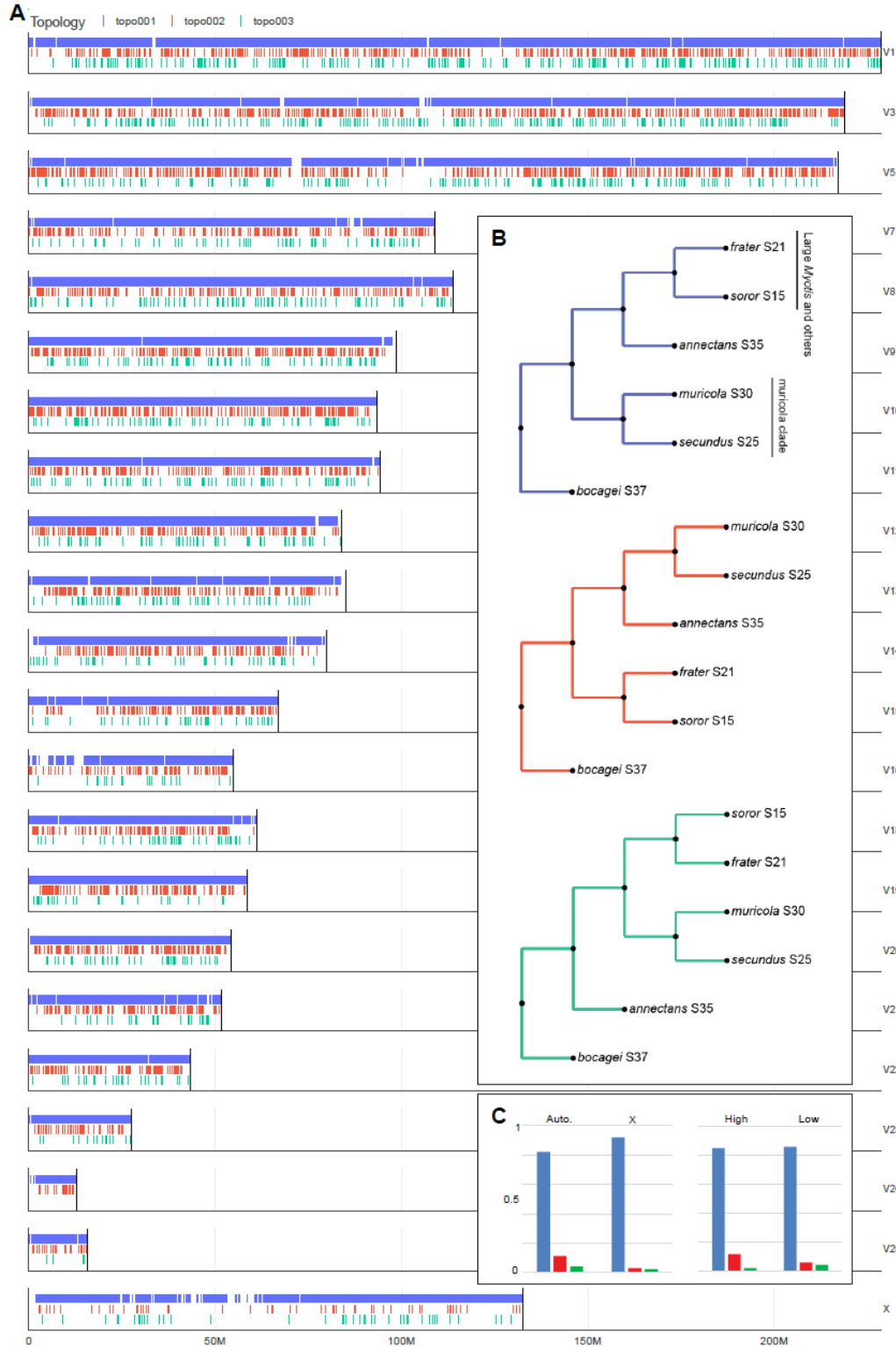
Figure S9: Genome-wide phylogenomic signal to determine the position of *M. annectans*, related to Figure 3. A) Genome-wide distribution of topologies shown in B). C) shows the frequency of each topology on the autosomes and X and in high and low recombining regions.
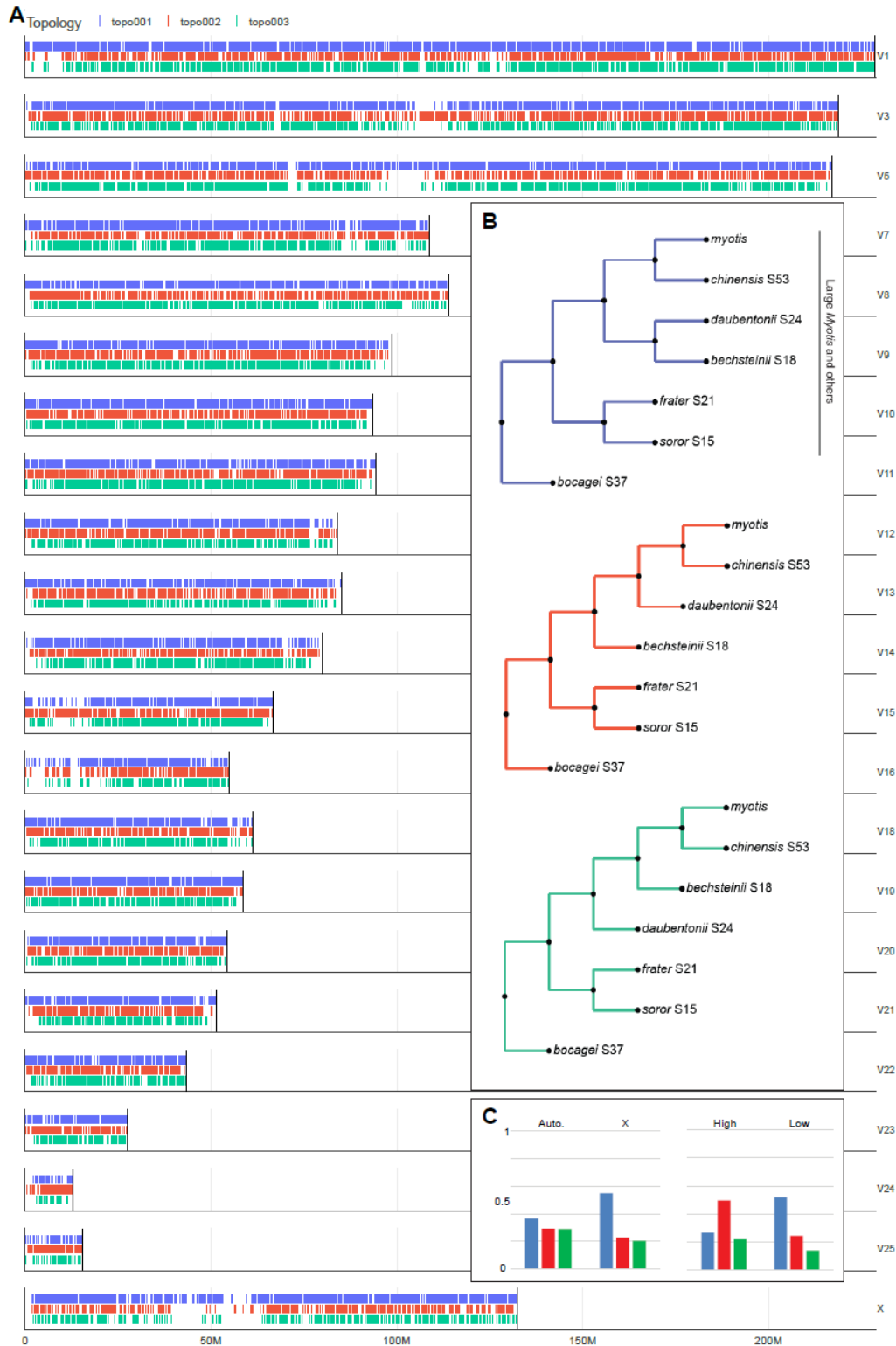
Figure S10: Genome-wide phylogenomic signal to determine the position of *M. bechsteinii*, related to Figure 3. A) Genome-wide distribution of topologies shown in B). C) shows the frequency of each topology on the autosomes and X and in high and low recombining regions.
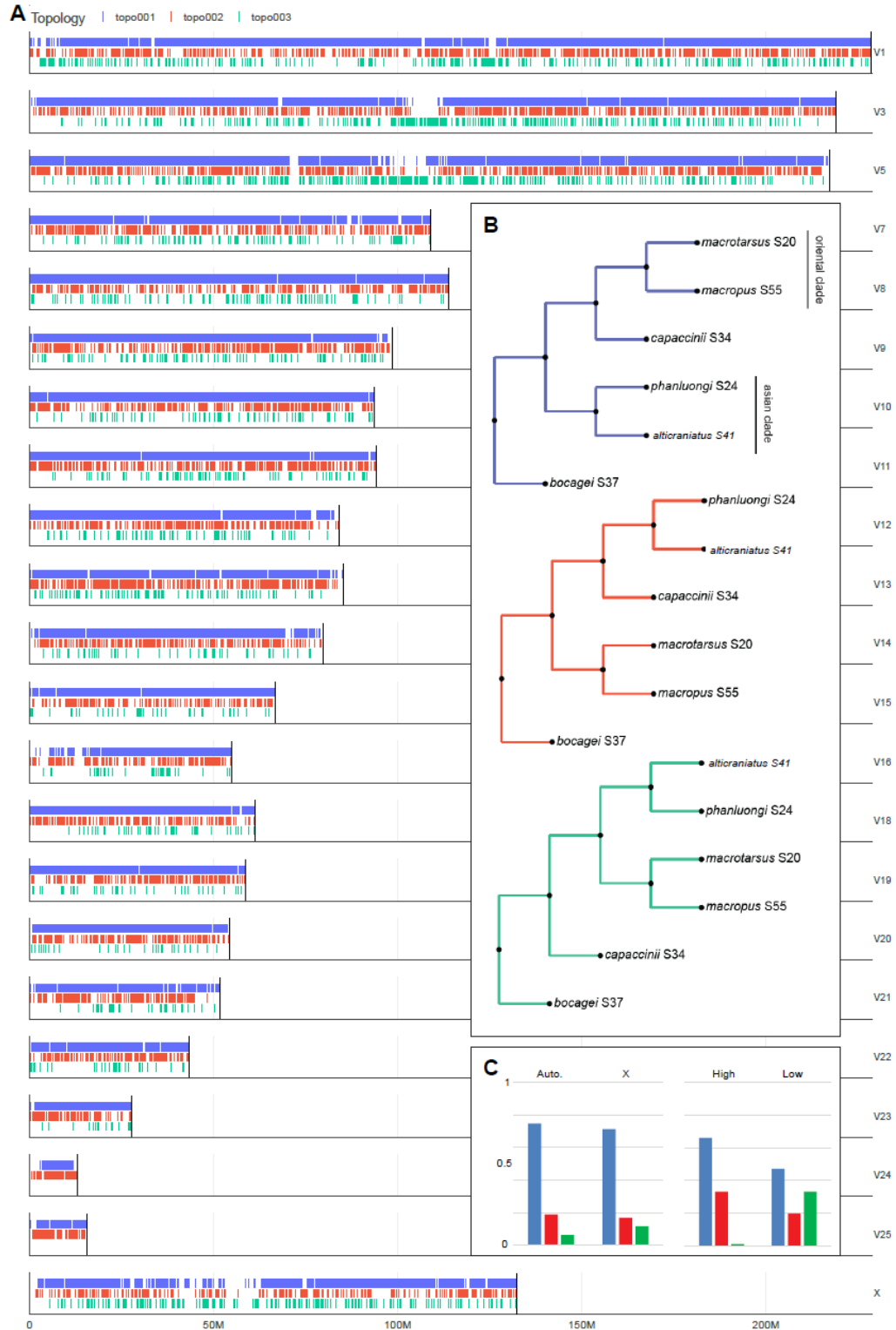
Figure S11: Genome-wide phylogenomic signal to determine the position of *M. capaccinii*, related to Figure 3. A) Genome-wide distribution of topologies shown in B). C) shows the frequency of each topology on the autosomes and X and in high and low recombining regions.
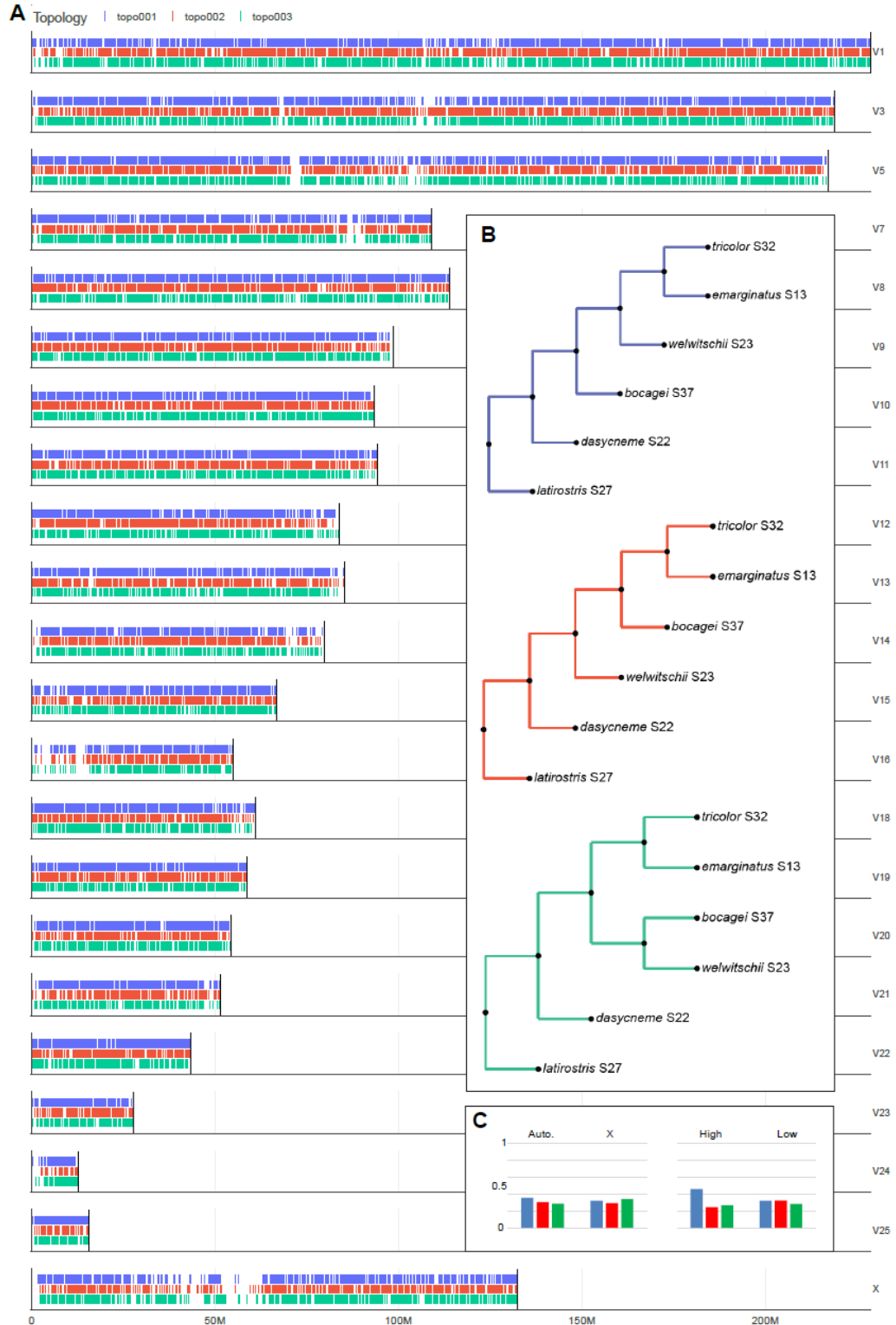
Figure S12: Genome-wide phylogenomic signal to determine the relationships among species in the Ethiopian clade, related to Figure 3. A) Genome-wide distribution of topologies shown in B). C) shows the frequency of each topology on the autosomes and X and in high and low recombining regions.

12
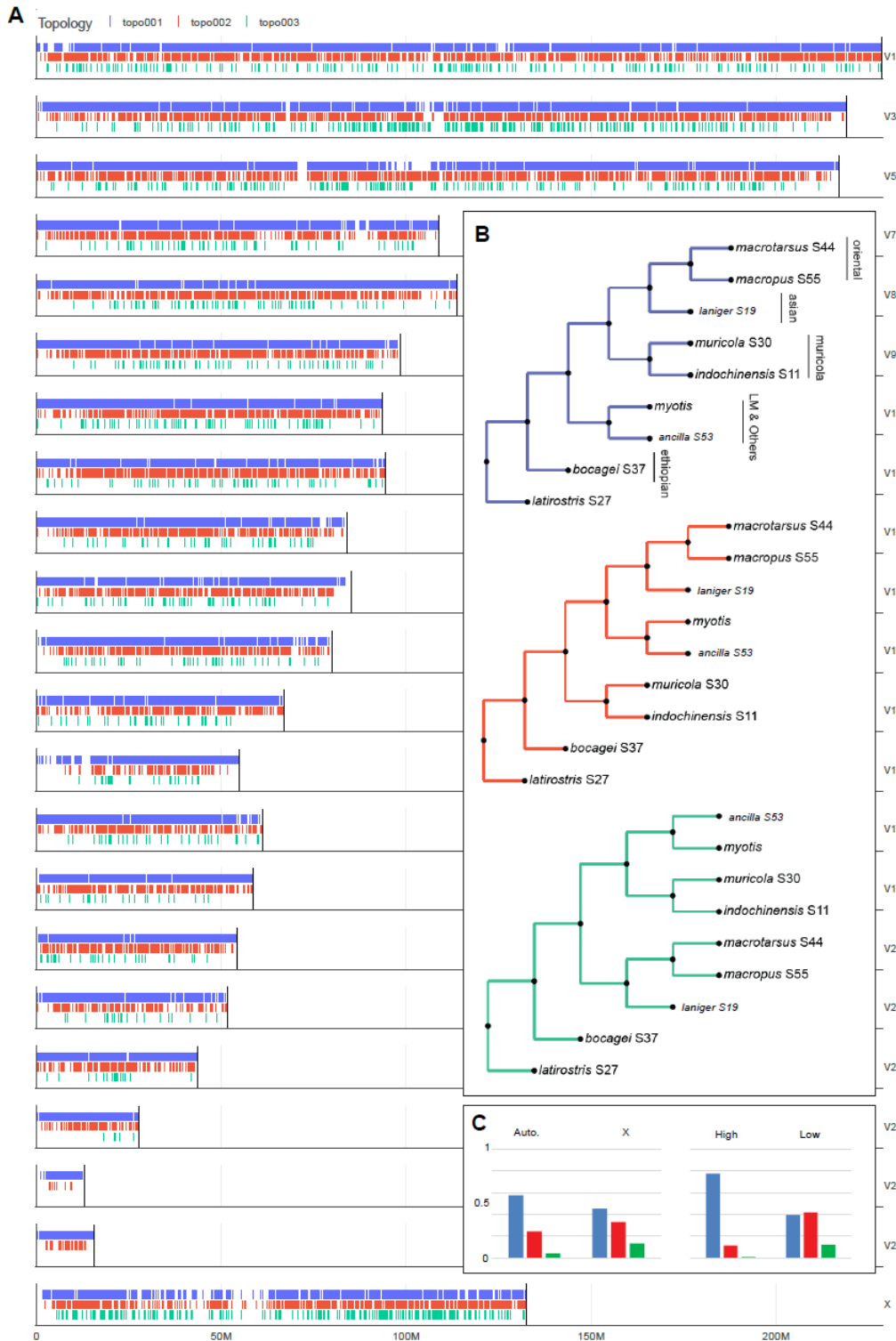
Figure S13: Genome-wide phylogenomic signal to determine the relationships among the major Old World Clades, related to Figure 3. A) Genome-wide distribution of topologies shown in B). C) shows the frequency of each topology on the autosomes and X and in high and low recombining regions.

13
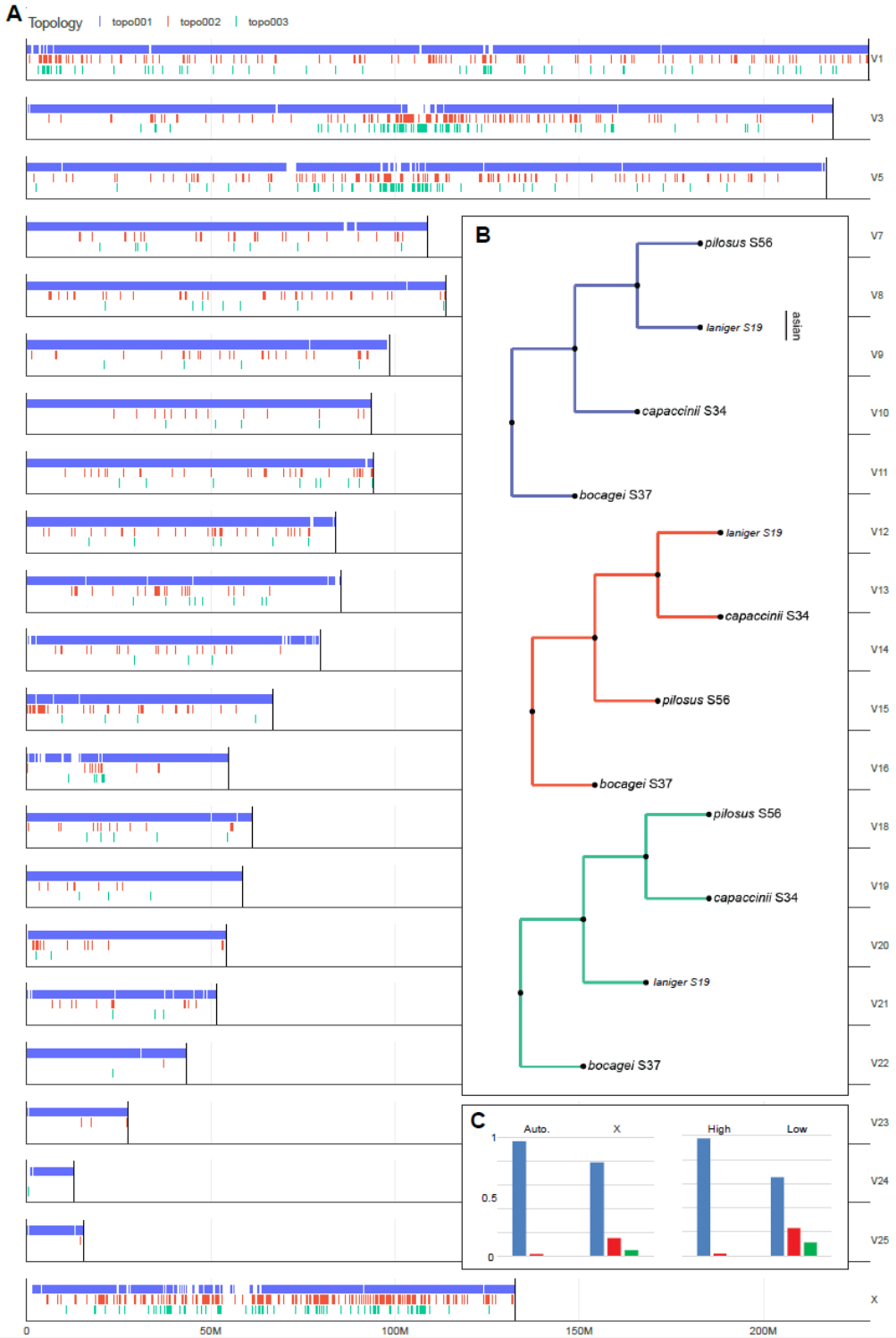
Figure S14: Genome-wide phylogenomic signal to determine the relationship between *M. pilosus, M. capaccinii* and *M. laniger*, related to Figure 3. A) Genome-wide distribution of topologies shown in B). C) shows the frequency of each topology on the autosomes and X and in high and low recombining regions.

14
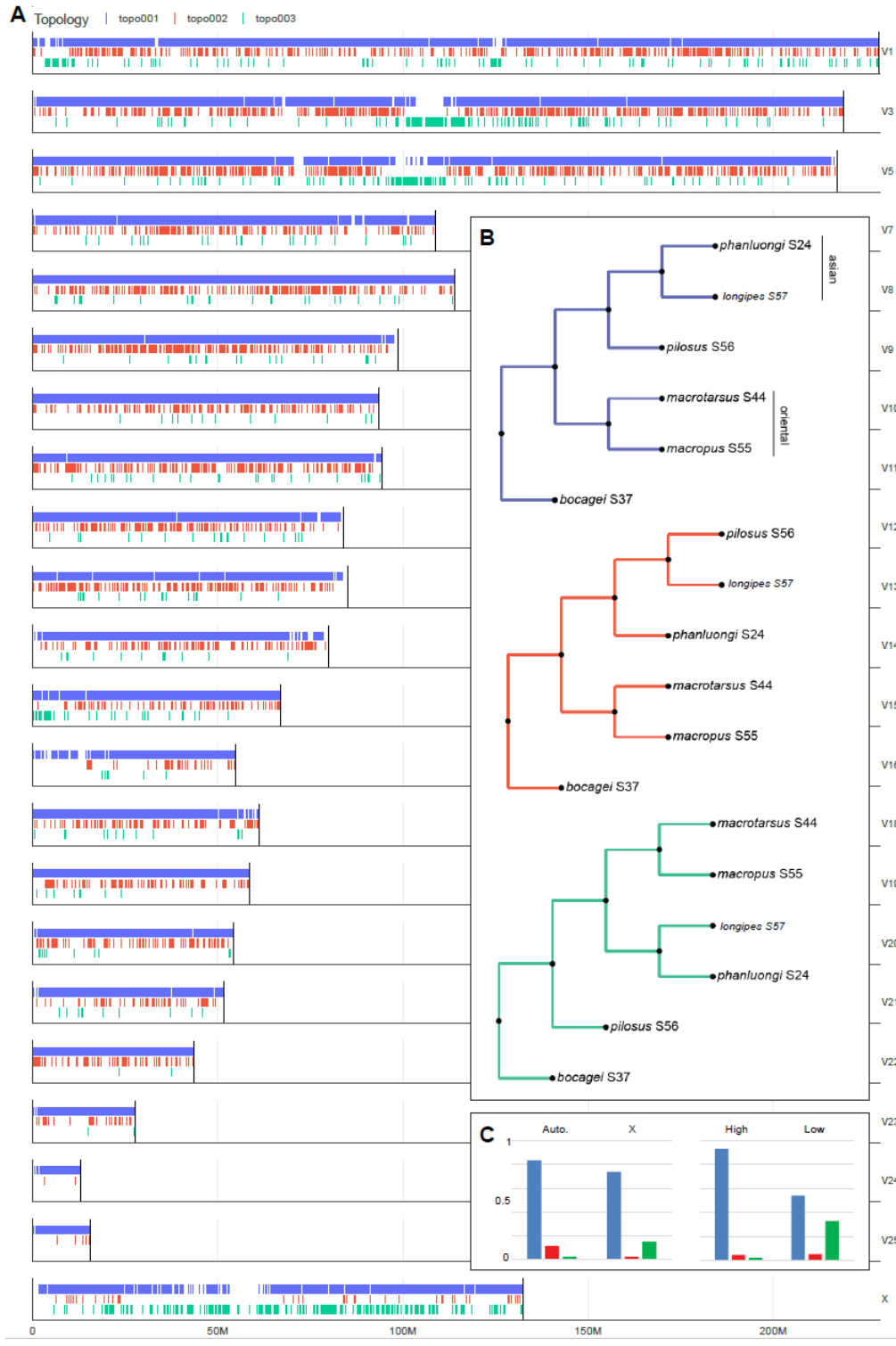
Figure S15: Genome-wide phylogenomic signal to determine the position of *M. pilosus*, related to Figure 3. A) Genome-wide distribution of topologies shown in B). C) shows the frequency of each topology on the autosomes and X and in high and low recombining regions.
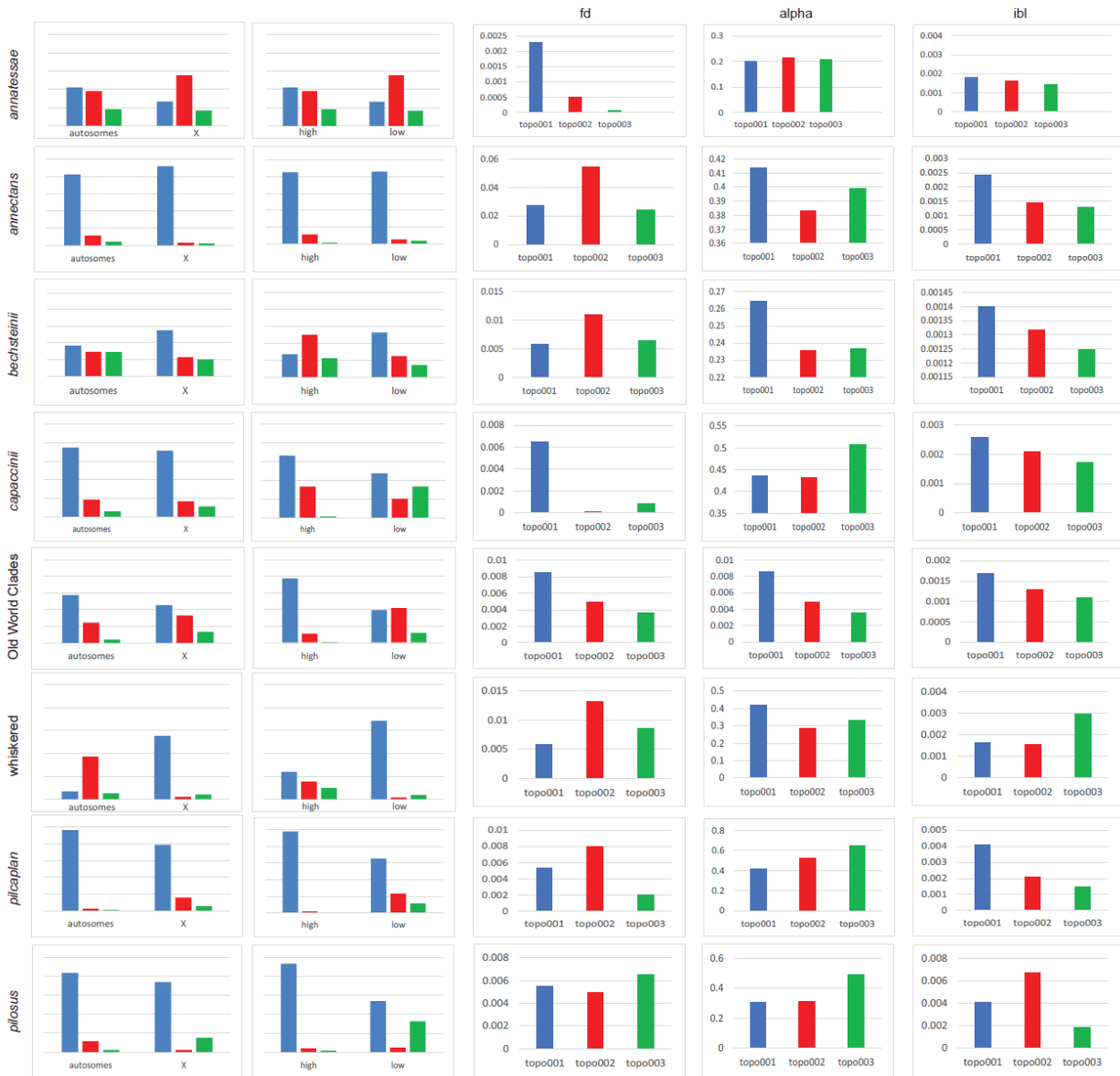
Figure S16: Phylogenomic discordance, related to Figure 3. Topological frequency is calculated comparing the Autosomes and X and comparing low and high recombining regions. Average values of f(*D*), alpha and ibl per clade.
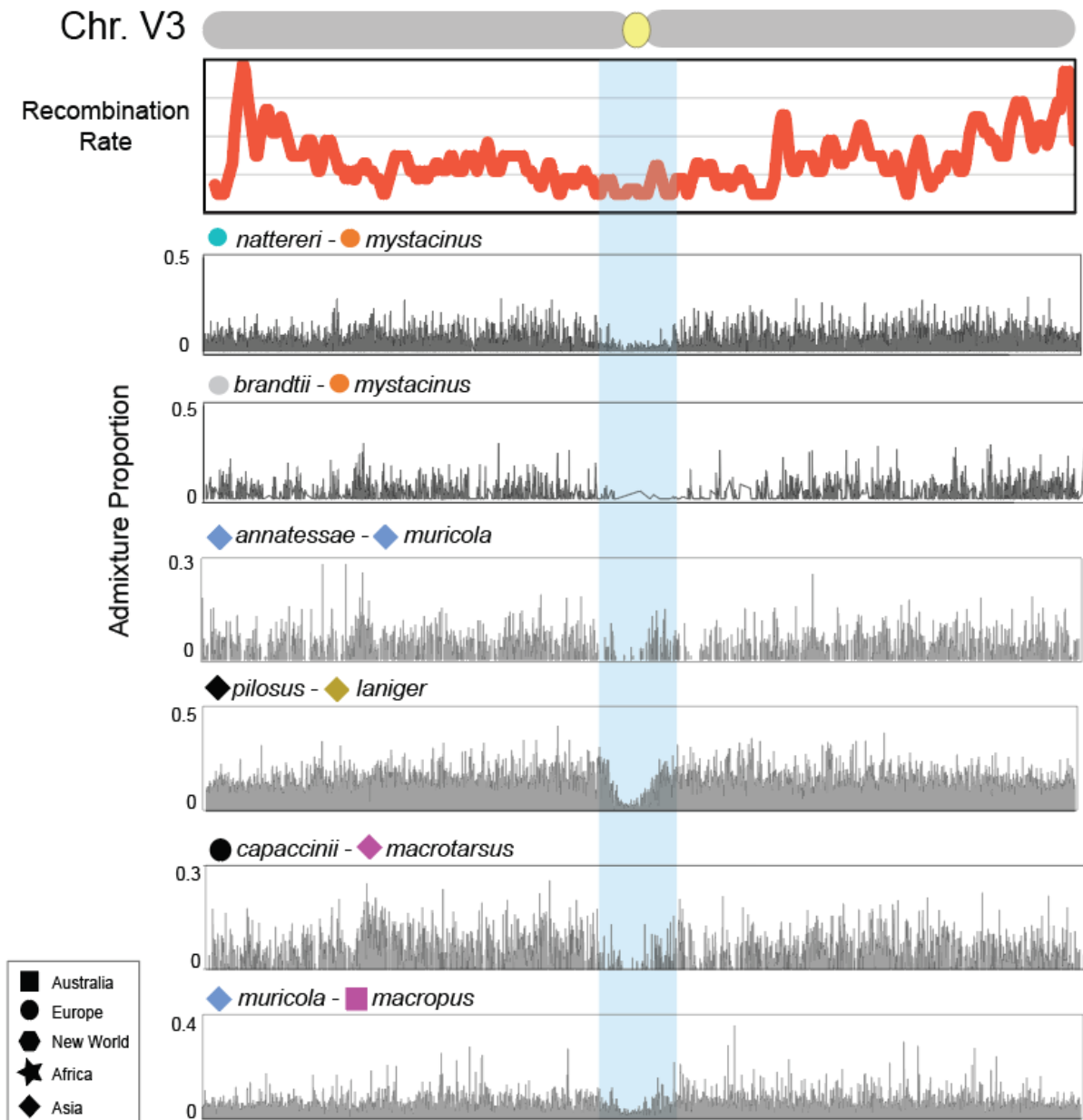
Figure S17: The f(*D*) statistic calculated across chromosome V3 for various species pairs, related to Figure 4. Introgression is evident along chromosome arms while low recombining pericentromeric regions are relatively devoid of signal consistent with introgression.
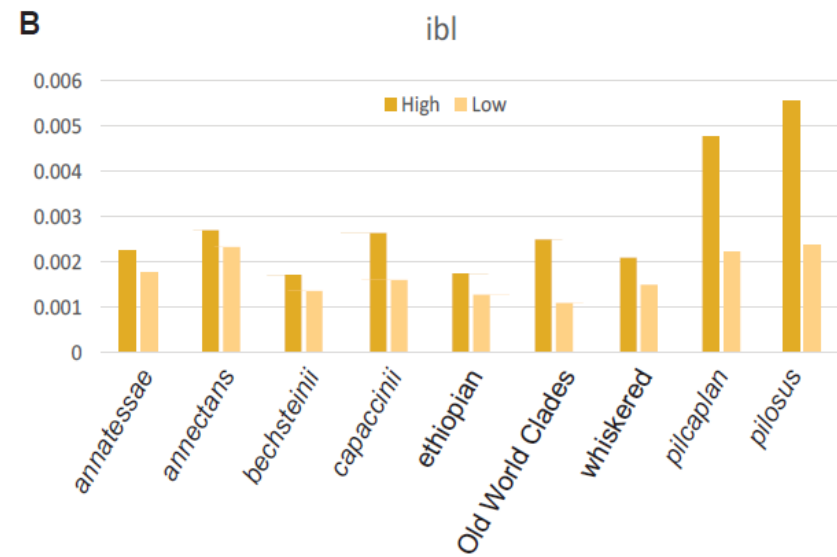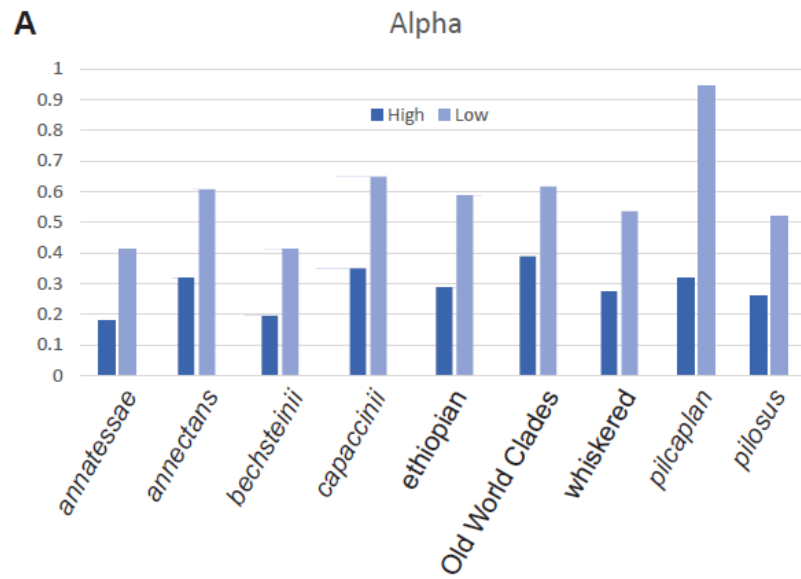
Figure S18: Distribution of alpha and internal branch length (ibl) in regions of high and low recombination, related to Figure 4.
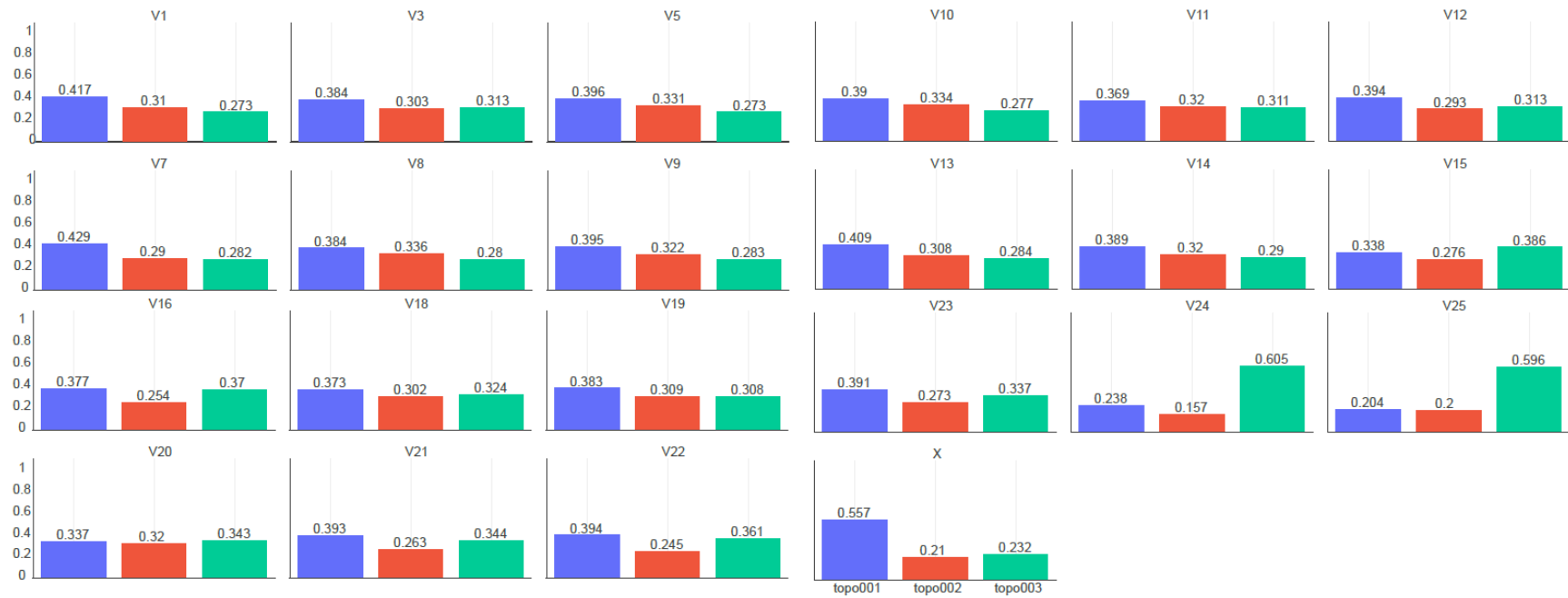
Figure S19: Topology frequency on each chromosome representing within clade relationships among species present at swarming sites, related to Figure 5.
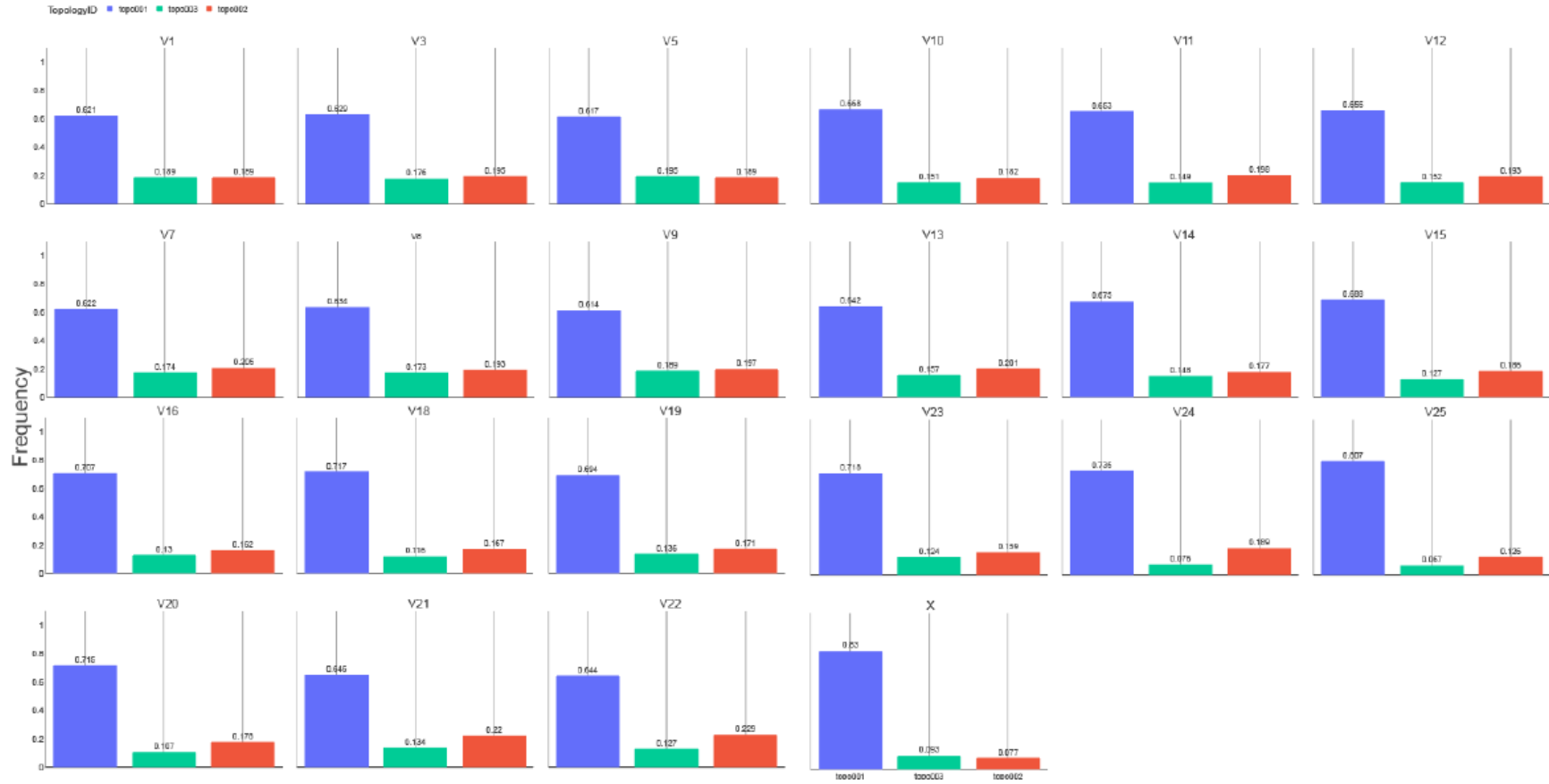
Figure S20: Topology frequency on each chromosome representing between clade relationships for *M. brandtii, M. mystacinus* and *M. alcathoe* at swarming sites, related to Figure 5.
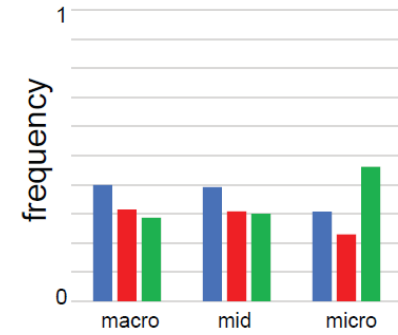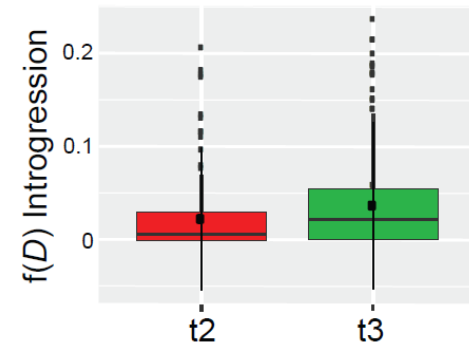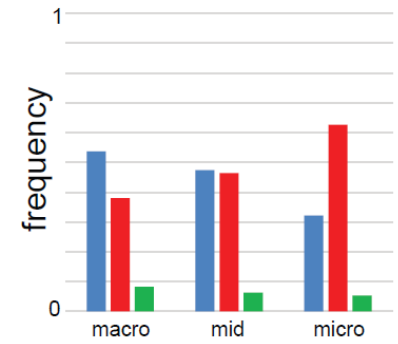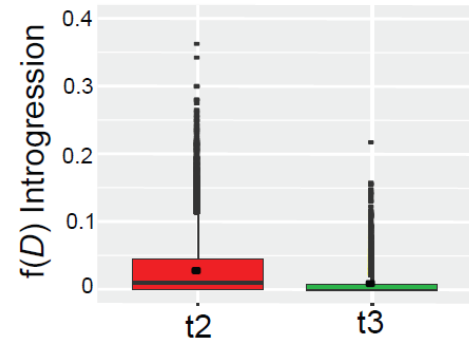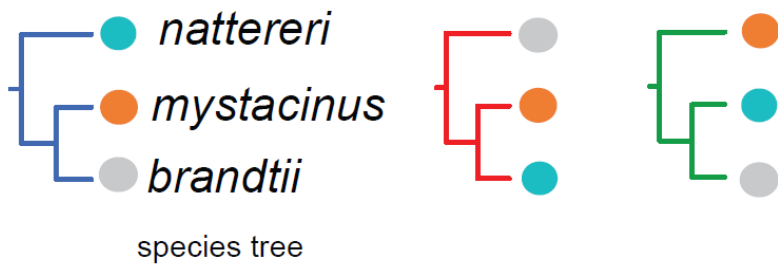
Figure S21: Introgressed topologies with the highest f(*D*) values are the most enriched on microchromosomes, related to Figure 6.
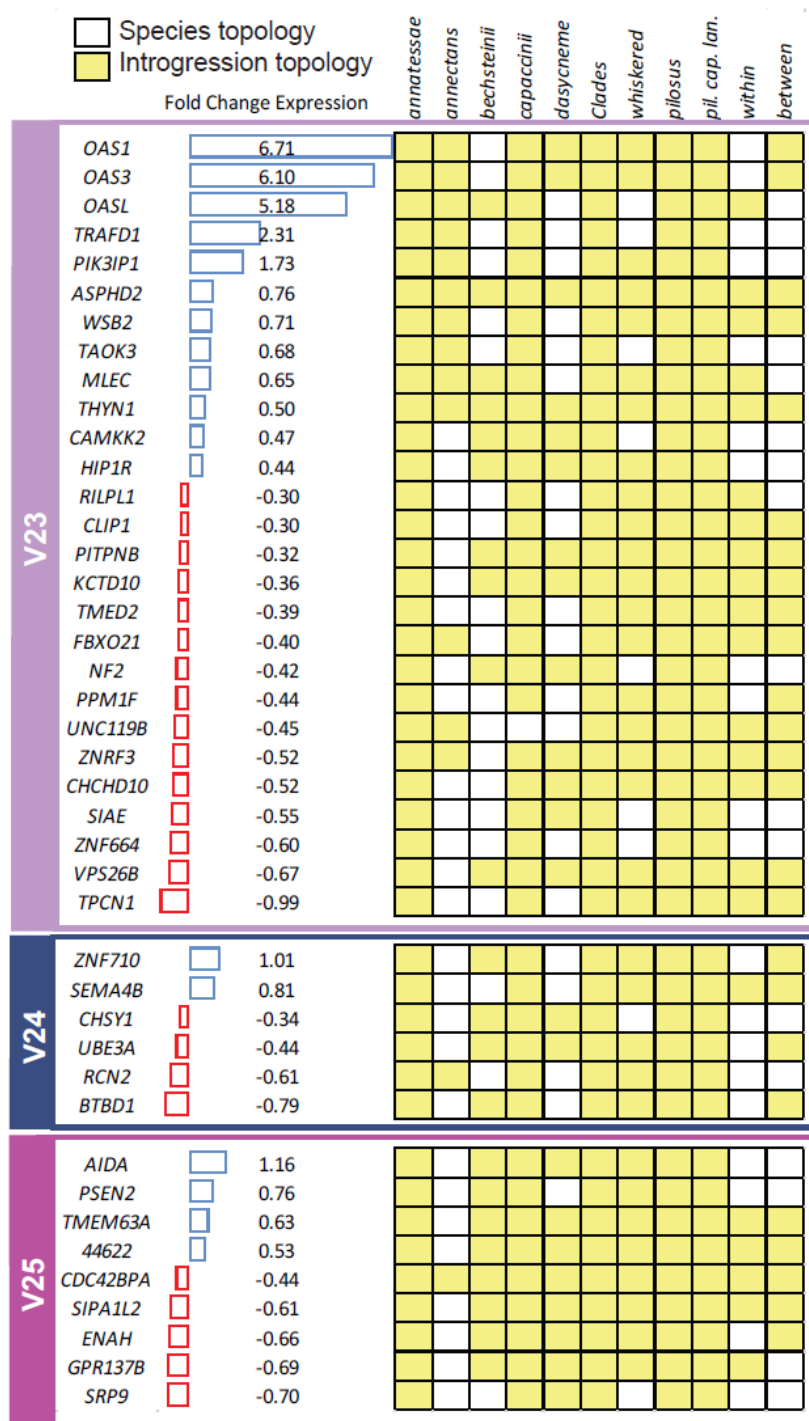
Figure S22: Genes that are differentially expressed in response to viral challenges in *M. daubentonii* were among the most frequently introgressed across microchromosomes, related to Figure 6.
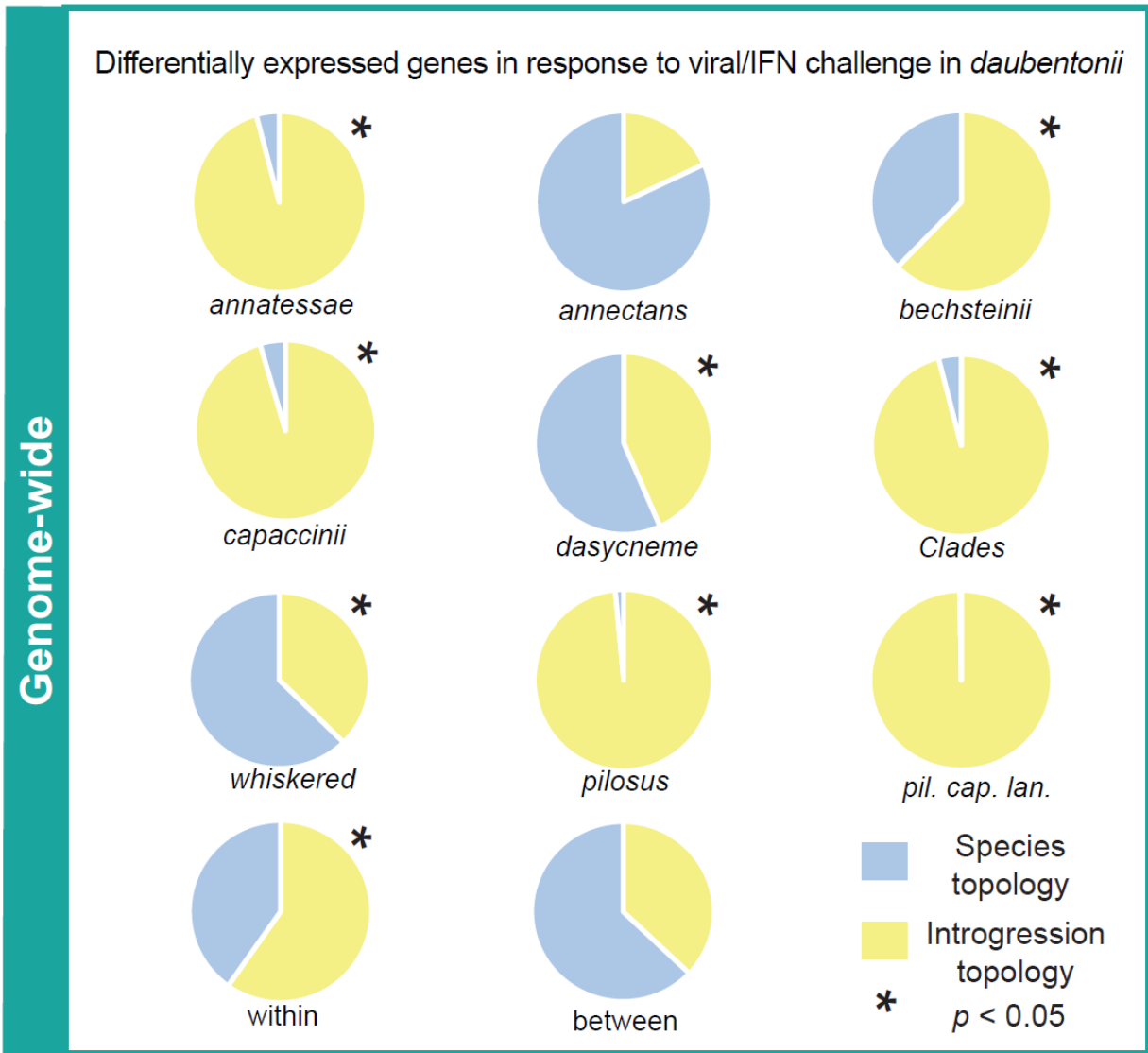
Figure S23: Significant overlap between introgressed genomic windows and genes that are differentially expressed in response to viral challenges in *M. daubentonii*, related to Figure 6.
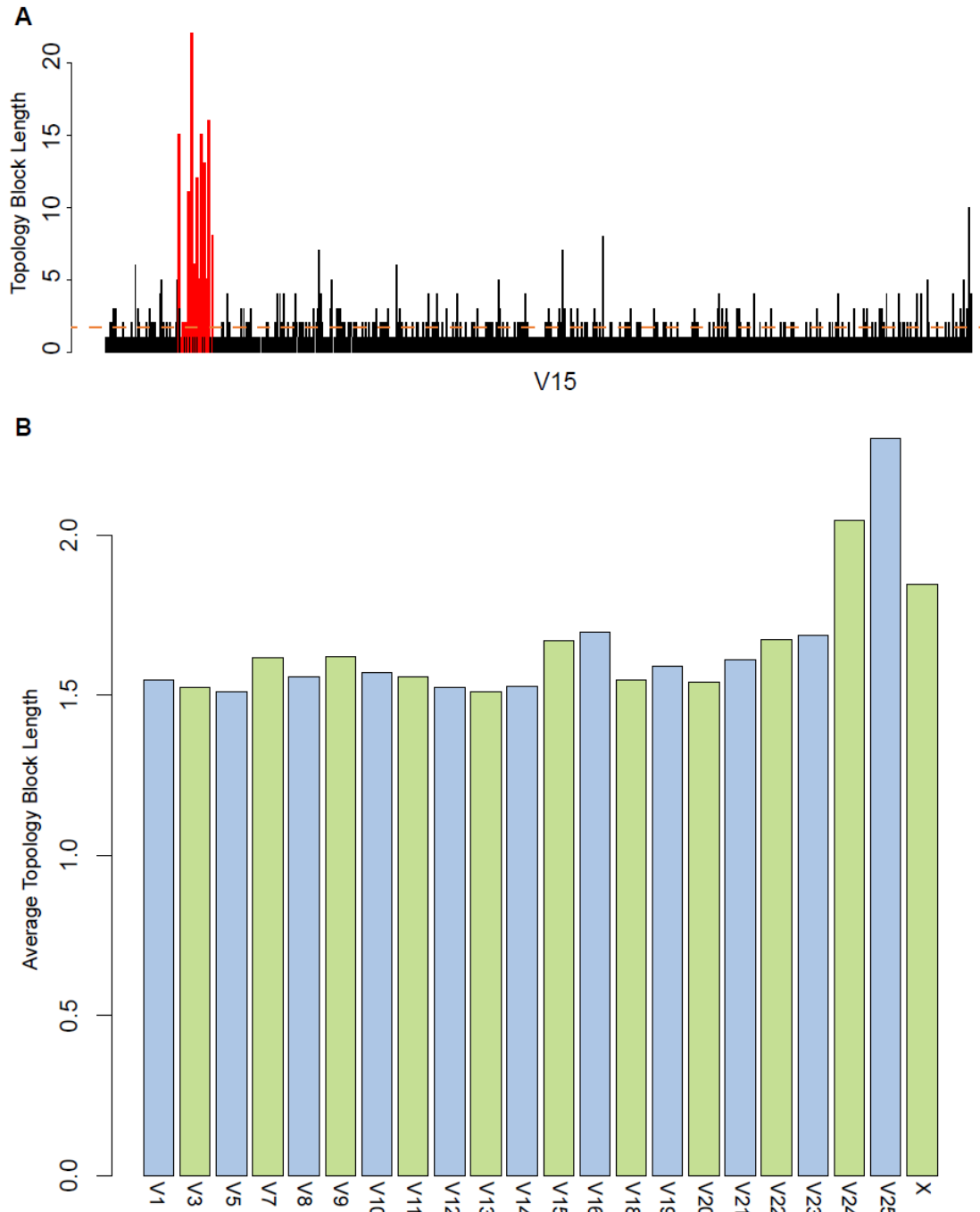
Figure S24: Plots of topology block length (=number of consecutive identical topologies) along chromosomes for the red topology uniting *M. myotis* and *M. daubentonii*, related to Figure 6. A) shows topology block length along chromosome V15. B) Microchromosomes V24 and V25 also exhibit elevated topology block lengths.
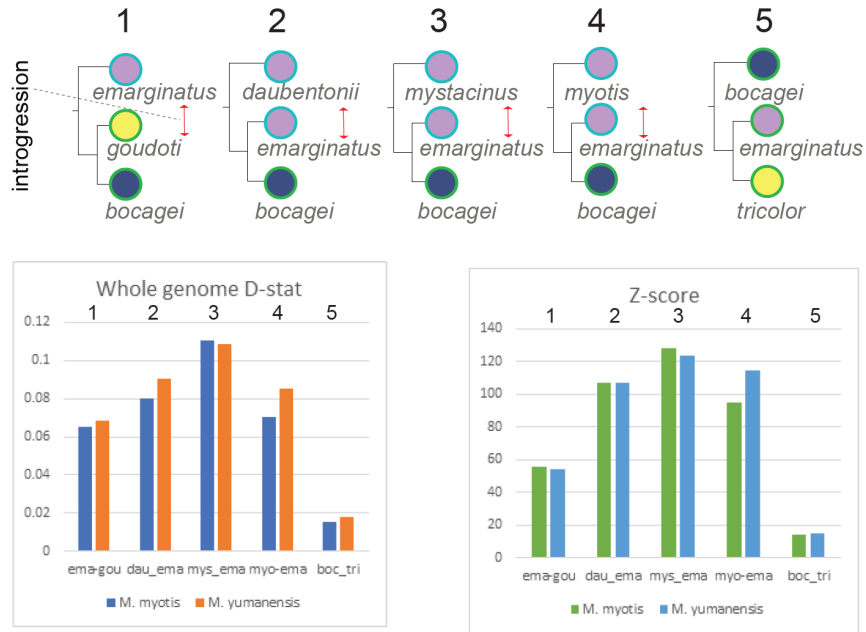
Figure S25: No impact of reference bias on whole genome tests of introgression, related to Figures 4, 5 and 6. *D*-statistics and Z-scores derived from data mapped to the *M. myotis* reference genome or the *M. yumanensis* genome are highly similar indicating the absence of reference bias

Table S1: Sample Information, related to Figure 1. Voucher or sample name, source and sampling locality for each sample used in this study. Categorization of broad scale species distributions as either tropical or temperate or spanning both. Abbreviations in sample source correspond to MHNG – Natural History Museum of Geneva, FMNH – Field Museum of Natural History Chicago, ZMMU – Zoological Museum Moscow Lomonosov State University, ROM – Royal Ontario Museum, EBD –Estacion Biologica de Doñana, AGS – Antonio Guillen-Servant, CMF – Charles M. Francis, SJP – Sebastien J. Puechmaille, MR – Manuel Ruedi

Voucher or Sample Name	Species	Sequencing Sample Number	Source	Locality	Clade
M2148	*latirostris*	S27	MHNG 1998.057	Taïwan.	
unknown	*spp.*	S37	MR		New World
M941	*alcathoe*	S26	MHNG 1828.073	Switzerland.	whiskered
M1575	*alcathoe*	S49	MHNG 1970.099	France.	whiskered
M803	*davidii*	S5	MHNG 1807.035	Greece	whiskered
M1993	*mystacinus*	S20	MHNG 1991.045	Switzerland.	whiskered
FMNH151200	*bocagei*	S42	FMNH	Tanzania	ethiopian
MZ004	*bocagei*	S37	MHNG 1971.027	Mozambique.	ethiopian
FMNH172095	*goudoti*	S45	MR/ FMNH	Madagascar.	ethiopian
FMNH173041	*goudoti*	S51	MR/ FMNH	Madagascar.	ethiopian
TM39421	*welwitschii*	S23	MR/ Transvaal Museum	South Africa.	ethiopian
FMNH144313	*welwitschii*	S47	MR/ FMNH	Uganda.	ethiopian
M733	*emarginatus*	S13	MHNG 1807.040	Greece.	ethiopian
MZ425	*tricolor*	S8	MHNG 1971.030	Mozambique.	ethiopian
TM40300	*tricolor*	S32	MR/ Transvaal Museum	South Africa.	ethiopian
Mdas1	*dasycneme*	S22	MHNG 1805.052	The Netherlands.	ethiopian
M1606	*laniger*	S57	MHNG 1981.074	India.	asian
AG 950116.6	*cf laniger*	S19	AG/ SMF 86179	Laos.	asian
M629	*laniger*	S50	MR	Taiwan.	asian
M1637	*siligorensis*	S31	MHNG 1981.073	India.	asian
N194	*alticraniatus*	S41	MHNG 1956.089	Laos.	asian
S175154	*phanluongi*	S24	MR/ ZMMU		asian
CMF960418.17	*pilosus*	S10	CMF	Laos.	asian
M2065	*pilosus*	S56	MR	India.	asian
CMF960522.46	*macrotarsus*	S20	CMF	Borneo.	oriental
EAR122	*macrotarsus*	S44	MR	Philippines.	oriental
M	*macropus*	S55	MR	Australia.	oriental
CMF960523.40	*horsfieldii*	S12	CMF	Borneo.	oriental

Voucher or Sample Name	Species	Sequencing Sample Number	Source	Locality	Clade
M1551	*horsfieldii*	S28	MHNG 1970.049	Malaysia.	oriental
M1184	*horsfieldii*	S2	MHNG 1926.038	Laos.	oriental
LRH3168	*browni*	S39	MR	Philippines.	oriental
Mca1	*capaccinii*	S34	MHNG 1805.050	Italy.	oriental
AGS980326.44	*montivagus*	S11	AGS	Laos.	muricola
M1208	*indochinensis*	S17	MHNG 1926.043	Laos.	muricola
CMF960408.3	*federatus*	S29	CMF/ROM 106389	Laos.	muricola
M1200	*annatessae*	S7	MHNG 1926.044	Laos.	muricola
M1165	*ater*	S9	MHNG 1926.036	Laos.	muricola
M1569	*muricola*	S30	MHNG 1970.064	Malaysia.	muricola
M1600	*muricola*	S40	MHNG 1972.084	Indonesia.	muricola
M2152	*secundus*	S25	MHNG 1998.058	Taïwan.	muricola
CMF960406.5	*annectans*	S35	CMF/ ROM 106376	Laos	muricola
M2139	*frater*	S21	MHNG 1998.053	Taïwan.	Large *Myotis* & others
M2163	*soror*	S15	MHNG 1998.05	Taïwan.	Large *Myotis* & others
M2009	*bechsteinii*	S18	MHNG 1991.067	Switzerland.	Large *Myotis* & others
M2187	*daubentonii*	S24	MHNG 1999.098	Switzerland.	Large *Myotis* & others
M301	*daubentonii nathalinae*	S54	MR	Spain	Large *Myotis* & others
M303	*daubentonii nathalinae*	S52	MR	Spain.	Large *Myotis* & others
EBD25765	*escalerai*	S36	EBD	Spain	Large *Myotis* & others
M2096	*crypticus*	S38	MHNG 1996.094	Switzerland.	Large *Myotis* & others
M764	*nattereri*	S33	MHNG 1807.049	Greece.	Large *Myotis* & others
MM4SA	*punicus*	S1	MHNG 1805.092	Italy.	Large *Myotis* & others
Mb203	*blythii*	S3	MHNG 1805.026	Kyrgyzstan.	Large *Myotis* & others
631D	*blythii*	S14	MHNG 1805.037	Switzerland.	Large *Myotis* & others
M867	*blythii*	S6	MHNG 1807.099	Greece.	Large *Myotis* & others
Mb3	*blythii*	S4	MHNG 1805.041	Spain.	Large *Myotis* & others
SP.C.47	*blythii*	S43	SJP	Iran	Large *Myotis* & others
SP.C.48	*blythii*	S48	SJP	Iran	Large *Myotis* & others
Mchin1	*ancilla*	S53	MR	China	Large *Myotis* & others

Table S2: Mapping Statistics, related to Figure 1.

Voucher or Sample Name	Species	Sequencing Sample Number	% Reference Covered	reads mapped	mean coverage
M2148	*latirostris*	S27	78.6	94.56%	25
unknown	*spp.*	S37	79.6	96.33%	12
M941	*alcathoe*	S26	82.1	97.68%	16
M1575	*alcathoe*	S49	84.4	97.44%	26
M803	*davidii*	S5	85	98.51%	23
M1993	*mystacinus*	S20	84.8	96.86%	22
FMNH144313	*welwitschii*	S47	83.1	95.94%	18
MZ004	*bocagei*	S37	84.8	97.17%	29
FMNH172095	*goudoti*	S45	81.5	95.22%	12
FMNH173041	*goudoti*	S51	84.8	96.80%	19
TM39421	*welwitschii*	S23	83.3	97.77%	17
FMNH151200	*bocagei*	S42	84	95.01%	19
M733	*emarginatus*	S13	86.1	98.32%	25
MZ425	*tricolor*	S8	85.4	97.52%	21
TM40300	*tricolor*	S32	86.2	98.11%	27
Mdas1	*dasycneme*	S22	79.5	98.70%	20
M1606	*laniger*	S57	85	98.78%	18
AG950116.6	*laniger*	S19	85.6	97.27%	23
M629	*laniger*	S50	85.8	98.33%	26
M1637	*siligorensis*	S31	84.8	97.39%	18
N194	*alticraniatus*	S41	86.6	98.29%	29
S175154	*phanluongi*	S24	81.3	97.45%	16
CMF960418.17	*pilosus*	S10	85.9	98.56%	24
M2065	*pilosus*	S56	86.1	98.68%	27
CMF960522.46	*macrotarsus*	S20	83	97.69%	14
EAR122	*macrotarsus*	S44	83.8	96.5%	16
M	*macropus*	S55	84.5	98.84%	20
CMF960523.40	*horsfieldii*	S12	86.1	97.91%	25

Voucher or Sample Name	Species	Sequencing Sample Number	% Reference Covered	reads mapped	mean coverage
M1551	*horsfieldii*	S28	83.5	97.01%	15
M1184	*horsfieldii*	S2	86.6	98.16%	28
LRH3168	*browni*	S39	83.9	96.62%	19
Mca1	*capaccinii*	S34	82.2	97.98%	13
AGS980326.44	*montivagus*	S11	85.2	97.63%	24
M1208	*indochinensis*	S17	85.4	97.06%	25
CMF960408.3	*federatus*	S29	85.7	97.62%	27
M1200	*annatessae*	S7	85.1	98.17%	20
M1165	*ater*	S9	85.9	98.04%	29
M1569	*muricola*	S30	84.9	96.57%	23
M1600	*muricola*	S40	84.6	94.99%	20
M2152	*secundus*	S25	86.7	96.75%	27
CMF960406.5	*annectans*	S35	82.4	97.80%	12
M2139	*frater*	S21	86.5	96.04%	20
M2163	*soror*	S15	86.4	97.90%	17
M2009	*bechsteinii*	S18	89.5	98.97%	27
M2187	*daubentonii*	S24	88.6	98.31%	20
M301	*daubentonii nathalinae*	S54	88.9	99.01%	23
M303	*daubentonii nathalinae*	S52	89	98.96%	26
EBD25765	*escalerai*	S36	90.5	96.94%	23
M2096	*crypticus*	S38	91.4	98.30%	28
M764	*nattereri*	S33	90.9	98.23%	24
MM4SA	*punicus*	S1	94.1	99.18%	20
Mb203	*blythii*	S3	94.1	98.86%	23
631D	*blythii*	S14	94.2	98.71%	24
M867	*blythii*	S6	93.5	99.35%	18
Mb3	*blythii*	S4	94.2	99.11%	22
SP.C.47	*blythii*	S43	93.3	98.64%	17
SP.C.48	*blythii*	S48	89.2	99.34%	17
Mchin1	*ancilla*	S53	93.1	98.44%	25

29

Table S3: Quast summary of difference between the original *Myotis myotis* assembly (HLmyoMyo6) and the improved assembly (Myotismyotis_assembly_V2), related to the improved *Myotis myotis* assembly described in the main text.

	HLmyoMyo	Myotismyotis_assembly_V2
# contigs	92	55
Largest contig	223369599	228434895
Total Length	2003238046	2003245946
GC%	43.11	43.11
N50	94448911	108770286
N75	74216526	79764552
L50	7	6
L75	12	12
# N's per 100kbp	1468.17	1468.56

Table S4: Species composition for each subclade examined in the analysis of genome-wide phylogenomic signal, related to Figure 3.

annatessae	annectans	bechsteinii	capaccinii	ethiopian	Old World Clades	whiskered	pilcaplan	pilosus
bocagei S37	soror S15	bocagei S37	bocagei S37	latirostris S27	latirostris S27	latirostris S27	bocagei S37	bocagei S37
muricola S30	frater S21	bechsteinii S18	capaccinii S34	tricolor S32	laniger S19	mystacinus S20	capaccinii S34	macropus S55
ater S9	annectans S35	daubentonii S24	macropus S55	welwitschii S23	macropus S55	alcathoe S49	laniger S19	macrotarsus S44
muricola S40	secundus S25	ancilla S53	macrotarsus S20	bocagei S37	macrotarsus S44	brandtii	pilosus S56	pilosus S56
federatus S29	muricola S30	myotis	phanluongi S24	emarginatus S13	muricola S30	bocagei S37		phanluongi S24
montivagus S11	bocagei S37	soror S15	alticraniatus S41	dasycneme S22	montivagus S11	myotis		laniger S57
annatessae S7		frater S21			myotis			
					ancilla S53			
					bocagei S37			

Table S5: Detailed breakdown of results for genome wide *D*-statistic tests, related to Figure 4. Trees were analyzed in the format (((H1, H2), H3,) Outgroup) where the outgroup was *S. latirostris* for all tests. A Z score above 3 is considered significant.

Reference genome	H1	H2	H3	nABBA	nBABA	Dstat	jackEst	SE	Z
Myotis myotis	MZ004_bocagei_S37	**M733_emarginatus_S13**	**M2187_daubentonii_S24**	1791427	1511330	0.084807	0.084807	0.00079	**107.3416**
Myotis yumanensis	MZ004_bocagei_S37	**M733_emarginatus_S13**	**M2187_daubentonii_S24**	1711426	1427716	0.090378	0.090378	0.000843	**107.2569**
Myotis myotis	MZ004_bocagei_S37	**M733_emarginatus_S13**	**myo_BROAD**	1800187	1563127	0.070484	0.070484	0.00074	**95.21591**
Myotis yumanensis	MZ004_bocagei_S37	**M733_emarginatus_S13**	**myo_BROAD**	1733777	1460703	0.085483	0.085483	0.000746	**114.6314**
Myotis myotis	MZ004_bocagei_S37	**M733_emarginatus_S13**	**M1993_mystacinus_S20**	1627722	1303891	0.110462	0.110462	0.000861	**128.308**
Myotis yumanensis	MZ004_bocagei_S37	**M733_emarginatus_S13**	**M1993_mystacinus_S20**	1548282	1244630	0.108722	0.108722	0.000881	**123.4457**
Myotis myotis	MZ004_bocagei_S37	**fmnh172095_goudoti_S45**	**M733_emarginatus_S13**	2226221	1954903	0.064891	0.064891	0.001166	**55.66637**
Myotis yumanensis	MZ004_bocagei_S37	**fmnh172095_goudoti_S45**	**M733_emarginatus_S13**	2135239	1861688	0.06844	0.06844	0.001266	**54.08118**
Myotis myotis	**TM40300_tricolor_S32**	M733_emarginatus_S13	**MZ004_bocagei_S37**	1981908	2042725	-0.01511	-0.01511	0.001075	**-14.0531**
Myotis yumanensis	**TM40300_tricolor_S32**	M733_emarginatus_S13	**MZ004_bocagei_S37**	1895093	1963687	-0.01778	-0.01778	0.001175	**-15.128**
Myotis myotis	myo_BROAD	**M2187_daubentonii_S24**	S175154_phanluongi_S24	2058223	1844105	0.054869	0.054869	0.001072	**51.19208**
Myotis myotis	M2009_bechsteinii_S18	**M2187_daubentonii_S24**	**myo_BROAD**	2580187	2536752	0.008488	0.008488	0.002327	**3.648049**
Myotis myotis	**CMF960522_46_macrotarsus_S20**	M2009_bechsteinii_S18	**M1569_muricola_S30**	2926327	3861014	-0.13771	-0.13771	0.001369	**-100.559**
Myotis myotis	**M2009_bechsteinii_S18**	M2096_nattereri_S38	**Mbrandtii**	1202345	1248347	-0.01877	-0.01877	0.000794	**-23.6339**
Myotis myotis	**M2187_daubentonii_S24**	M2096_nattereri_S38	**M1993_mystacinus_S20**	1394982	1545713	-0.05126	-0.05126	0.000799	**-64.1663**
Myotis myotis	**M1993_mystacinus_S20**	Mbrandtii	**M2096_nattereri_S38**	2184190	3099853	-0.17329	-0.17329	0.002389	**-72.5429**
Myotis myotis	**M2139_frater_S21**	M2009_bechsteinii_S18	**CMF960406_5_annectans_S35**	2760696	3263672	-0.08349	-0.08349	0.002849	**-29.3023**
Myotis myotis	**M1993_mystacinus_S20**	M941_alcathoe_S26	**Mbrandtii**	2430561	2617513	-0.03703	-0.03703	0.001214	**-30.496**

Reference genome	H1	H2	H3	nABBA	nBABA	Dstat	jackEst	SE	Z
Myotis myotis	**CMF960522_46_macrotarsus_S20**	S175154_phanluongi_S24	**Mca1_capaccinii_S34**	3473250	4084785	-0.08091	-0.08091	0.00315	**-25.6831**
Myotis myotis	**M941_alcathoe_S26**	Mbrandtii	**Mdas1_dasycneme_S22**	2214338	3236368	-0.1875	-0.1875	0.00342	**-54.82**
Myotis myotis	**M1993_mystacinus_S20**	Mbrandtii	**Mdas1_dasycneme_S22**	2121574	3071673	-0.18295	-0.18295	0.002391	**-76.5191**
Myotis myotis	M733_emarginatus_S13	**Mdas1_dasycneme_S22**	**M2009_bechsteinii_S18**	2507335	2422351	0.017239	0.017239	0.001189	**14.49878**
Myotis myotis	**M2187_daubentonii_S24**	M2096_nattereri_S38	**Mdas1_dasycneme_S22**	1560422	1696782	-0.04186	-0.04186	0.000738	**-56.7437**
Myotis myotis	M733_emarginatus_S13	**Mdas1_dasycneme_S22**	**M1993_mystacinus_S20**	2131851	2029572	0.024578	0.024578	0.000942	**26.09706**
Myotis myotis	myo_BROAD	M733_emarginatus_S13	M1993_mystacinus_S20	2532201	2527665	0.000896	0.000896	0.001001	0.895467
Myotis myotis	M2009_bechsteinii_S18	**M2187_daubentonii_S24**	**M2096_nattereri_S38**	2621507	2579505	0.008076	0.008076	0.002248	3.592021
Myotis myotis	**M629_laniger_S50**	CMF960522_46_macrotarsus_S20	**M2065_pilosus_S56**	2361436	7045984	-0.49796	-0.49796	0.002534	**-196.503**
Myotis myotis	**M1569_muricola_S30**	M1208_indochinensis_S17	**M1200_annatessae_S7**	3455060	3730538	-0.03834	-0.03834	0.00132	**-29.0523**
Myotis myotis	**M2187_daubentonii_S24**	M2009_bechsteinii_S18	**myo_BROAD**	2536800	2581340	-0.0087	-0.0087	0.002334	**-3.72829**
Myotis myotis	**M2139_frater_S21**	M2187_daubentonii_S24	**M2065_pilosus_S56**	2650991	3062319	-0.07199	-0.07199	0.001695	**-42.4712**
Myotis myotis	M1569_muricola_S30	**M1208_indochinensis_S17**	CMF960406_5_annectans_S35	2093563	1918718	0.043577	0.043577	0.000709	**61.43691**
Myotis myotis	**M2096_nattereri_S38**	**M2187_daubentonii_S24**	**M733_emarginatus_S13**	**1610340**	**1590837**	**0.006092**	**0.006092**	**0.000795**	**7.668013**

Table S6: Results of the QuIBL analysis, related to Figure 4. The table shows the proportion of variation in discordant topologies explained by ILS alone or a combination of ILS and introgression. The difference in BIC estimates (delta) for each model indicates that the model with introgression and ILS (preferred at delta ≥-10) is the best fit for all relationships analyzed. Old World Clades refers to the relationship among the Muricola, Large Myotis, Asian, and Oriental clades shown in Figure 1. *pil.-cap.-lan.* refers to the relationship among *pilosus*, *capaccinii,* and *laniger*. Non-species trees are color-coded to correspond with data displayed in Figure 1.

Clade	non-species topology	tree	ILS	Introgression + ILS	delta
annatessae	topo002	*(annatessae, (indochinensis, muricola))*	0%	100%	-13383
	topo001	*indochinensis, (muricola ,annatessae))*	0%	100%	-17245
annectans	topo003	*(annectans, (frater, muricola))*	0%	100%	-995
	topo002	*(frater, (annectans, muricola))*	0%	100%	-3319
bechsteinii	topo002	*(bechsteinii, (daubentonii, myotis))*	0%	100%	-9038
	topo003	*(daubentonii, (bechsteinii, myotis))*	0%	100%	-9045
capaccinii	topo001	*(phanluongi, (capaccinii, macrotarsus))*	0%	100%	-30065
	topo002	*(macrotarsus, (capaccinii, phanluongi))*	0%	100%	-5825
dasycneme	topo004	*(mystacinus, (alcathoe, (dasycneme, bocagei)))*	0%	100%	-299
	topo002	*(bocagei, (dasyceneme, (mystacinus, alcathoe)))*	0%	100%	-44060
Clades	topo003	*(muricola, (myotis, macrotarsus))*	0%	100%	-9122
	topo001	*(myotis, (macrotarsus, muricola))*	0%	100%	-17445
whiskered	topo004	*(alcathoe, (mystacinus, brandtii))*	0%	100%	-4761

	topo006	*(mystacinus, alcathoe, brandtii))*	0%	100%	-4474
pil. cap. lan.	topo003	*(laniger, (capaccinii,pilosus))*	73%	27%	33
	topo001	*capaccinii, ((pilosus, laniger))*	0%	100%	-33039
pilosus	topo001	*(macropus, (pilosus, laniger))*	0%	100%	-32580
	topo005	*(pilosus, (macropus, laniger))*	28%	72%	-174

Table S7: Studies reporting species presence at swarming sites across Europe [S2-16], related to Figure 5. Although *M. myotis* and *M. blythii* are thought to use a lekking mating behavior

Paper / Country	Schunger et al (2004) / Bulgaria	Dundarova (2018) / Bulgaria	Rivers et al (2006) / UK	Parsons et al (2003) / UK	Piksa et al (2011) / Poland	Suba et al (2008) / Latvia	Schaik et al (2015) / Netherlands	Bogdanowicz et al 2012 / Poland	Suba et al (2011) / Latvia	Glover and Altringham (2008) / UK	Schmidbauer and Denzinger (2019) / Germany	Pocora et al (2012) / Romania	Dekeukeleire et al (2016) / Belgium and Netherlands	Thomas and Davison (2020) / Wales	Ignaczak et al (2019) / Poland
myotis	x	x			x		x				x	x	x		x
blythii	x	x													
bechsteinii	x	x		x	x		x					x	x	x	x
nattereri/crypticus	x	x	x	x	x	x				x	x	x	x	x	x
daubentonii	x	x	x	x	x	x	x		x	x			x		x
brandtii	x	x	x	x	x	x	x	x	x	x		x	x	x	x
alcathoe	x	x			x			x							
mystacinus		x	x	x	x	x	x	x		x		x	x	x	
emarginatus	x	x					x						x		
dasycneme					x	x	x		x				x		

36

Table S8: STRING enrichment analysis for an introgressed block on V15 which unites *M. myotis* and *M. daubentonii*, related to Figure 6. Enrichments are considered significant with an FDR value of ≥ 0.05.

Category	#term ID	term description	observed gene count	background gene count	strength	false discovery rate
Molecular Function	GO:0005149	interleukin-1 receptor binding	7	17	2.04	8.6E-09
Molecular Function	GO:0070851	Growth factor receptor binding	8	138	1.19	1.2E-04
Molecular Function	GO:0005126	Cytokine receptor binding	8	264	0.9	9.0E-03
KEGG Pathway	hsa04060	Cytokine-cytokine receptor interaction	7	282	0.82	3.6E-02
Reactome Pathway	HSA-446652	Interleukin-1 family signaling	7	136	1.13	2.4E-03
Reactome Pathway	HSA-9014826	Interleukin-36 pathway	3	6	2.12	4.6E-03

Table S9: Immunogenetic diversification mechanisms across the Tree of Life, related to Figure 6. Note that most of these mechanisms operate within the listed taxa. MHC allelic polymorphism has long been of interests to evolutionary biologists due to its function at the population level. Now adaptive immunogenetic introgression in *Myotis* bats appears to elevate such defense diversification strategies to the level of the multispecies community.

Taxa	Process	Genes Diversified	Evolutionary Facilitation	Mechanism
archaea/bacteria	adaptive anti-phage immunity	clustered regularly interspaced short palindromic repeats (CRISPR)	horizontal gene transfer	CRISPR/cas9 [S17]
arthropods	repertoire of pattern recognition receptors	down syndrome cell adhesion molecule (DSCAM)	exon family expansion	mutually exclusive alternative RNA exon splicing [S18]
jawless fishes	VLR repertoire diversification	variable lymphocyte receptors	copy-choice recombination	APOBEC family deaminases [S19]
jawed vertebrates	somatic cell gene rearrangement of lymphocyte antigen receptors	immunoglobulin, T cell receptor	horizontal transposon capture	recombination activating genes (RAG) [S20]
jawed vertebrates	antibody affinity maturation	immunoglobulin heavy and light chain variable genes	selection of controlled somatic hypermutation	activation induced cytidine deaminase (AID) [S21]
Bovidae	ultralong cattlebody knob diversification	third complementarity determining region (CDR3) of immunoglobulin heavy chain	bias for cysteine mutation, truncations in CDR3	activation induced cytidine deaminase (AID) [S22]
jawed vertebrates	allelic polymorphism	classical MHC antigen presentation	balancing selection, pathogen co-evolution	extreme allelic diversity in peptide binding – **Population** [S23]
Myotis **bats**	tunable immunogenetic viral tolerance	interferons, antigen processing, anti-viral signaling	swarming, interspecific hybridization	adaptive immunogenetic introgression – **Genus Community**

Supplementary References

S1. Jebb, D., Huang, Z., Pippel, M., Hughes, G.M., Lavrichenko, K., Devanna, P., Winkler, S., Jermiin, L.S., Skirmuntt, E.C., Katzourakis, A., et al. (2020). Six reference-quality genomes reveal evolution of bat adaptations. Nature *583*, 578–584.

S2. Schunger, I., Dietz, C., Merdschanova, D., Merdschanov, S., Christov, K., Borissov, I., Staneva, S., and Petrov, B. (2004). Swarming of bats (Chiroptera, Mammalia) in the Vodnite Dupki cave (Central Balkan National Park, Bulgaria). Acta Zool. *56*, 323–330.

S3. Dundarova, H. (2018). Bat diversity in Lednitsata and Forgovskata dupka Caves: two potentially important swarming sites in Western Rhodopes Mts., Bulgaria. Acta Zool. Bulg. *70*, 139–142.

S4. Rivers, N.M., and Butlin R. K. Altringham, J.D. (2006). Autumn swarming behaviour of Natterer's bats in the UK: population size, catchment area and dispersal. Biol. Conserv. *127*, 215–226.

S5. Parsons, K.N., Jones, G., and Greenaway, F. (2003). Swarming activity of temperate zone microchiropteran bats: effects of season, time of night and weather conditions. J. Zool. *261*, 257–264.

S6. Piksa, K., Bogdanowicz, W., and Tereba, A. (2011). Swarming of Bats at Different Elevations in the Carpathian Mountains. Acta Chiropterologica *13*, 113–122.

S7. Šuba, J., Vintulis, V., and Pētersons, G. (2008). Late summer and autumn swarming of bats at Sikspārņu caves in Gauja National Park. Acta Univ. Latv *745*, 43–52.

S8. van Schaik, J., Janssen, R., Bosch, T., Haarsma, A.-J., Dekker, J.J.A., and Kranstauber, B. (2015). Bats Swarm Where They Hibernate: Compositional Similarity between Autumn Swarming and Winter Hibernation Assemblages at Five Underground Sites. PLoS One *10*, e0130850.

S9. Bogdanowicz, W., Piksa, K., and Tereba, A. (2012). Hybridization hotspots at bat swarming sites. PLoS One *7*, e53334.

S10. Suba, J., Vintulis, V., and Petersons, G. (2010). Body weight provides insights into the feeding strategy of swarming bats. Hystrix, the Italian *22*, 1.

S11. Glover, A.M., and Altringham, J.D. (2008). Cave selection and use by swarming bat species. Biol. Conserv. *141*, 1493–1504.

S12. Schmidbauer, P., and Denzinger, A. (2019). Social calls of *Myotis nattereri* during swarming: Call structure mirrors the different behavioral context. PLoS One *14*, e0221792.

S13. Pocora, I., Pocora, V., and Baltag, E. (2012). Swarming activity of bats at the entrance of Liliecilor cave from Rarău Mountains. Analele Ştiinţifice ale *58*, 151–158.

S14. Dekeukeleire, D., Janssen, R., Haarsma, A.-J., Bosch, T., and Van Schaik, J. (2016). Swarming behaviour, catchment area and seasonal movement patterns of the Bechstein's bats: implications for conservation. Acta Chiropt. *18*, 349–358.

S15. Ignaczak, M., Postawa, T., Lesiński, G., and Gottfried, I. (2019). The role of autumnal swarming behaviour and ambient air temperature in the variation of body mass in temperate bat species. Hystrix *30*, 65–73.

S16. Thomas, R.J., and Davison, S.P. (2022). Seasonal swarming behavior of *Myotis* bats revealed by integrated monitoring, involving passive acoustic monitoring with automated analysis, trapping, and video monitoring. Ecol. Evol. *12*, e9344.

S17. Jinek, M., Chylinski, K., Fonfara, I., Hauer, M., Doudna, J.A., and Charpentier, E. (2012). A Programmable Dual-RNA–Guided DNA Endonuclease in Adaptive Bacterial Immunity. Science *337*, 816–821.

S18. Watson, F.L., Püttmann-Holgado, R., Thomas, F., Lamar, D.L., Hughes, M., Kondo, M., Rebel, V.I., and Schmucker, D. (2005). Extensive diversity of Ig-superfamily proteins in the immune system of insects. Science *309*, 1874–1878.

S19. Pancer, Z., Amemiya, C.T., Ehrhardt, G.R.A., Ceitlin, J., Gartland, G.L., and Cooper, M.D. (2004). Somatic diversification of variable lymphocyte receptors in the agnathan sea lamprey. Nature *430*, 174–180.

S20. Hozumi, N., and Tonegawa, S. (1976). Evidence for somatic rearrangement of immunoglobulin genes coding for variable and constant regions. Proc. Natl. Acad. Sci. U. S. A. *73*, 3628–3632.

S21. Muramatsu, M., Kinoshita, K., Fagarasan, S., Yamada, S., Shinkai, Y., and Honjo, T. (2000). Class switch recombination and hypermutation require activation-induced cytidine deaminase (*AID*), a potential RNA editing enzyme. Cell *102*, 553–563.

S22. Wang, F., Ekiert, D.C., Ahmad, I., Yu, W., Zhang, Y., Bazirgan, O., Torkamani, A., Raudsepp, T., Mwangi, W., Criscitiello, M.F., et al. (2013). Reshaping antibody diversity. Cell *153*, 1379–1393.

S23. Zinkernagel, R.M., and Doherty, P.C. (1974). Restriction of in vitro T cell-mediated cytotoxicity in lymphocytic choriomeningitis within a syngeneic or semiallogeneic system. Nature *248*, 701–702.